NASA CONTRACTOR REPORT

NASA CR-297

NASA CR-297

AN EXPERIMENTAL INVESTIGATION OF THRUST VECTOR CONTROL BY SECONDARY INJECTION

by Richard D. Guhse

Prepared under Grant No. NsG-592 *by*
PURDUE UNIVERSITY
Lafayette, Ind.
for

NATIONAL AERONAUTICS AND SPACE ADMINISTRATION • WASHINGTON, D. C. • SEPTEMBER 1965

NASA CR-297

AN EXPERIMENTAL INVESTIGATION OF THRUST VECTOR CONTROL BY SECONDARY INJECTION

By Richard D. Guhse

Prepared under Grant No. NsG-592 by
PURDUE UNIVERSITY
Lafayette, Ind.

for

NATIONAL AERONAUTICS AND SPACE ADMINISTRATION

For sale by the Clearinghouse for Federal Scientific and Technical Information
Springfield, Virginia 22151 – Price $4.00

TABLE OF CONTENTS

LIST OF TABLES

LIST OF FIGURES

ABSTRACT

An experimental investigation was conducted to examine the flow field produced when a secondary gas is injected into a supersonic primary stream. A preliminary analytical investigation revealed that several parameters (such as the primary and secondary gas properties, flow conditions and geometrical parameters) were influential in determining the nature of the flow field produced by secondary injection and the resulting side force. The investigation reported herein is concerned with the results of a systematic variation of these parameters.

Experiments were conducted in a Mach 2.0, two-dimensional blow down wind tunnel utilizing air as the primary and secondary gases. The secondary gas was injected through a rectangular slot extending the width of the primary nozzle. The area of the slot was varied from 1/2% to 10% of the primary nozzle throat area in five increments. For each value of slot area the secondary to primary stagnation pressure ratio was varied from 0.301 to 1.175 in six increments. The experiments were conducted for injection normal to the nozzle axis and at an angle of 10° upstream of this normal at an axial position where the primary Mach number was 1.90. In each case preliminary diagnostic investigations (optical) were conducted to determine the nature of the flow field.

Secondly, the measured experimental data were used to calculate the side force produced by secondary injection. and

These results were compared with the values of side force computed with the aid of the two theories (due to Wu, Chapkis and Mager (5) and Broadwell (6)) available at the present time. It was found that the theoretical results compared favorably with experimental results only over a specific range of the variables, thus indicating ranges of applicability for each of the proposed theories.

1. INTRODUCTION

A problem of considerable theoretical and practical interest is the description of the flow field produced by the injection of a secondary gas into a supersonic primary stream at an inclination. Flows of that type occur during thrust vector control of rocket motors, during jet reaction (attitude) control of vehicles moving through the atmosphere, and during fuel injection into a supersonic burner. In all of those applications, when a gas is injected into a supersonic primary flow, the injected material acts as an obstruction to the primary flow and, as such, causes the formation of a strong shock wave. The shock and the boundary layer present on the wall form a complex flow pattern in which both high and low pressure regions exist in the neighborhood of the injector.

Although much work has been done to investigate the phenomena associated with such injection, the interaction processes are still not well understood. With regard to thrust vector control, which is the application of major interest here, most of the experimental studies reported to date have been concerned with the measurement of gross quantities, such as the side force produced in a given system, without delving too deeply into the phenomena taking place in the nozzle.

The purpose of the research, the results of which are presented here, is to gain insight into the phenomenological processes that occur when a gas is injected into a supersonic stream. It is hoped that the conditions under which several theoretical models (that have been postulated to date)

may be applied for analytical study may be determined. Furthermore, the experimental results may be employed in the development of more realistic theoretical models.

Before outlining the method of attacking the problem (Section 1.2), a brief survey of the pertinent literature is in order. The literature reviewed in Section 1.1 is limited to studies that have resulted in well defined theoretical models and does not include studies that are solely experimental.

1.1 Survey of Pertinent Literature

Several theories have been proposed for the study of phenomena associated with the secondary injection of a gas into a supersonic flow. The more significant of those theories may be classified as follows:

1. linearized supersonic flow theory due to Walker, Stone and Shandor (1962)(1),* (1962)(2), (1963)(3), (1964)(4),
2. boundary layer separation theory due to Wu, Chapkis and Mager (1961)(5),
3. blast wave theory due to Broadwell (1962)(6), (1963)(7),
4. theory to replace the injected gas with a blunt axisymmetric body for analytical purposes (hereafter referred to as the blunt axisymmetric body theory) due to Zukoski and Spaid (1964)(8), and
5. the injection model due to Charwat and Allegre (1964)(9).

* Numbers in parenthesis refer to references listed in the BIBLIOGRAPHY. Preceding many of the references will be the date the article was published, also in parenthesis.

Of the theories proposed, only the analyses by Wu, Chapkis and Mager and Broadwell present specific relations for determining the side force produced by the injection of a gas into a supersonic stream. Those theories may be employed (see Chapter 4), under certain conditions, for a theoretical determination of the values of the side force generated in a given system which may be compared with the results obtained from the experimental studies reported herein. The remaining three theories are essentially in the nature of phenomenological discussions.

1.1.1 Linearized Supersonic Flow Theory

Walker, Stone and Shandor (1962)(2) propose the model shown in Fig. 1. The authors idealize the problem in terms of the study of mixing between a trace of injectant, $d\dot{W}$, and a portion of supersonic flow, $\dot{W}$. The mixing is assumed to occur in a length of flow passage of constant area giving rise to an instantaneous dissipation of the transverse jet momentum. This is a theory based on one dimensional gas dynamics. The rise of static pressure in the mixing region induces a compression Mach wave (weak shock wave) in the enveloping flow. Expansion waves in the supersonic flow maintain the pressure continuity along the dividing streamline separating the mixing region from the unaffected stream. The authors assume small flow deflections so that linear supersonic flow theory is valid. The side force is then found by integrating the pressure rise along the dividing streamline.

In addition to the theoretical model proposed, the authors also provide (1),(2),(3),(4) a considerable amount of experimental data.

The principal conclusions derived from the theoretical study in relation to the data obtained in the experimental research are as follows:

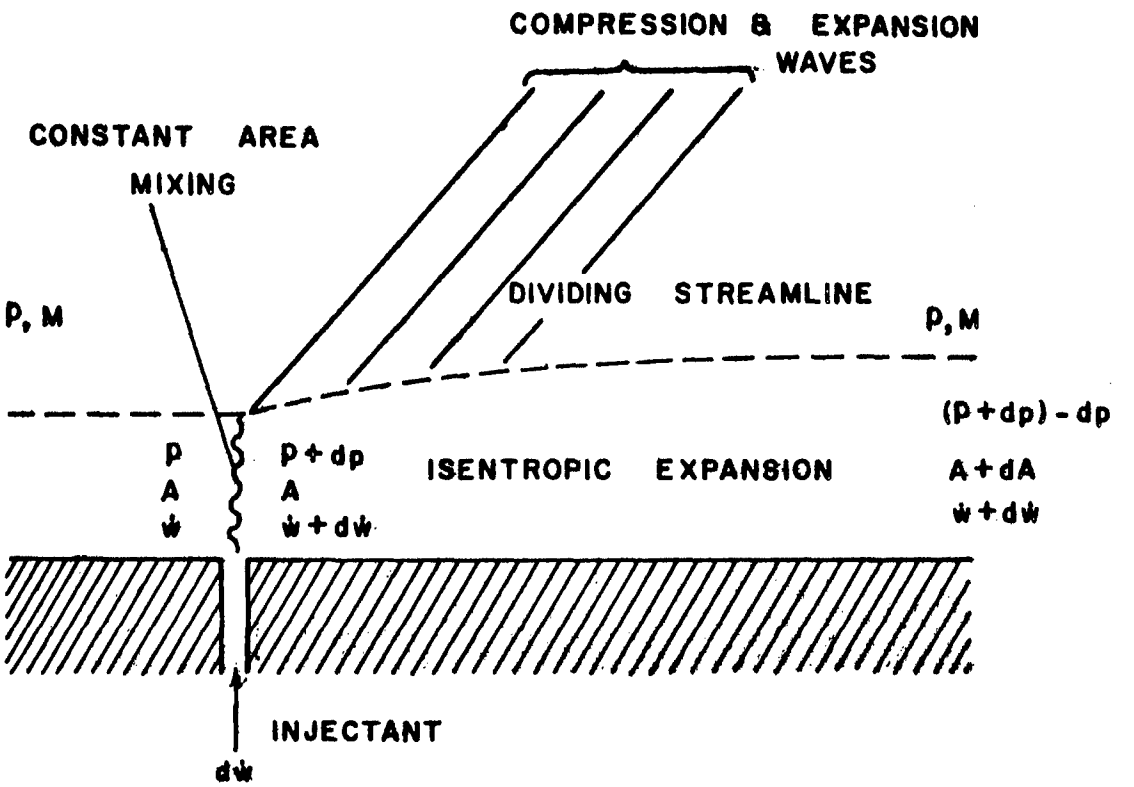

FIG. 1 LINEARIZED SUPERSONIC FLOW THEORY MODEL BY WALKER, STONE AND SHANDOR

1. the maximum observed effective specific impulse is only slightly above the predictions of linear theory, and

2. a group of dimensionless parameters have been deduced from the theoretical analysis as follows:

   a. I_s/I_s^*

   b. $(\dot{W}_j/\dot{W})^*$

   c. R/D

   d. $\ell/h\sqrt{M^2 - 1}$

   where the symbols are defined in Appendix I. The parameters stated above have enabled the authors to reduce a large quantity of data (see reference (2)).

1.1.2 Boundary Layer Separation Model

The model proposed by Wu, Chapkis and Mager (5) is shown in Fig. 2. The primary gas stream flowing at a supersonic speed encounters a secondary stream injected through a port in the wall at station j. As a result the turbulent boundary layer of the primary stream is assumed to separate from the nozzle wall causing the formation of a conical shock, AD. The position of the vertex, A, of the conical shock depends upon the main stream conditions, the flow rate of the injectant and the physical properties of the secondary stream.

The shock angle, the separation angle, and the conditions behind the shock and in the separated flow region are determined from a knowledge of the upstream Mach number by a method due to Mager (10). In that article a semi-empirical relation is developed between the values of pressure on either side of a shock which is induced by the separation of a turbulent

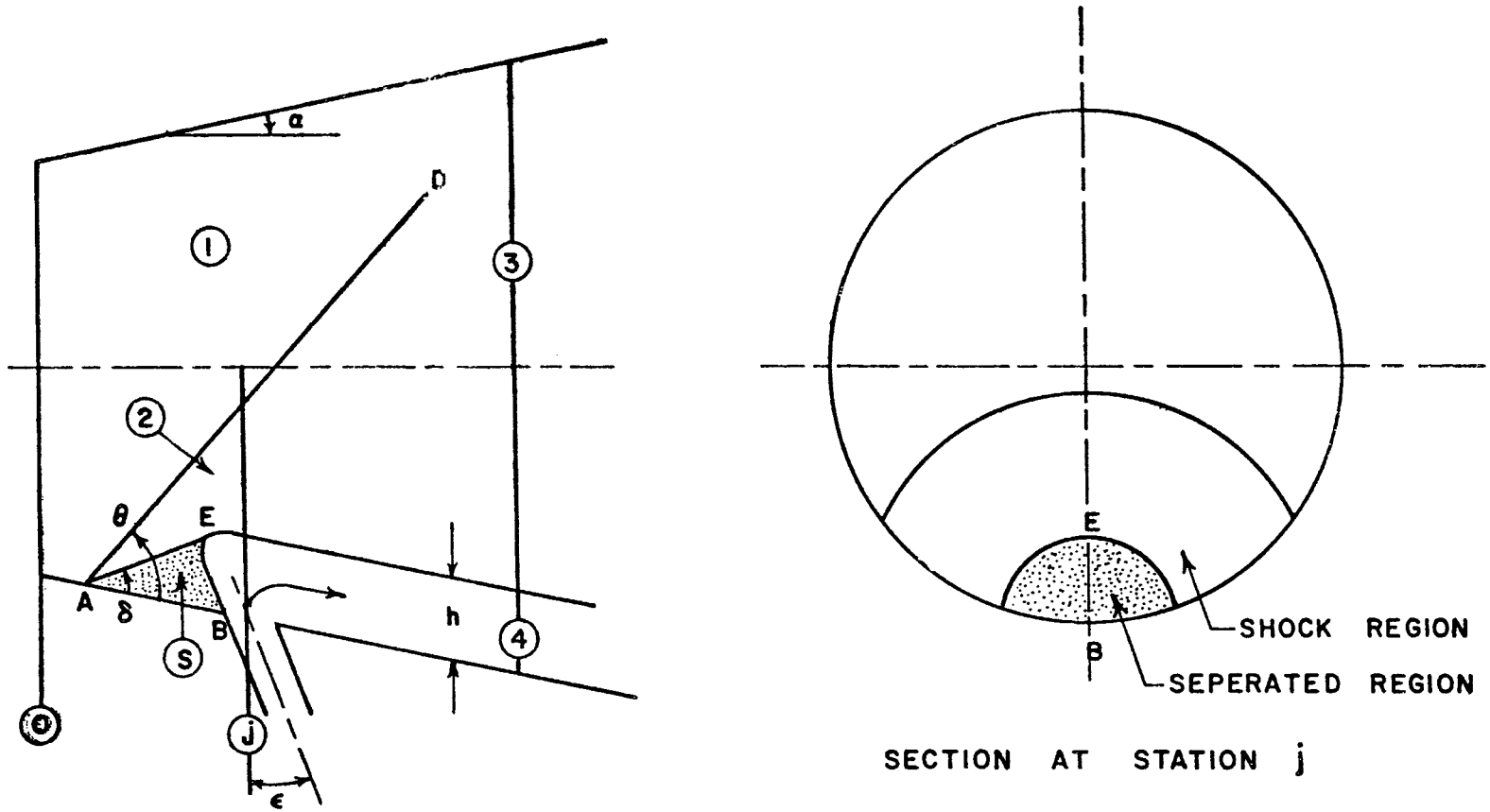

FIG. 2 BOUNDARY LAYER SEPARATION MODEL BY WU, CHAPKIS AND MAGER

boundary layer due to an adverse pressure gradient. The equation developed for the ratio of the upstream pressure to downstream pressure is a function of the free stream Mach number, the specific heat ratio of the gas, and certain experimentally determined constants.

Knowing the pressure ratio across the shock, the specific heat ratio and the free stream Mach number, one can determine the separation angle, the shock angle and the gas properties behind the shock from standard oblique shock relations.

Thus the principal assumptions and approximations introduced in developing this analysis are:

1. use of semi-empirical turbulent incompressible boundary layer equations for the turbulent compressible boundary layer case with the aid of suitable transformations;
2. oblique shock approximations;
3. the semi-empirical relation utilized in developing the equation reported in reference (10) using data for shocks produced ahead of steps and wedges is applicable for shocks produced by injection of a secondary gas; and
4. the pressure ratio required for separation at the outer boundary of a conical separated region is the same as that for the two-dimensional case.

The side force results from the higher pressure behind the shock acting on the projected area of the shock and the separated region. Since the separation angle is known, the vertex, A, of the conical shock can be determined once the accomodation height, EB, is known. To

determine the accomodation height it is assumed that the gas, after injection, makes a sharp turn and flows parallel to the wall without mixing with the main stream. One may then solve the conservation equations for mass, energy and momentum of the primary and the secondary streams to obtain the side force. The boundary conditions are that the static pressures of the primary and secondary streams are equal at the exit plane of the nozzle and the geometrical relationship that the cross-sectional area of the primary nozzle at the injection point is equal to the sum of the cross-sectional areas of the primary and secondary gases at the exit plane (see Fig. 2).

Within the aforementioned limitations in the model, the side force produced by the injection of a gas is shown to be the sum of three components. The first results from the pressure increase in the separated region. The second is due to a similar increase in pressure occurring between the shock and the separated region. The third component is due to the momentum of the injected gas.

The authors neglect any possible contribution to the side force downstream of the injection port. This is justified by the authors in the following manner. Any forces present in that region cancel one another. Thus, for example, it is argued that since experimental results seem to indicate that the secondary gas tends to overexpand, that expansion may cancel any pressure increases due to shock reflection from the walls.

It is evident that the analysis by Wu, et al (5) is based on a rather idealized model in that, apart from the fact that it does not take

into account the mixing processes occuring downstream of the point of injection or the possible side force contributions therein, many aspects of the upstream phenomena have also not been fully taken into account as shown by Murthy (1963)(11). Thus it appears that the following features of the region upstream of the point of injection must be taken into account:

1. the three dimensional nature of the boundary layer,
2. the shape of the surface of the shock,
3. the vorticity that is generated in the separated region,
4. the location of the shock on the nozzle wall, and
5. the pattern of the shock in this region.

1.1.3 Blast Wave Theory

Broadwell (6), (7) utilizes the so-called blast wave theory for an analysis of the problem of thrust vector control by secondary injection. Blast wave theory is based on an analogy between the cylindrical unsteady flow produced by the explosion of a line charge and an axi-symmetric steady flow. That analogy has been applied to the flow about blunt bodies at high supersonic speeds. The flow field is determined in the blast wave theory from the energy added per unit length of gas (charge). In the application of the theory the energy is considered analogous to the drag of the body under consideration. In the present case of secondary gas injection, Broadwell reasons that if the injected fluid enters normal to the primary stream (i.e., with no axial momentum), mixes with it and attains free stream velocity, then an effective force on the primary stream (in analogy to the drag on a blunt body) is the momentum of this

injected gas after it has reached the free stream velocity.

Broadwell has derived a semi-empirical equation (6) for the side force produced by secondary injection utilizing blast wave theory. The results of the theoretical analysis are compared (7) with experimental results reported by Walker, et al (3). Qualitative agreement is obtained between theory and experiment although, generally, the theoretically predicted results for the side force are lower than the experimental values. The author attributes this to the relatively low Mach numbers employed in the experimental study. A serious defect of blast wave theory is that it is strictly valid only for high Mach numbers of the primary stream and becomes increasingly inaccurate quantitatively as the value of Mach number is decreased.

A feature of the theory of some importance is that it does correctly predict the qualitative dependence of the side force on the molecular weight and pressure of the injected gas.

1.1.4 Blunt Axisymmetric Body Theory

Recently an experimental and theoretical program has been completed by Zukoski and Spaid (1964)(8). The experiments were conducted at freestream Mach numbers of 1.38 to 4.54. On the basis of Schlieren and shadowgraph pictures of the interaction region the models in Fig. 3 have been proposed.

In those models the injected material enters through a circular orifice, with a static pressure much higher than that in the undisturbed primary flow. The flow is sonic at the injector and expands rapidly into the primary stream through a Prandtl-Meyer expansion fan. The interaction

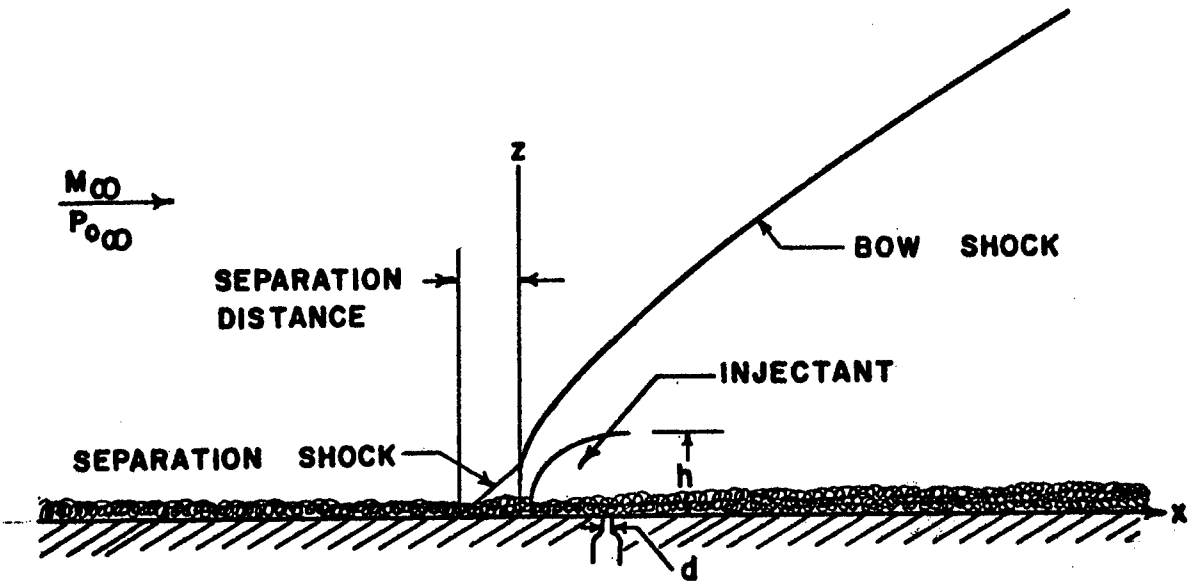

a) TURBULENT BOUNDARY LAYER

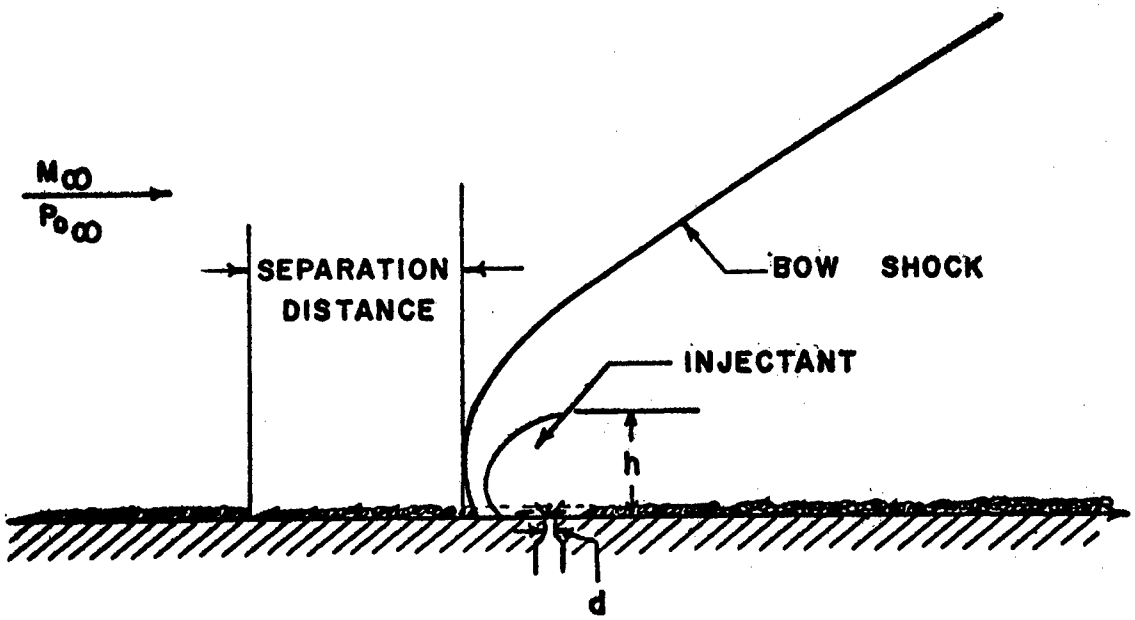

b) LAMINAR BOUNDARY LAYER

FIG. 3. BLUNT AXISYMETRIC BODY MODEL BY ZUKOSKI AND SPAID

of the two streams produces a strong bow shock on the upstream side of the injector, and the shock induced pressure field turns the injectant until it moves approximately parallel to the wall.

The shock-boundary layer interaction produces a region of boundary layer separation upstream of the shock. For the case of a turbulent boundary layer (see Fig. 3a) the separated region is short and the oblique shock produced by separation is usually sufficiently strong to be observed. When the boundary layer is laminar (see Fig. 3b) the separated region is much larger and the angle between the separated flow and the wall is assumed to be never more than a few degrees.

Zukoski and Spaid, after observing the Schlieren and shadowgraph pictures, propose finding a blunt axi-symmetric body with a shape equivalent to the obstruction caused by the secondary injectant and then calculating the characteristic dimensions of that body by balancing the drag of the nose section of the body against the momentum flux of the injectant. Thus it is apparent that this is essentially the same basis that Broadwell has utilized in applying the blast wave theory discussed in the previous section.

Unlike Broadwell, however, Zukoski and Spaid employ a modified Newtonian theory in developing the equations (8). The assumptions made in developing the model and subsequent equations may be summarized as follows:

1. a sonic jet is injected into a uniform supersonic flow with no wall boundary layer,
2. no mixing occurs between the injectant and either the primary

flow or the separated flow near the injector,

3. the interface between the injectant and primary flow is a quarter sphere followed by an axisymmetric half body,
4. the interface between the separated flow downstream of the injector and the injectant always lies inside the surface described in item 3,
5. the pressure forces on the sphere due to the primary flow can be calculated by the use of a modified Newtonian flow,
6. the injectant expands isentropically to the ambient pressure with its velocity parallel to the wall at the downstream face of the sphere, and
7. the contribution to the momentum flux perpendicular to the free stream velocity due to flow in the separated region downstream of the injector can be neglected.

It has been proposed by the authors that the radius, h, (see Fig. 3) can be used as a scale of the disturbance produced by injection. An equation for the determination of the radius has also been developed.

The data from a large number of experiments have been satisfactorily reduced by normalizing the dimensions of the system with the aid of the radius, h. Quantitatively, the results of the shock shape, concentration and pressure measurements indicate that the scaling parameter, h, is satisfactory for the particular range of variables which has been investigated.

The authors have also performed measurements of the concentration of the injected fluid in the region downstream of the injector. Those data indicate the following:

1. the secondary gas has mixed appreciably with the primary flow within a short distance from the injection port, and
2. the secondary gas is turned toward the wall by the primary gas and is forced to move downstream practically along the wall as mixing occurs.

The data which Zukoski and Spaid have used for developing their theoretical model involve flow rate ratios of the secondary to primary streams which are considerably less than the minimum practical values for thrust vector control by secondary injection. The equations which have been derived are of course not governed by this restriction; however, it appears clear that the correctness of the theoretical models proposed (see Fig. 3) is questionable for larger flow rates as borne out by experiments conducted by Charwat and Allegre (9) (also see Section 1.1.5). The results of the experiments conducted as part of the experimental program, reported in Chapter 3, also will bear out the same conclusion. There is also reason to believe that the separated region exerts a greater influence on the side force produced by secondary injection than what Zukoski and Spaid have indicated.

1.1.5 Injection Model

An experimental study of the phenomena associated with secondary injection has been conducted by Charwat and Allegre (1964)(9) to clarify the details of the flow. Results of wall and impact pressure measurements throughout the core of the interaction field, as well as flow visualization tests, are reported for eleven tests in which the injected mass flow rate, injection station Mach number, and the primary to secondary

stagnation pressure ratio have been varied systematically. Those measurements are used in an effort to reconstruct theoretically the true structure of the flow field.

The authors have proposed the models shown in Fig. 4, for the region near the injection port. In Fig. 4a the static pressure of the secondary injectant at the throat is greater than that of the separated region and, therefore, the gas expands upstream to equalize pressures. Because the gas is also expanding around the downstream edge of the port, the secondary gas flows at supersonic speeds and the boundary between the primary and secondary fluids is taken to be a slip line. In Fig. 4b the static pressure of the jet at the injector throat is less than the pressure in the separated region and therefore, a shock is assumed to originate from the upstream edge of the injection port and extends over the port as a "cap". Such speculations have been based upon impact pressure measurements in the region immediately above the injection port.

Several other conclusions have been derived by Charwat and Allegre based on their experimental study. They are as follows:

1. the strength and location of the leading shock is a function of the momentum of the injected mass flow and the Mach number of the primary stream at the injection station;
2. the wall pressure distribution is a function of the parameters included under 1, and, also, of the ratio of the secondary to the primary stagnation pressures;
3. the momentum of the injected fluid is the principal, physical similarity parameter in the over-all problem;

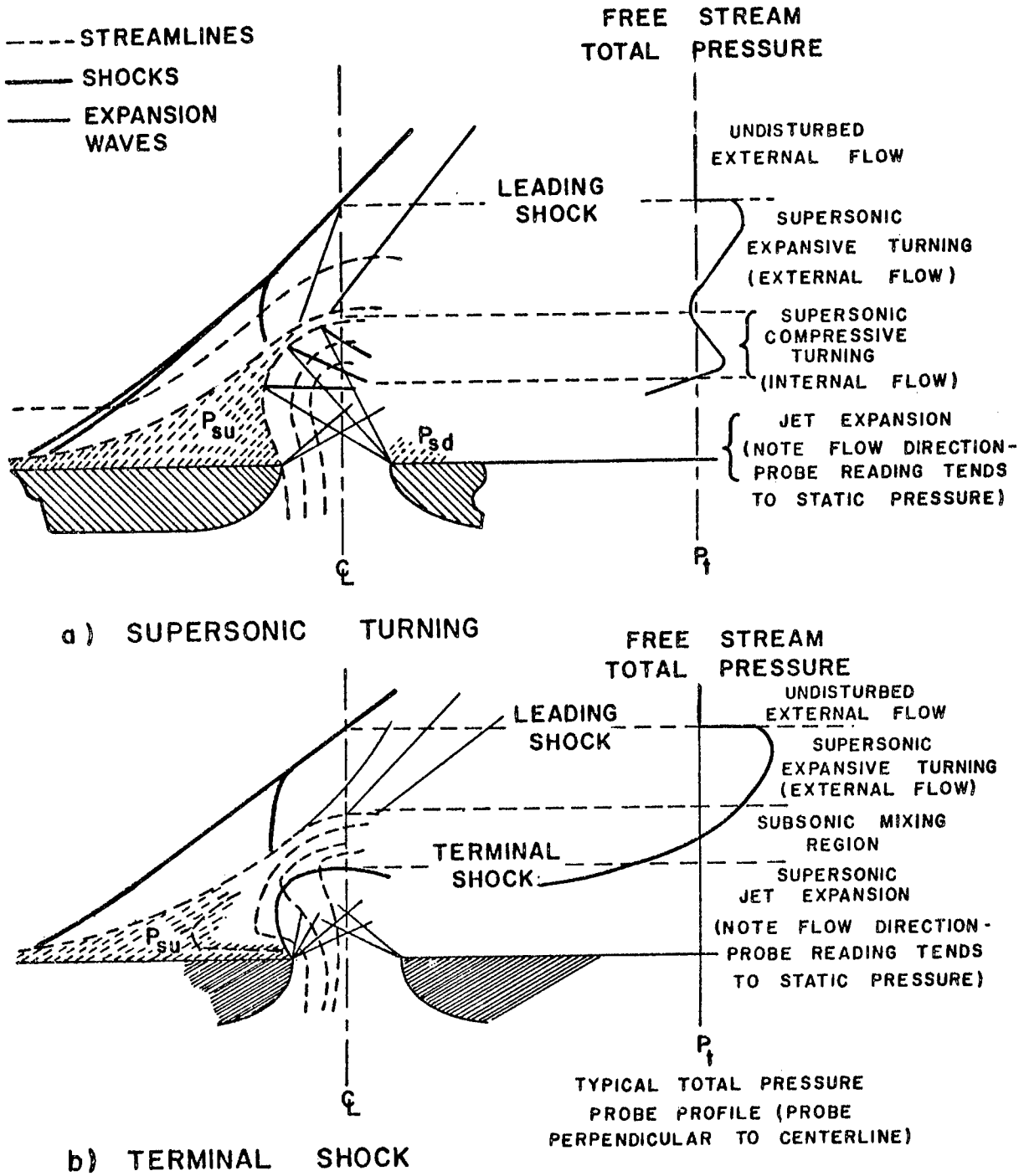

FIG. 4 INJECTION MODEL BY CHARWAT AND ALLEGRE

4. the flow speed of the secondary fluid has little influence on the formation of the main shock (i.e., for a given secondary stagnation pressure, injection at sonic or supersonic speeds has approximately the same effect), and
5. the height of penetration of the secondary jet is not a simple function of the jet momentum. For example, it increases with the Mach number of the primary stream at the injection station, all other factors remaining constant.

1.1.6 Discussion of the Various Studies

Each of the aforementioned studies has contributed to a better understanding of the complicated flow phenomena associated with the injection of a gas into a supersonic stream. In particular the article by Charwat and Allegre (9) has clarified many aspects of the flow field heretofore unknown.

The most noticable feature of the theories discussed is that none of the authors appear to indicate clearly under what conditions and over what range of variables a particular model may be more successful.

Several of the conclusions reached by different authors also appear contradictory. Such differences pertain both to the estimated values of side force under given conditions as well as to the understanding of the details of the phenomena involved in secondary gas injection.

Thus a comparison of the different theories should take into account the following features.

1. Flow Parameters

    a. Upstream effects,

    b. the region around the point of injection, and

    c. downstream effects.

2. Physical Parameters

    a. Density ratio,

    b. molecular weight ratio, and

    c. ratio of specific heats for the primary and secondary gases.

Considering the upstream effects, the different theories depend upon several assumptions pertaining to each of the following:

1. the cause of separation of the boundary layer,

2. the shock formation, and

3. the spread of the injected stream of gas.

Similarly, for the region around the point of injection, the assumptions made pertain to:

1. the expansion characteristics of the jet,

2. the accomodation height,

3. additional shock formations, and

4. turning of the secondary stream.

Lastly, in regard to the downstream effects, it may be stated that there appears to be little understanding related to any of the following:

1. mixing of the primary and secondary gases,

2. additional shock formation, and

3. interaction of boundary layer flow, injected gas and the primary stream.

Considering next the physical properties, except in the theories postulated in (5) and (6), there is no specific relationship available between the magnitude of the side force produced and the ratio of molecular weight of the primary and secondary streams or the ratio of the specific heats.

1.2 Details of the Method of Attack

In the light of the theoretical models that have been developed and the type of experimental results which have been obtained to date, it is considered that further systematic experimental studies are required before a comprehensive theory may be postulated. The experimental studies, it is felt, should be conducted in a wind tunnel-like apparatus with a two-dimensional slot on one wall of the tunnel for injection of the secondary gas.

In order that a systematic experimental program could be conducted, a parametric analysis presented originally by Thompson, Hoffman and Murthy (1963)(12) utilizing a model similar to the one proposed by Wu, et al (5) (see Fig. 2), has been adapted for use in the present research program.

A useful measure of the effectiveness of secondary injection, for thrust vector control purposes, is the amplification factor, AK, which is defined as the ratio of the effective specific impulse of the secondary stream to the specific impulse of the primary stream.

From the parametric analysis it has been established that the amplification factor is directly proportional to the ratio of the

stagnation acoustic speeds of the secondary and primary gases and a function of five parameters as follows:

1. the point of injection,
2. the angle of injection,
3. the secondary gas flow rate,
4. the secondary gas properties (P, T, γ, η), and
5. the injection port geometry.

The amplification factor is then shown to be given by the relation,

$$AK = \frac{a_{o_s}}{a_{o_p}} \cdot f\left(\epsilon, M_p, M_s, P_{o_s}, \gamma_s\right) \tag{1.1}$$

$$= \sqrt{\frac{\gamma_s T_{o_s} \eta_p}{\gamma_p T_{o_p} \eta_s}} \; f\left(\epsilon, M_p, M_s, P_{o_s}, \gamma_s\right) \tag{1.2}$$

On the basis of the findings of the parametric analysis it is clear that an experimental program should include the determination of the influence of all of the primary parameters influencing the overall side force produced. The parameters to be investigated and their ranges in the experimental program are outlined in Table 1.

From the experimental results obtained by the variation of the parameters over the ranges indicated in Table 1, it is proposed that two objectives may be fulfilled as follows:

1. the determination of the influence of some of the parameters upon the value of side force that may be generated, and

2. the determination of the conditions under which the several theories that have been proposed may be applied with or without modification.

Table 1

Experimental Program for Secondary Injection

Parameter	Range
(1) primary Mach number, M_p	inject at axial positions where a) $M_p \approx 1.90$ b) $M_p \approx 1.70$
(2) angle of injection, ϵ	from normal to the nozzle axis to 10° upstream
(3) secondary stagnation pressure, P_{o_s}	vary from 20 psig to 120 psig in increments of 20 psi
(4) area of slot, A_s	vary from 1/2% to 10% of throat area of primary nozzle in 5 increments
(5) molecular weight, η, and specific heat ratio, γ, of secondary gas	use both a heavier and lighter gas (CO_2 and He)

1.3 Outline of the Thesis

The report is concerned with the experimental and analytical studies conducted in relation to the problem of the injection of a secondary gas at an angle into a supersonic primary stream. While the subject has several practical applications, the particular aspect of the problem studied is that

which arises in the thrust vector control of rocket motors by secondary gas injection.

The experimental apparatus and procedure for testing are included in Chapter 2. Essentially the apparatus consists of a wind tunnel into which a secondary gas is injected through a port in one of the walls. Both diagnostic investigations involving optical observations of flow patterns as well as measurements of physical and flow properties have been undertaken. The side force produced during an experiment is calculated by integrating the static pressure along the wall of the nozzle. The experimental results are presented in Chapter 3.

The results of calculations employing two of the theoretical models proposed on this subject are presented in Chapter 4. The ranges of variables employed therein are identical to those in the experimental study. Therefore, one can compare the results of the analysis with the experimental results. Such a comparison of results has been included in Chapter 4.

In combination with the measured and calculated results, one can employ the optical observations of the flow field to determine qualitatively the ranges of parameters over which the different theories may prove successful.

The conclusions derived from such studies and some recommendations for further work are presented in Chapter 5.

2. EXPERIMENTAL APPARATUS AND PROCEDURE

The object of the experimental program was to investigate the changes in the flow field produced when a gas is injected into a supersonic stream. The apparatus that has been employed to accomplish this is a two-dimensional supersonic nozzle appropriately modified to permit the injection of a secondary gas and the inclusion of the necessary instrumentation. The details of the experimental apparatus, the instrumentation and the experimental procedure are described in this chapter.

2.1 The Wind Tunnel

The experiments have been conducted in the 2 inch x 6 inch blow-down supersonic wind tunnel, which is designed to produce a uniform parallel flow with a Mach number of 2.0 at the exit section. The details of the design of the tunnel are given in Appendix II. The tunnel is operated with air, which therefore constitutes the primary flow of the system. Air is supplied from a bank of high-pressure tanks shown in Fig. 5 with the flow rate controlled by a hydraulic pressure regulator. The temperature of the air supplied to the tunnel is not controllable. Figure 6 is a schematic diagram of the apparatus. The supply system for the secondary fluid is included in the diagram but will be discussed later.

The nozzle blocks for the wind tunnel have been fabricated from 303 stainless steel. The contour was rough-cut .005 inch oversize with a planer and hand polished to the specified dimensions. Tolerances on the contour

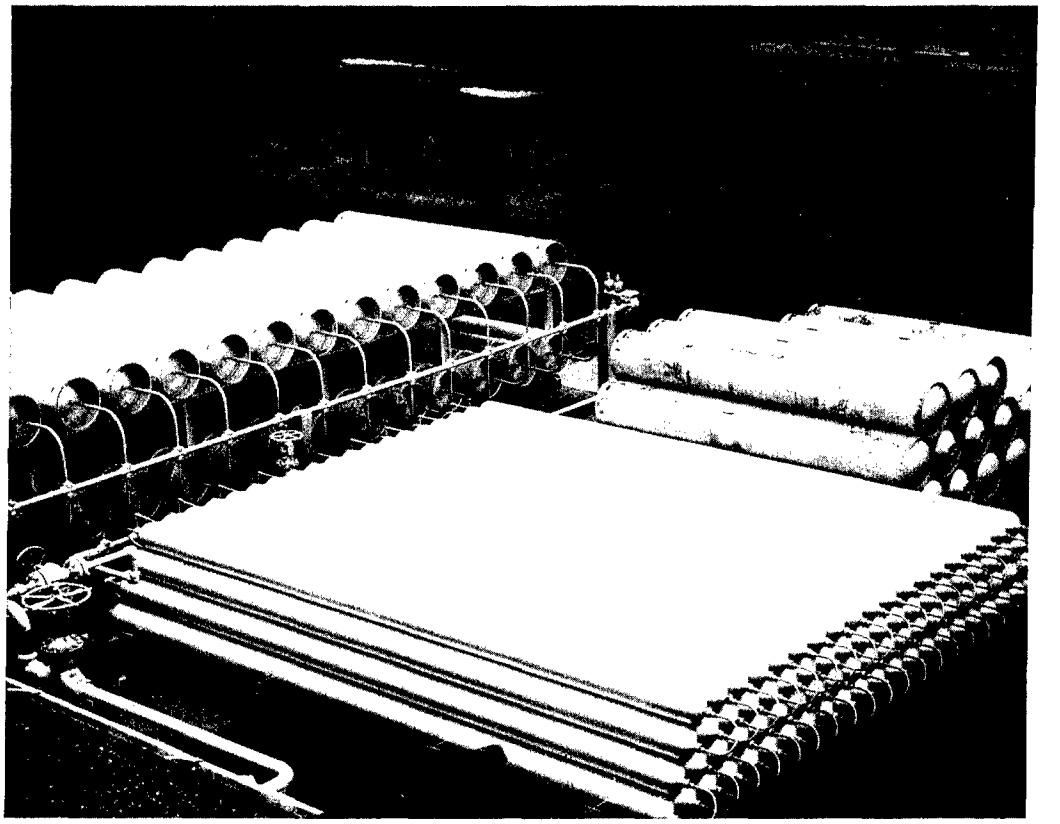

FIG. 5 HIGH PRESSURE AIR SUPPLY TANKS

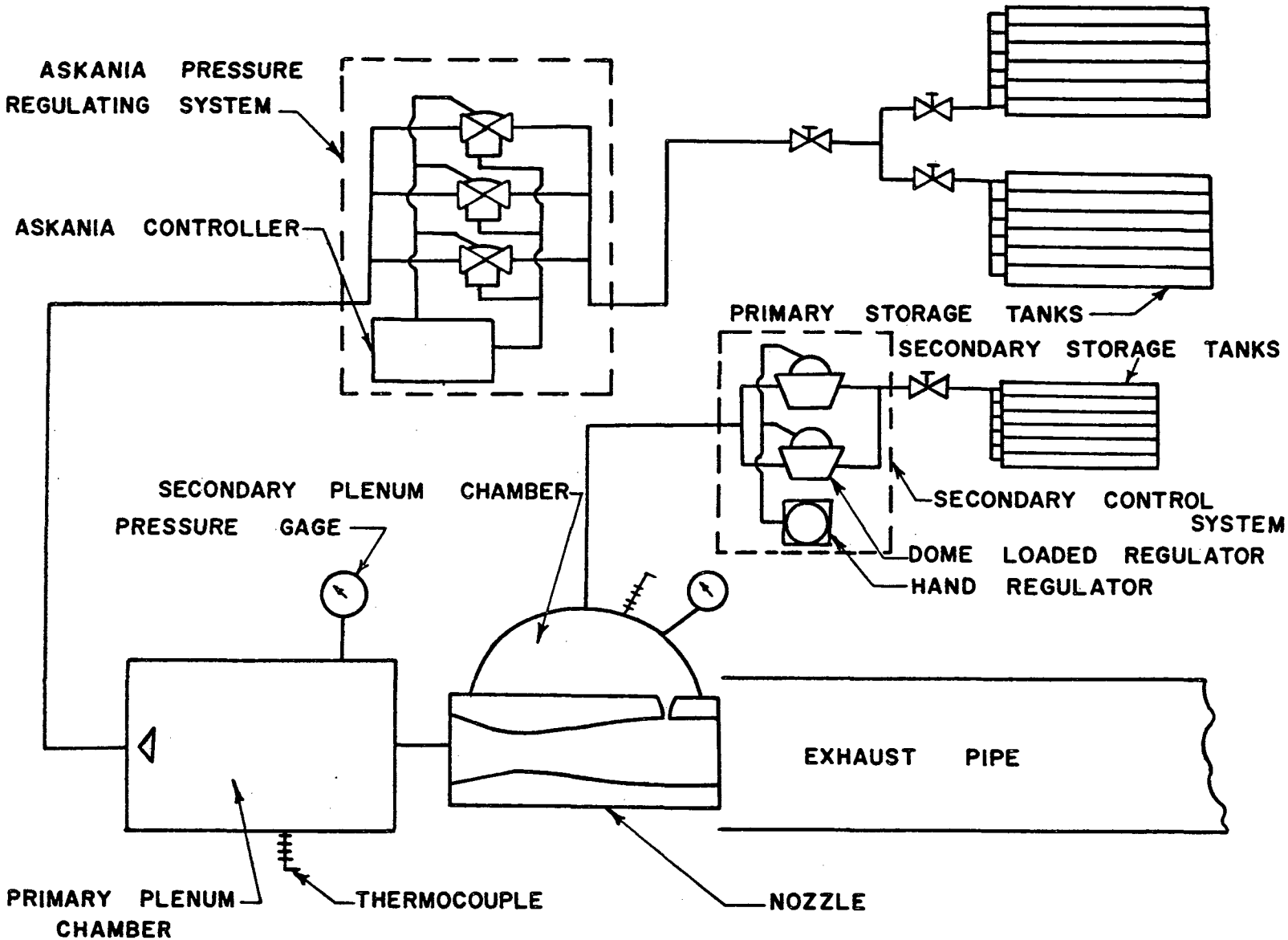

FIG. 6 SHEMATIC DIAGRAM OF THE FLOW SYSTEM

have been held to ± .003 inch throughout the 19.722 inch length of the nozzle. The sides are parallel to within .001 inch through the entire length.

The nozzle blocks are fitted with 0.5 inch thick plexiglass sidewalls to enable visual observation of the flow field. Steel retainer plates have been used to support the sidewalls and locate the nozzle blocks. By means of dowels inserted through the nozzle blocks and the retainer plates, the throat and exit heights of the nozzle have been held to within ± .003 inches of the design calculations. Figure 7 is a photograph of the assembled nozzle with the sidewall and retainer removed from one side.

2.2 The Secondary Gas Injection System

To retain the two-dimensional character of the flow system, as far as practicable, both with respect to the primary flow and the secondary flow, it was decided to inject gas through a slot extending over the width of the nozzle and oriented at right angles to the side walls. This necessitated cutting one of the nozzle blocks at some desired position along the nozzle length and modifying the block in this region to produce a desired width of passage for the secondary gas to flow into the primary system when the nozzle blocks were assembled. The secondary gas is admitted into the nozzle slot through a converging passage supplied from a plenum chamber which is located immediately upstream of the converging passage. The plenum chamber enables accurate measurements to be made of the total pressure and total temperature of the secondary gas immediately upstream of the point of injection. The secondary plenum chamber is fed by a set of high pressure tanks and the flow is controlled

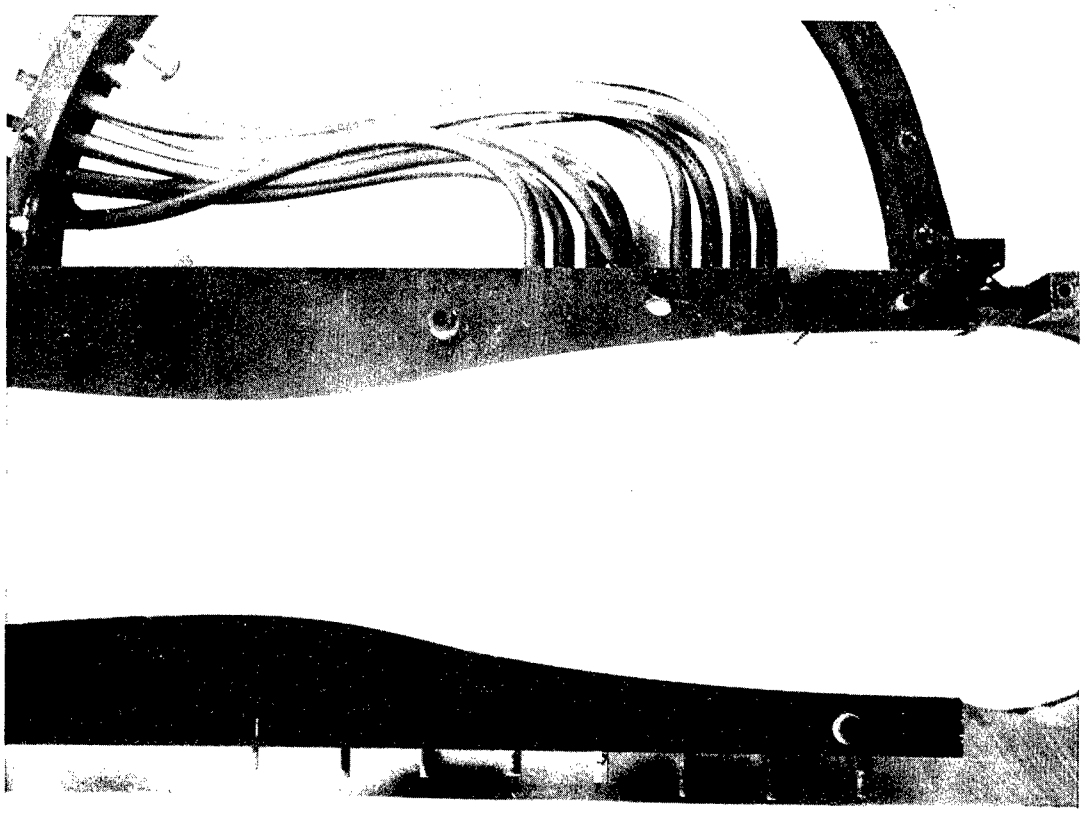

FIG. 7 THE ASSEMBLED NOZZLE WITH SIDEWALL REMOVED

by two dome loaded regulators as shown schematically in Fig. 6.

Figure 8 is a photograph of the nozzle blocks with the secondary plenum chamber attached. It may be observed that the portion of the nozzle downstream of the slot is fitted with an adjusting screw to enable the slot area to be varied through a prescribed range. The secondary plenum chamber has been designed such that it is suitable for any axial position of injection without modification.

2.3 Instrumentation

The instrumentation employed in the experimental investigation has been designed for the following:

(a) to visually observe the flow field,

(b) to obtain static pressure measurements on the nozzle walls, and

(c) to determine the flow properties of the primary and the secondary gases, such as total temperature and pressure.

2.3.1 Optical Apparatus

A shadowgraph system is employed for examining the flow field. The arrangement of the apparatus is shown in Fig. 9. The light source for the system is a Sylvania concentrated-arc, 300 watt lamp. From this source the light beams diverge to the parabolic mirror where they are reflected as parallel beams of light. After passing through the test section the light beams are incident on a section of ground glass. A 35 mm camera is employed to photograph the image on the ground glass. The visual observations are made primarily in the flow region surrounding the point of injection.

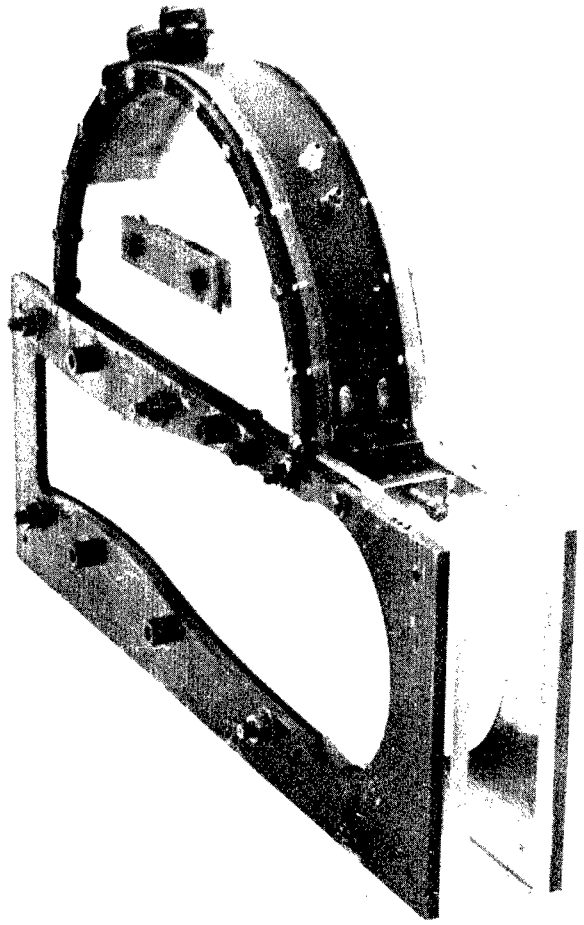

FIG. 8 THE NOZZLE BLOCKS WITH THE SECONDARY PLENUM CHAMBER ATTACHED

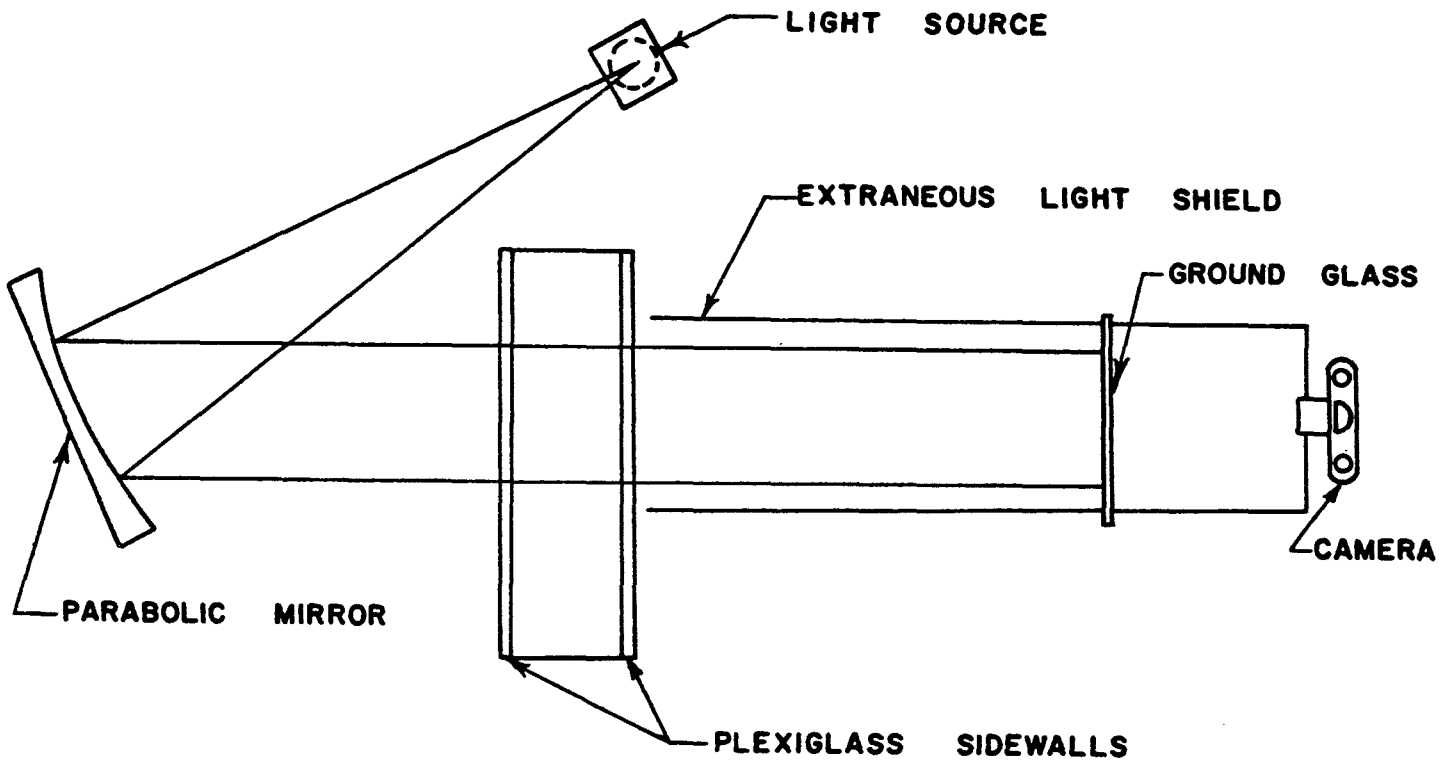

FIG. 9 SCHEMATIC DIAGRAM OF ARRANGEMENT OF THE SHADOWGRAPH APPARATUS

2.3.2 Pressure and Temperature Measurements

Total pressure measurements are recorded in both the primary and secondary plenum chambers by means of Bourdon gages. It is assumed that the flow velocity in these chambers is low enough so that stagnation conditions exit. The temperature in each chamber is measured by a copper-constantan thermocouple. The cold junction of the thermocouple is maintained at $32^{\circ}F$ in an ice bath and the voltages fed to a Brown recorder.

A total of 22 static pressure taps have been placed in the nozzle walls, their location measured with respect to the entrance of the nozzle and the angles which the contour made with the nozzle axis at the respective locations being presented in Table 2.

The procedure for fabricating these pressure taps is as follows. A .020 inch diameter hole is drilled at each location, a depth of approximately .125 inch into the nozzle block perpendicular to the wall. A .25 inch hole is then back-drilled to connect with the .020 inch diameter hole. The pressure taps are then fed to a bank of manometers through flexible Tygon tubing.

During the experiments the manometer banks are photographed and the pressures read from the photographs at a later date.

A photograph of the entire system in location is shown in Fig. 10.

Table 2

Location and Orientation of Pressure Taps

in the Nozzle Walls

Pressure tap No.	Distance from nozzle entrance (inches) Side without slot	Side with slot	Angle with respect to nozzle axis (degrees)
1	7.540		0.
2	9.250		7.38
3	10.750		12.71
4	12.210		9.50
5	13.725		6.92
6	15.230		4.79
7	16.723		3.00
8	18.226		1.40
9		12.490	8.97
10		12.990	8.09
11		13.468	7.31
12		14.003	6.48
13		14.488	5.79
14		15.028	5.06
15		15.503	4.43
16		16.003	3.83
17		16.488	3.26
18		17.413 + SW*	2.22
19		17.858 + SW*	1.73
20		18.343 + SW*	1.19
21		18.837 + SW*	.76
22		19.353 + SW*	.30

* SW = slot width

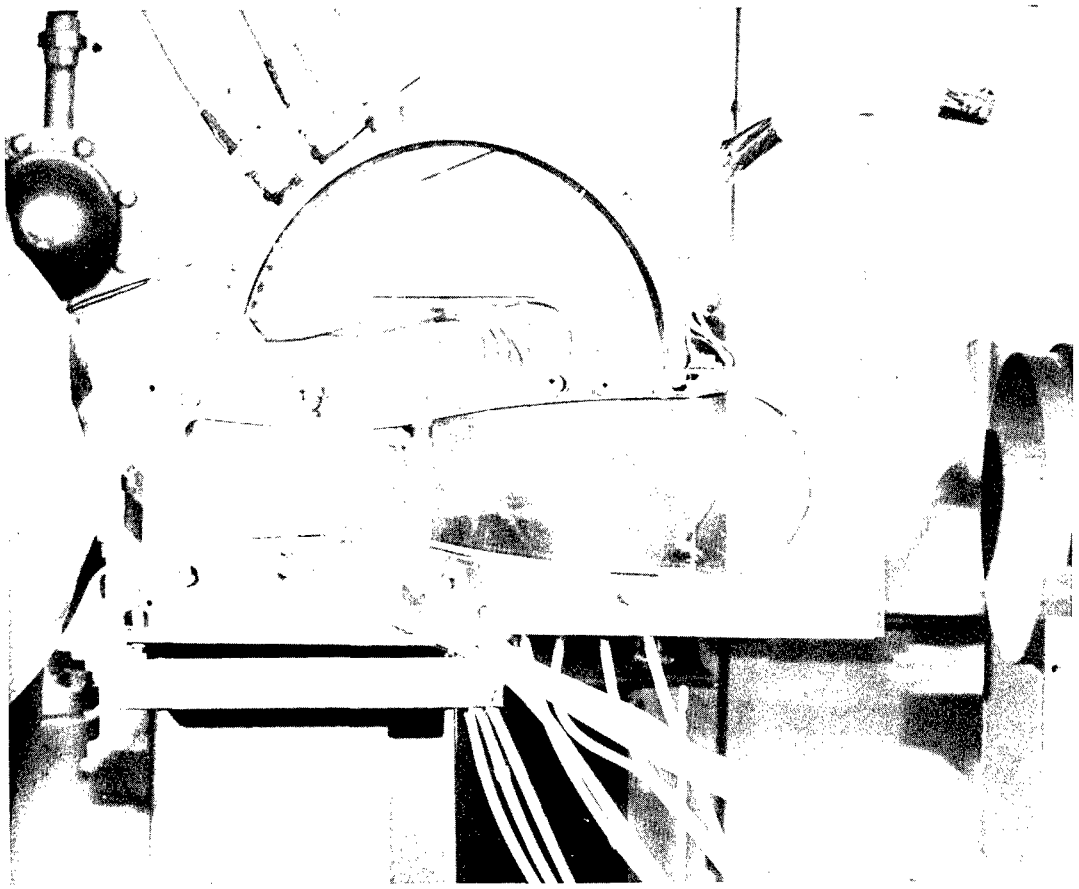

FIG. 10 THE ENTIRE SYSTEM IN LOCATION

2.4 Experimental Procedure

Prior to performing experiments involving actual gaseous injection into a particular injection configuration, it was necessary to ensure that the actual flow field in the wind tunnel nozzle corresponded to the design conditions within a desired accuracy. Tests were therefore performed to determine the flow conditions in the wind tunnel nozzle while operating with the primary air stream alone. This aspect of the program is discussed in Appendix III. It may be stated here that every attempt was made to obtain uniform parallel flow at the exit plane of the nozzle while it was assumed that the entire flow in the nozzle corresponded to design conditions to the same accuracy as the exit flow. In all such experiments, visual observations were also made at least in the region of the secondary gas injection port to ensure shock free flow under the conditions of no injection.

After completing the uniform parallel flow studies, the procedure for preparing the apparatus for an experiment was as follows:

1. place the modified nozzle block in the nozzle assembly and set the slot width at a value of .017 inch (1/2% of the primary nozzle throat height) by means of the adjusting screw,
2. assemble the apparatus by connecting
   a. the nozzle to the primary plenum chamber,
   b. the secondary supply lines,
   c. the secondary plenum chamber thermocouples, and
   d. the presure lines,
3. check out the control valves on the primary and secondary gas

supplies, and

4. calibrate the Brown recorder and associated equipment.

Upon completion of these preliminary steps the experiment itself could be conducted. The procedure that was followed during the course of an experimental run is detailed in the following.

1. Obtain steady state flow in the primary plenum chamber at correct operating pressure ($p_e = p_a$) with no secondary injection;
2. introduce the secondary gas into the primary stream and obtain steady state conditions at a secondary plenum chamber pressure of 20 psig;
3. record primary and secondary stagnation temperatures on the Brown recorder, photograph the manometer banks and photograph the projected image on the ground glass of the shadowgraph apparatus;
4. increase the secondary stagnation pressure through 120 psig in increments of 20 psi making sure that, at each value of pressure, steady state conditions existed before repeating step 3; and
5. upon completing step 4 for the complete range of secondary stagnation pressures, the system was shut down and the slot width increased to .035 (1% of the primary nozzle throat height). Steps 1 through 4 were repeated again for this new value of slot width. The slot width was set at 1/2, 1, 2, 5 and 10% of the primary nozzle throat height during the course of the experiments.

Because of the limited air supply it was possible to complete the steps outlined above for only one slot width during an individual experimental run. Ambient conditions were, therefore, recorded for each run.

Experiments were repeated for injection at an angle of 10° measured upstream with respect to a normal to the nozzle axis. This necessitated modifying the injection side nozzle block and repeating the aforementioned procedure. At the 10° upstream inclined injection position, a limited number of experiments were also conducted using helium as the secondary injectant.

Before examining the experimental results (see Chapter 3) a short discussion of the accuracy of the measured quantities is in order.

As was mentioned previously the primary and secondary gas temperatures were not controllable and varied throughout an experimental run. To circumvent this it was necessary to record the temperatures at the same instant as when the manometer bank was photographed. It was then assumed that sufficient correspondence could be established among the various readings.

During all of the experimental runs the system performed quite satisfactorily; that is, no fluctuations in the primary or the secondary stagnation pressures were observable during any of the experiments.

As was mentioned previously no recordings were made until the system had reached steady state operating conditions. Such a condition could be ensured by allowing the total and static pressure fluctuations to die out. During most of the experimental runs the static pressure values stabilized within 5 seconds after the total pressure values

reached a steady state.

Table 3 contains the maximum errors in recorded measurements.

Table 3

Maximum Errors of Measurements

Measurement	Maximum Error
static wall pressure	± 0.2 in Hg
stagnation pressure	± 1.0 psi
stagnation temperature	± 1.0 ^{o}F

3. EXPERIMENTAL RESULTS

The experimental program has been undertaken in two phases, namely

1. diagnostic investigations relating to optical observations of the flow pattern in the vicinity of the point of injection; and
2. detailed measurements of the relevant physical and flow parameters of the primary and secondary flows.

The primary objective of the diagnostic investigations was to obtain qualitative data regarding the flow pattern in the immediate vicinity of the point of injection. It is obvious that any physical instrumentation employed in that region should interfere with the flow pattern itself as little as possible. It was therefore decided that only optical observations, employing the shadowgraph apparatus, and static pressure measurements at the nozzle wall would be employed to obtain information in this region.

The diagnostic observations served a purpose other than providing qualitative data regarding the flow pattern. Visual observations were useful in determining the regions where standard instrumentation should be employed. The results of these diagnostic observations are presented in Section 3.1.

The method of obtaining detailed measurements of the relevant physical and flow parameters has been outlined in Section 2.4. These measurements are used in determining the side force produced under given

flow conditions, the details of which are presented in Section 3.2. Sections 3.3 and 3.4 contain the results of these calculations.

3.1 Diagnostic Observations

Shadowgraphs of the flow field produced when a gas is injected into a supersonic stream are presented in Figs. 11,12,13 and 14. Values of the significant parameters are presented below the photographs. The upstream edge of the injection slot can be determined by tracing the line on the photograph representing the line etched in the plexiglass sidewall, to the nozzle wall.

In those photographs the flow is from left to right. The injected gas apparently causes a boundary layer separation upstream of the injection port with a resulting shock structure consisting of an oblique shock originating at the upstream edge of the separated region (hereafter referred to as the leading shock) and a weaker oblique shock originating at a point near the region of maximum penetration of the secondary gas and intersecting the first shock at some point in the free stream.

Another shock (hereafter referred to as the trailing shock) is located downstream of the inflection point. This shock is apparently caused by one of two factors or a combination of both:

1. turning of the supersonic secondary gas stream by the wall, and/or
2. boundary layer separation caused by an adverse pressure gradient. This adverse pressure gradient is due to a low pressure region (pressures as low as 10 psi vacuum have been recorded) immediately downstream of the injection port caused by the Prandtl-Meyer

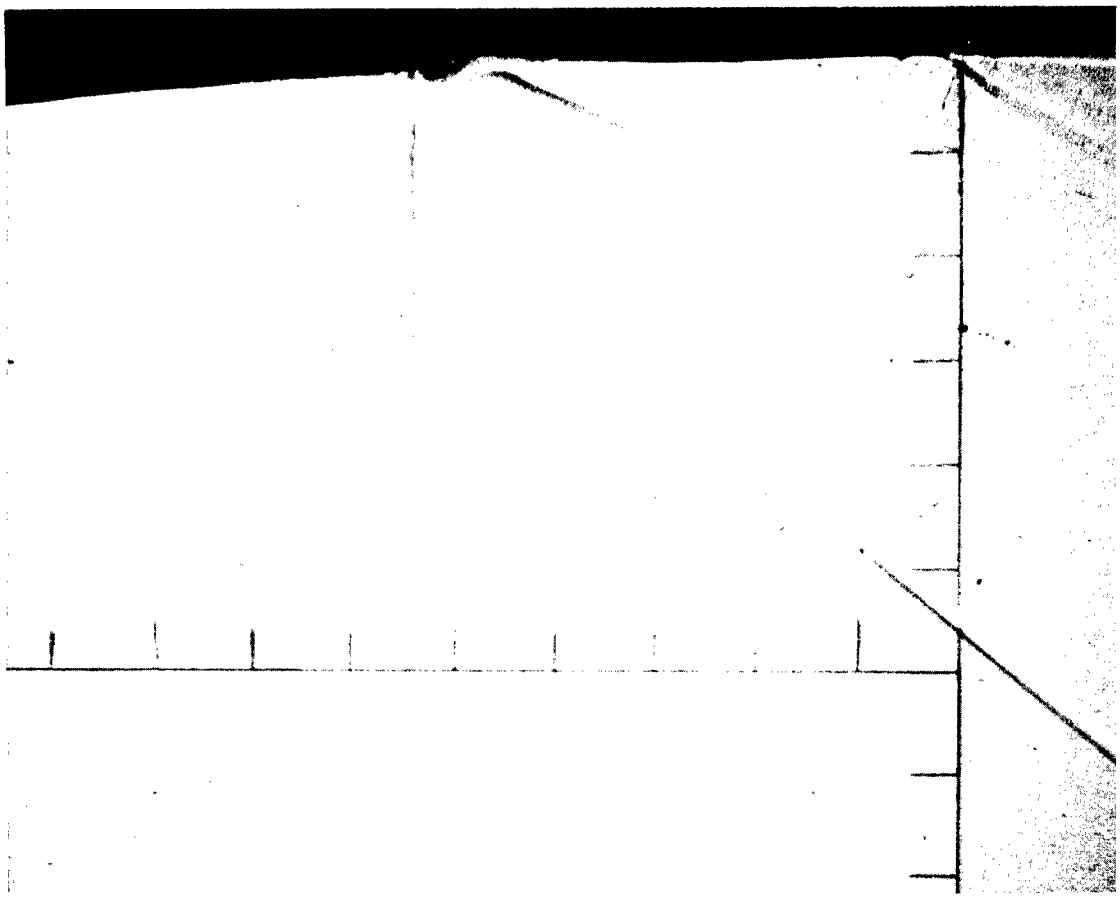

$P_{o_s} = P_{o_p} = 100$ PSIG

$T_{o_s} = 515°R$

$T_{o_p} = 451°R$

$A_s = .0416\ IN^2$

NORMAL INJECTION

FIG. 11 SHADOWGRAPH OF SHOCK SYSTEM

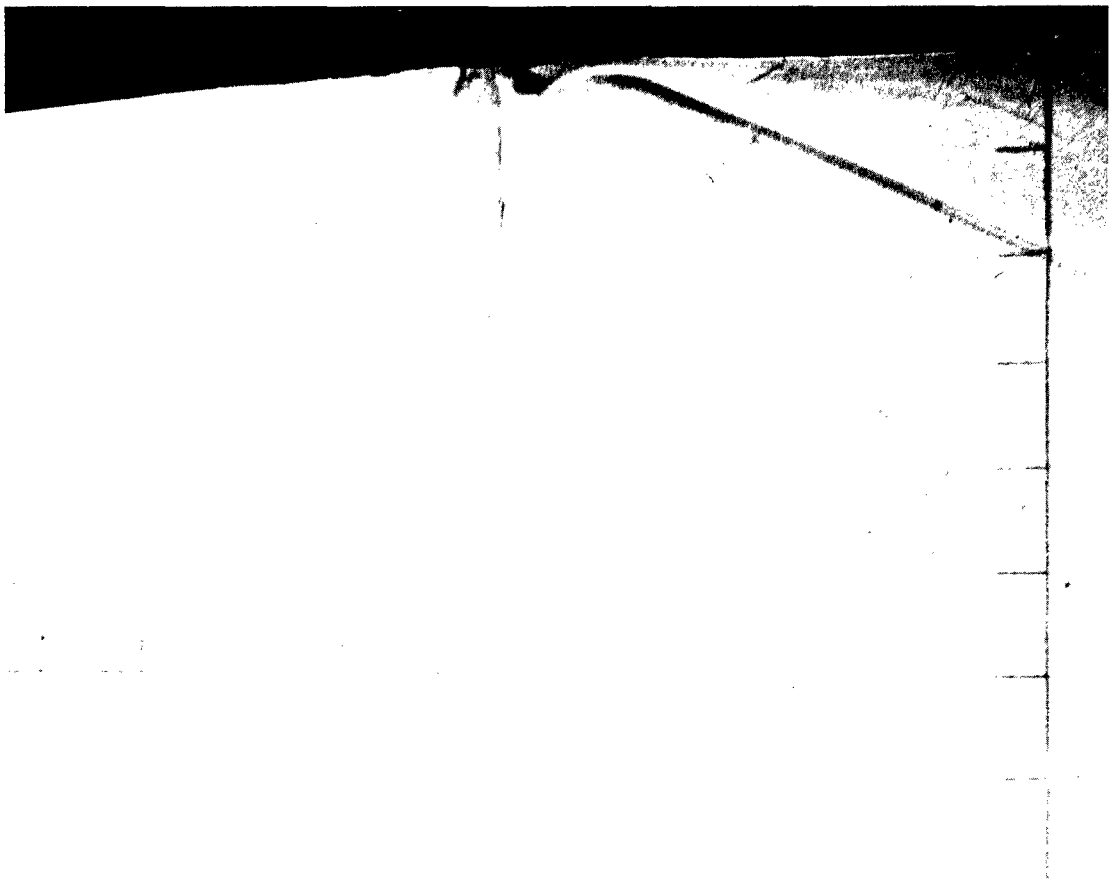

$P_{o_s} = P_{o_p} = 100$ PSIG

$T_{o_s} = 512°R$

$T_{o_p} = 453°R$

$A_s = .0812$ IN^2

NORMAL INJECTION

FIG. 12 SHADOWGRAPH OF SHOCK SYSTEM

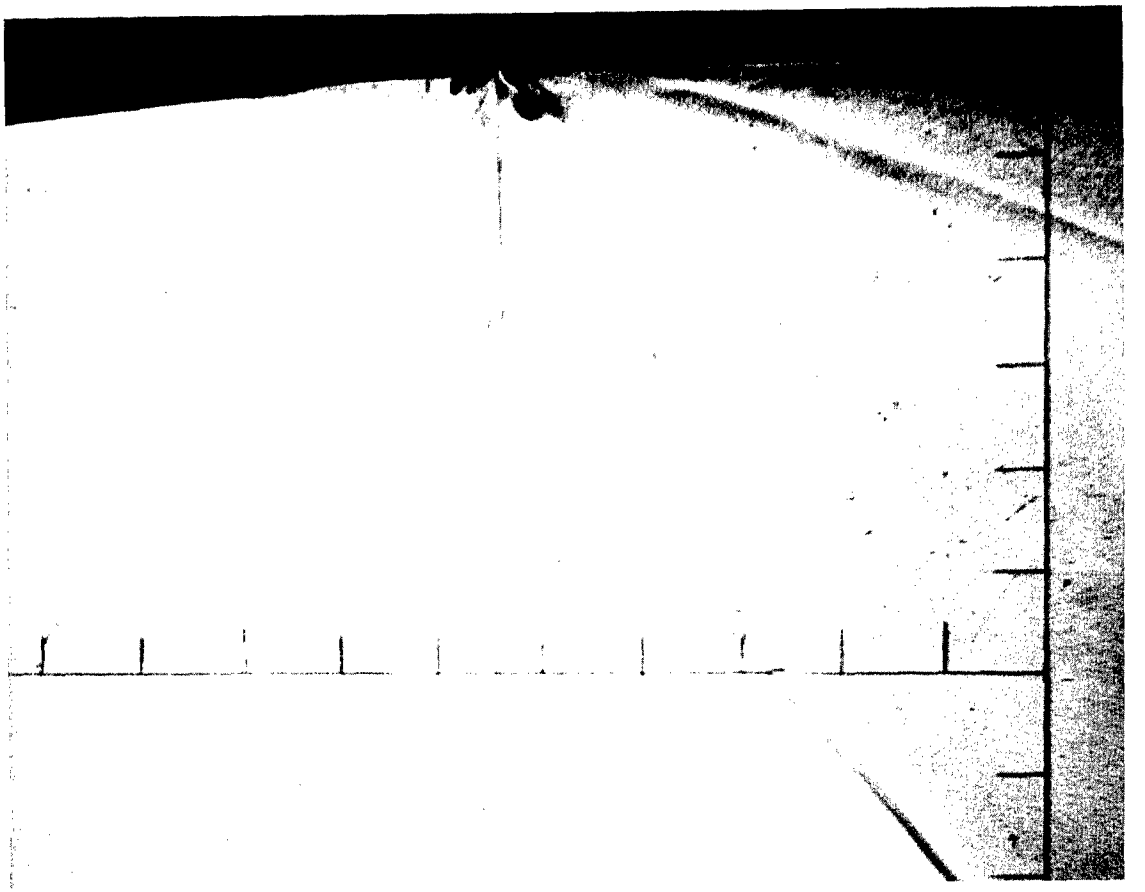

$P_{o_s} = P_{o_p} = 100$ PSIG

$T_{o_s} = 501°R$

$T_{o_p} = 449°R$

$A_s = .1604$ IN^2

NORMAL INJECTION

FIG. 13 SHADOWGRAPH OF SHOCK SYSTEM

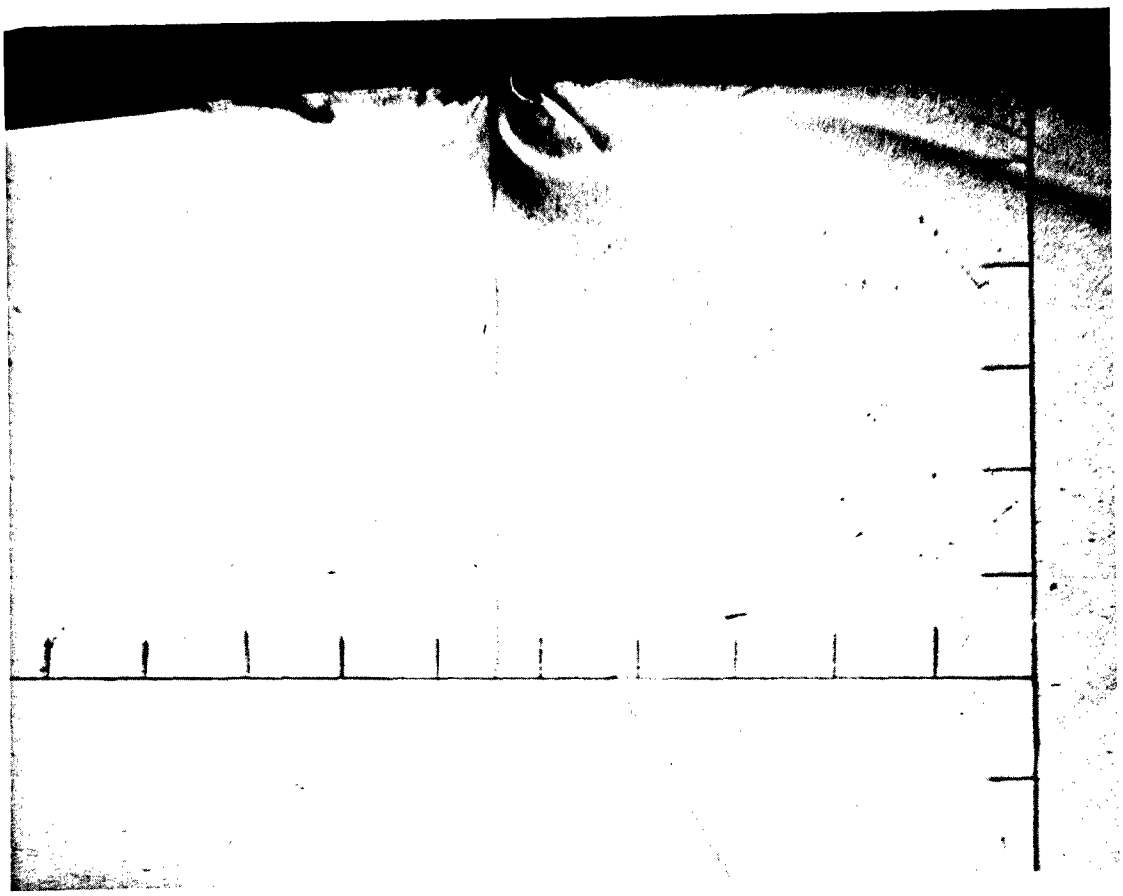

$P_{o_s} = P_{o_p} = 100$ PSIG

$T_{o_s} = 490°R$

$T_{o_p} = 467°R$

$A_s = .3663\ IN^2$

NORMAL INJECTION

FIG. 14 SHADOWGRAPH OF SHOCK SYSTEM

expansion of the secondary gas around the downstream edge of the injection slot. The low pressure region coupled with atmospheric pressure at the exit produces the adverse pressure gradient.

It should be noted that if injection were through a circular orifice or a slot not extending the entire width of the nozzle, the primary gas would tend to flow into this low pressure region thereby increasing the pressure immediately downstream of the injection port and possibly weakening or even eliminating the trailing shock. Charwat and Allegre (9) have noted a shock in this region whereas Zukoski and Spaid (8) have not.

Some qualitative observations may be made after examination of the shadowgraphs and pressure measurements. They are as follows.

1. Increasing the secondary stagnation pressure while holding all other parameters constant (secondary mass flow rate necessarily increases for a constant slot area) tends to move the leading shock further upstream.
2. Increasing the slot area while holding the secondary stagnation pressure constant also moves the leading shock upstream.
3. The trailing shock tends to move downstream under the influence of increasing secondary stagnation pressure or increasing slot area.
4. The oblique shock originating near the point of maximum penetration and intersecting the leading shock is, by two-dimensional oblique shock calculations, a weak shock of secondary strength when compared to the leading shock.
5. From considerations in item 4 it is apparent that the flow

direction of the secondary gas at the origin of the weak shock is approximately parallel to the boundary between the separated region and the free stream.

6. Pressure measurements indicate that the pressure in the separated region is not constant.

7. The low pressure region downstream of the injection port is detrimental to the side force produced and, in addition, the condition in this region becomes more unfavorable as the angle of injection (measured upstream from a normal to the axis) increases.

3.2 Calculation of Side Thrust

Reduction of the experimental data has been accomplished with the aid of the IBM 7090 computer. Because measurements consisted of wall static pressures it was necessary to integrate these values along both walls and the difference between the two forces plus the momentum thrust of the secondary jet provided the value of the net side thrust produced under given operating conditions.

The procedure used to calculate the force on a wall is as follows:

1. the area of interest is divided into several equal increments (approximately 5 per inch) in the axial direction;

2. using experimentally measured values of pressure at the physical pressure taps, the pressure at the end point of each increment is found by use of a subprogram which utilizes a cubic equation, written between three physical pressure taps enclosing the point in question, to determine the interpolated value of pressure;

3. the pressure is integrated across each increment by use of Simpson's rule (13);

4. the net force due to pressure acting on the walls is determined by taking the difference between the force acting on the full nozzle wall and the injection nozzle wall; and

5. the momentum thrust of the secondary jet is added to the foregoing. The momentum thrust of the secondary jet is calculated using as back pressure (for the jet) the static pressure on the opposite wall at the same axial position as the injection slot.

It should be noted that the slope of the contour of the nozzle wall is taken into account in all of the calculations as is the angle of injection.

The following is an illustrative example pertaining to a typical set of measured data. The operating conditions, for example, are as follows.

Ambient temperature	$= T_{amb}$	$= 76^{\circ}F$
Ambient pressure	$= P_{amb}$	$= 29.46$ in Hg
Injection slot width	$= SW$	$= .178$ in.
Freestream Mach number at the injection station	$= M_p$	$= 1.904$
Secondary stagnation temperature	$= T_{o_s}$	$= 490^{\circ}R$
Primary stagnation temperature	$= T_{o_p}$	$= 465^{\circ}R$
Secondary stagnation pressure	$= P_{o_s}$	$=$ 60 psig
Primary stagnation pressure	$= P_{o_p}$	$=$ 100 psig
Angle of injection measured upstream of a normal to the axis	$= \epsilon$	$= 0^{\circ}$

The static wall pressures recorded are listed below (refer to Table 2 for location of pressure taps).

Side without slot		Side with slot			
		Upstream		Downstream	
Pressure Tap No.	Static Pressure (in.Hg.)	Pressure Tap No.	Static Pressure (in.Hg.)	Pressure Tap No.	Static Pressure (in.Hg.)
4	21.6	9	21.3	18	-14.4
5	16.9	10	19.2	19	- 1.8
6	11.3	11	17.8	20	3.2
7	6.7	12	16.1	21	1.4
8	2.4	13	14.6	22	- 0.6
		14	11.7		
		15	11.0		
		16	10.7		
		17	44.9		

Pressure taps 4 through 8 are located on the nozzle block without the slot. Assuming that at the exit of the nozzle the wall static pressure is ambient the region to be examined is from 12.210 inches to 19.722 inches measured with respect to the entrance plane of the nozzle. The region, 7.512 inches long, is divided into 25 equal increments with the end point of each increment being assigned a value of pressure found from the subprogram using a cubic equation to interpolate between the value of pressure at three physical pressure taps. For example, to find the value of pressure at the end of the first increment the subprogram would utilize the values of pressure at tap numbers 4, 5, and 6 to determine this value. The pressures at each end point are then converted to psig. Simpson's rule is then utilized to integrate these pressures over each increment, the result being multiplied by the cosine of

the angle the nozzle wall makes with respect to the nozzle axis at the end point, and the nozzle width. Summing up the forces on each increment of the wall results in the total force acting on the wall between 12.210 inches and the exit.

The same procedure is used on the wall with the injection slot. Since this integration must be over the same region as on the opposite wall, the value of the pressure at tap number 4 is used as the starting point. This is allowable since this tap is well upstream of any disturbances caused by secondary injection.

Since pressure taps could not be located exactly at the upstream or downstream edges of the injection slot which are the end point and the starting point of calculations of forces on the upstream and the downstream sides of the injection port, respectively, the boundary condition that the pressure at these points was equal to the static pressure at the throat of the sonic converging injection slot was imposed. The manner of calculation of the wall force on the nozzle side with injection is then entirely analagous to the procedure for the opposite wall. The calculated wall forces for the example being considered here are:

force acting on side without slot = 69.41 lbs

force acting on side with slot

upstream of slot = 94.71 lbs

downstream of slot = 2.27 lbs

Thus a net wall side force of 27.57 lbs is produced. The momentum thrust of the secondary jet must be added to this to obtain the total side force produced under the given operating conditions.

The secondary jet momentum thrust is calculated by assuming isentropic flow with a discharge coefficient of unity. The back pressure used in the calculation is the experimentally determined static pressure on the opposite wall. For the problem under consideration the secondary jet momentum thrust is found to be 30.40 lbs. resulting in a total side force of 57.97 lbs. Other parameters of interest are easily calculated from these results.

The results from the observations made during the experimental study have been calculated on a basis similar to the example presented in the foregoing.

3.3 Influence of Selected Parameters

The parameters influencing the side force produced by secondary gas injection are as follows:

1. the point of injection,
2. the angle of injection, ϵ,
3. the secondary gas flow rate, $\dot{W}_s$, determined by
   a. the injection slot area, A_s, and
   b. the secondary stagnation pressure, P_{o_s},
4. the secondary gas properties (P, T, γ, M), and
5. the injection port geometry.

Among those, the effect of varying the angle of injection, the injection slot area and the secondary stagnation pressure have been studied in the experimental program and are presented in the following graphical form.

The side force, F_s, is plotted in Fig. 15 versus the secondary

stagnation pressure, P_{o_s}, for normal injection, with slot area, A_s, as the parameter.

Figure 16 presents the side force, F_s, plotted versus the secondary weight flow rate, $\dot{W}_s$, for normal injection, with the secondary stagnation pressure, P_{o_s}, as the parameter.

Figures 17 and 18 present corresponding curves for injection at an angle of 10^o directed upstream of a normal to the nozzle axis.

3.3.1 Correlation of Experimental Results

The experimental results may now be considered in relation to the following non-dimensional parameters.

1. $AK = \dfrac{F_s/\dot{W}_s}{F_p/\dot{W}_p}$

   = ratio of the effective specific impulse of the secondary stream to the undisturbed specific impulse of the primary stream,

2. $\dfrac{P_{o_s}}{P_{o_p}}$ = ratio of secondary to primary stagnation pressures,

3. $\dfrac{\dot{W}_s}{\dot{W}_p}$ = ratio of secondary to primary weight flow rates, and

4. $\dfrac{A_s}{A_t}$ = ratio of the area of the injection slot to the throat area of the primary nozzle.

Figure 19 presents AK versus P_{o_s}/P_{o_p}, for normal injection, with

A_s/A_t as parameter.

Figure 20 presents AK versus $\dot{W}_s/\dot{W}_p$, for normal injection, with P_{o_s}/P_{o_p} as parameter.

Figures 21 and 22 present corresponding results for injection 10^o upstream of a normal to the nozzle axis.

3.3.2 Discussion of the Results

Some qualitative results may be derived after examination of Figs. 15 through 22. They are as follows.

1. The side force produced increases as the secondary stagnation pressure is increased (necessarily increasing the secondary weight flow rate), for a constant injection slot area.
2. The side force produced increases as the injection slot area is increased (again increasing the secondary weight flow rate), for a constant secondary stagnation pressure.
3. At larger injection slot areas (5% of primary nozzle throat area and above) the side force increases for 10^o upstream injection as compared to normal injection. For smaller injection slot areas the angle of injection does not effect the side force produced.
4. The amplification factor increases as the ratio of secondary to primary stagnation pressures is increased (necessarily increasing the secondary to primary weight flow rate ratio) for a constant ratio of injection slot area to nozzle throat area.

5. The amplification factor decreases as the secondary to primary weight flow rate ratio is increased, for a constant secondary to primary stagnation pressure ratio.

6. The amplification factor increases for 10^{o} upstream injection as compared to normal injection, the greatest increase being at the lower pressures.

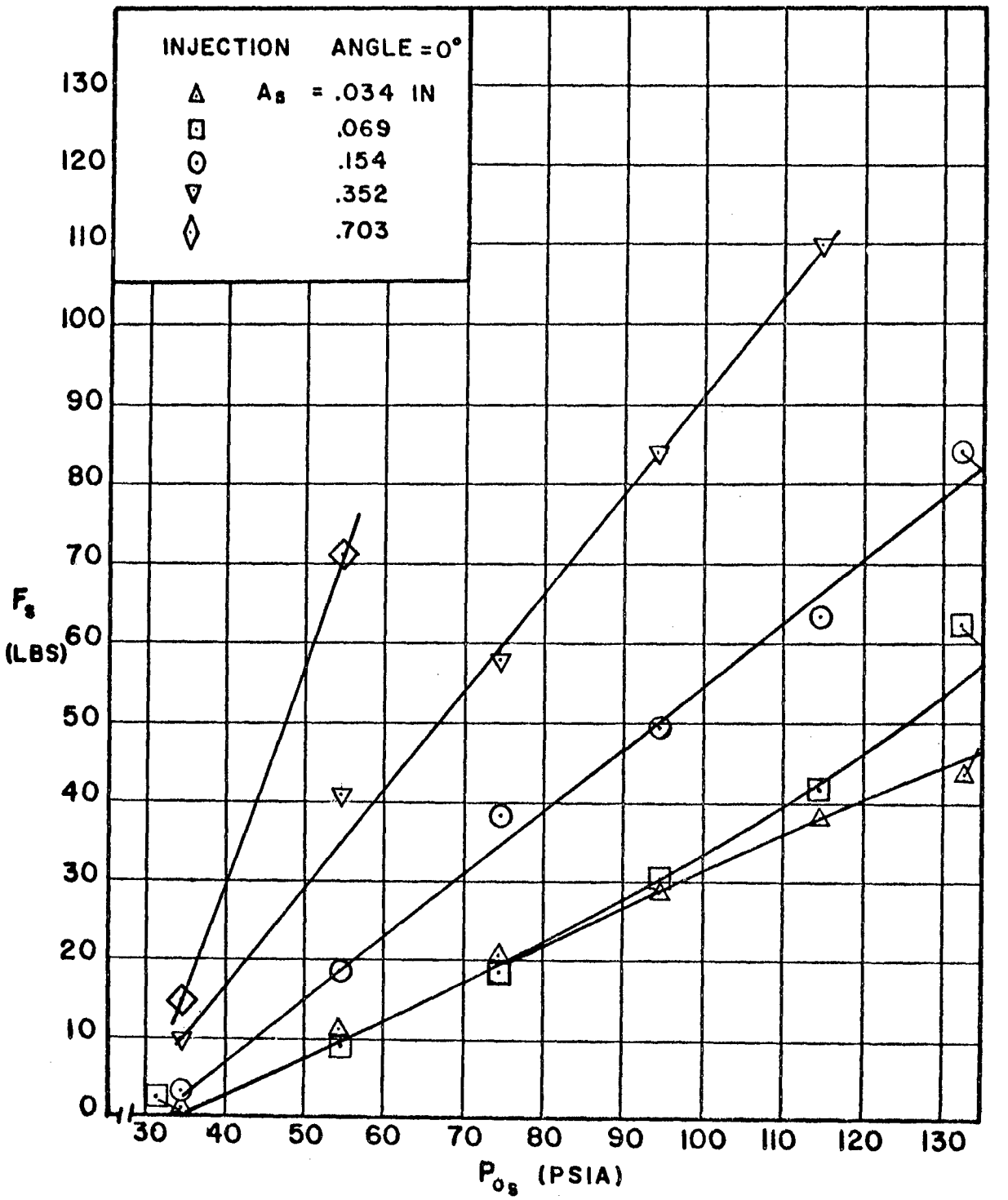

FIG. 15 EFFECT OF P_{os} ON F_s WITH A_s AS PARAMETER ($\epsilon = 0°$) (EXPERIMENTAL)

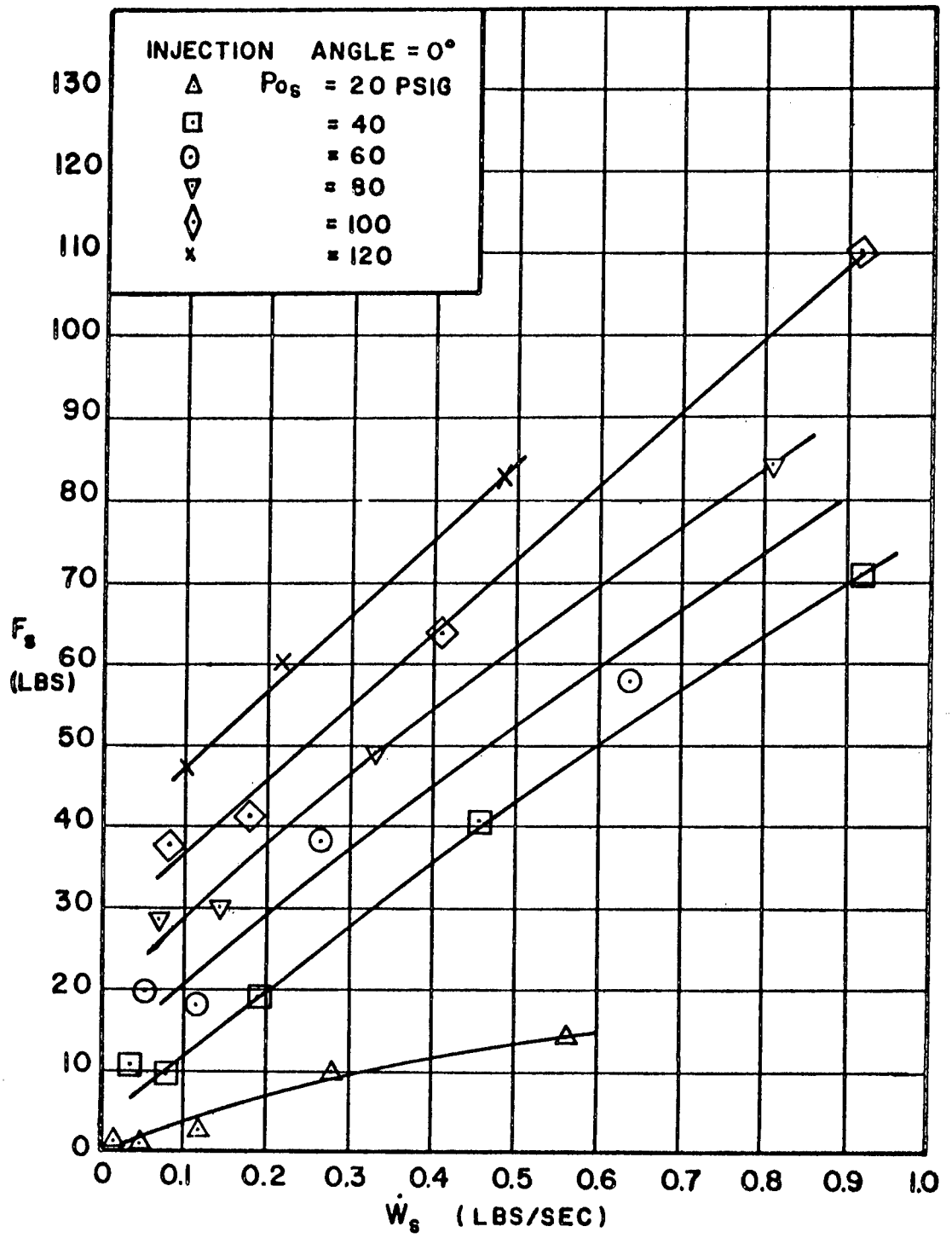

FIG. 16 EFFECT OF $\dot{W}_s$ ON F_s WITH P_{os} AS PARAMETER ($\epsilon = 0°$) (EXPERIMENTAL)

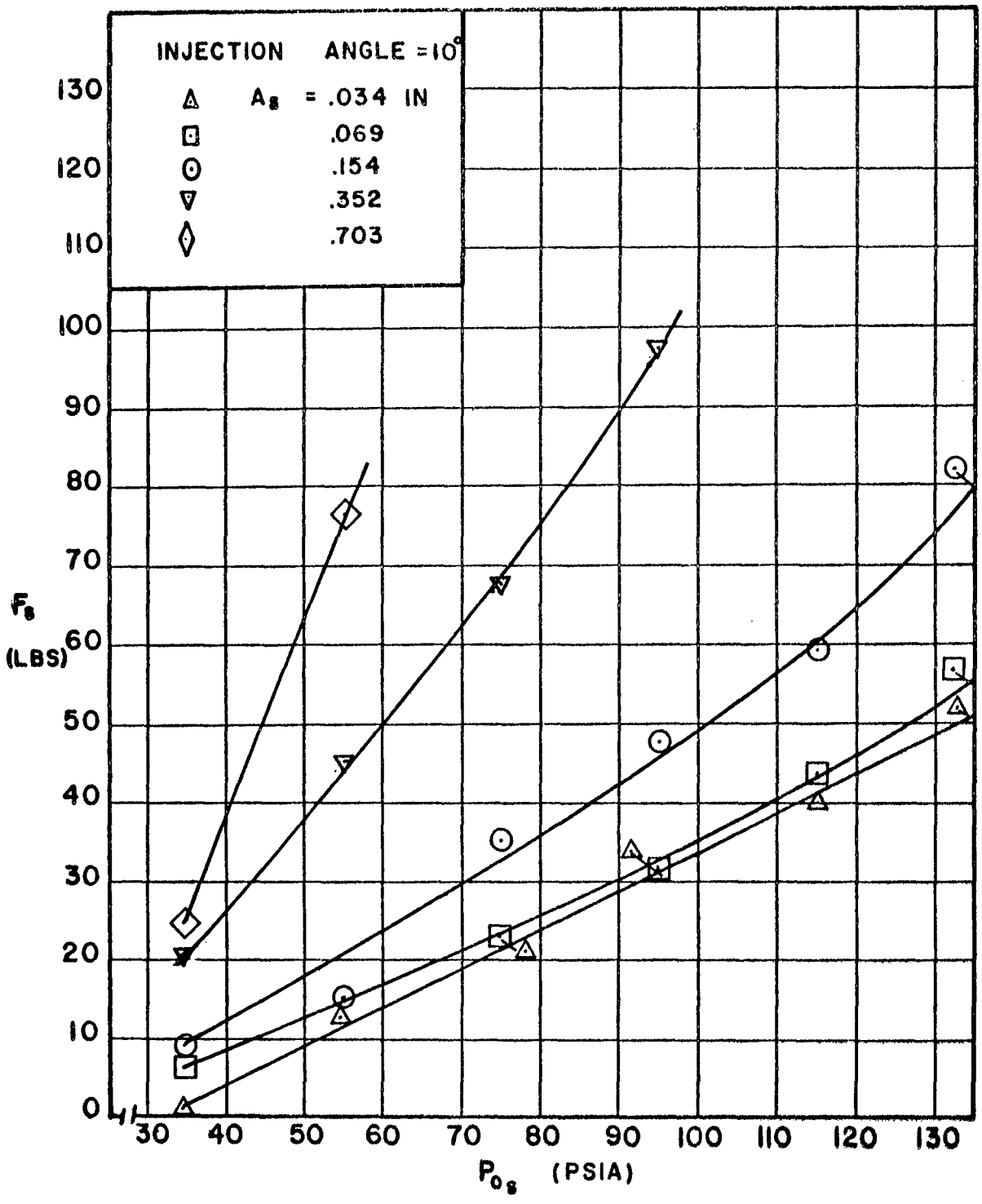

FIG. 17 EFFECT OF P_{os} ON F_s WITH A_s AS PARAMETER ($\epsilon = 10°$) (EXPERIMENTAL)

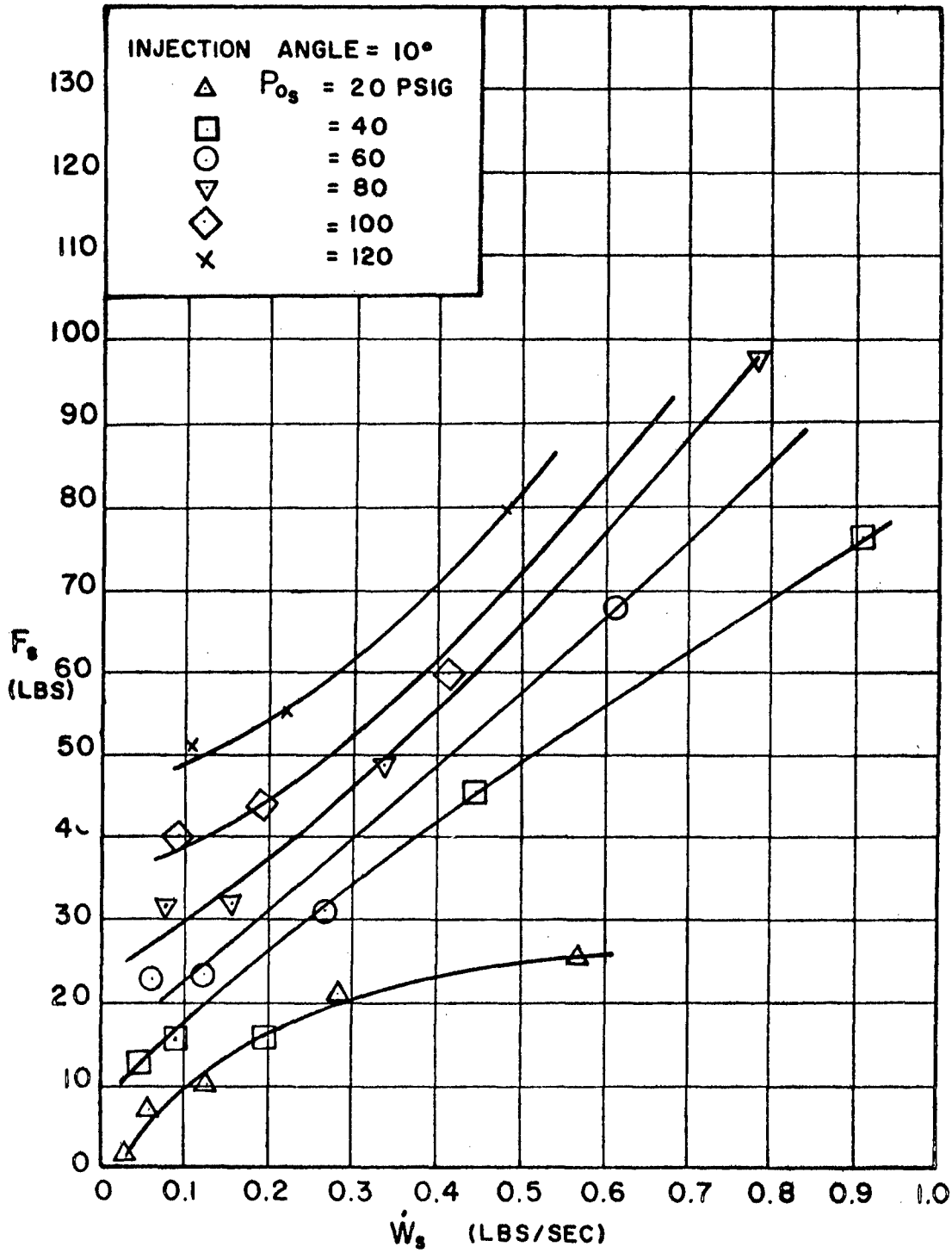

FIG. 18 EFFECT OF $\dot{W}_s$ ON F_s WITH P_{0_s} AS PARAMETER ($\epsilon = 10°$) (EXPERIMENTAL)

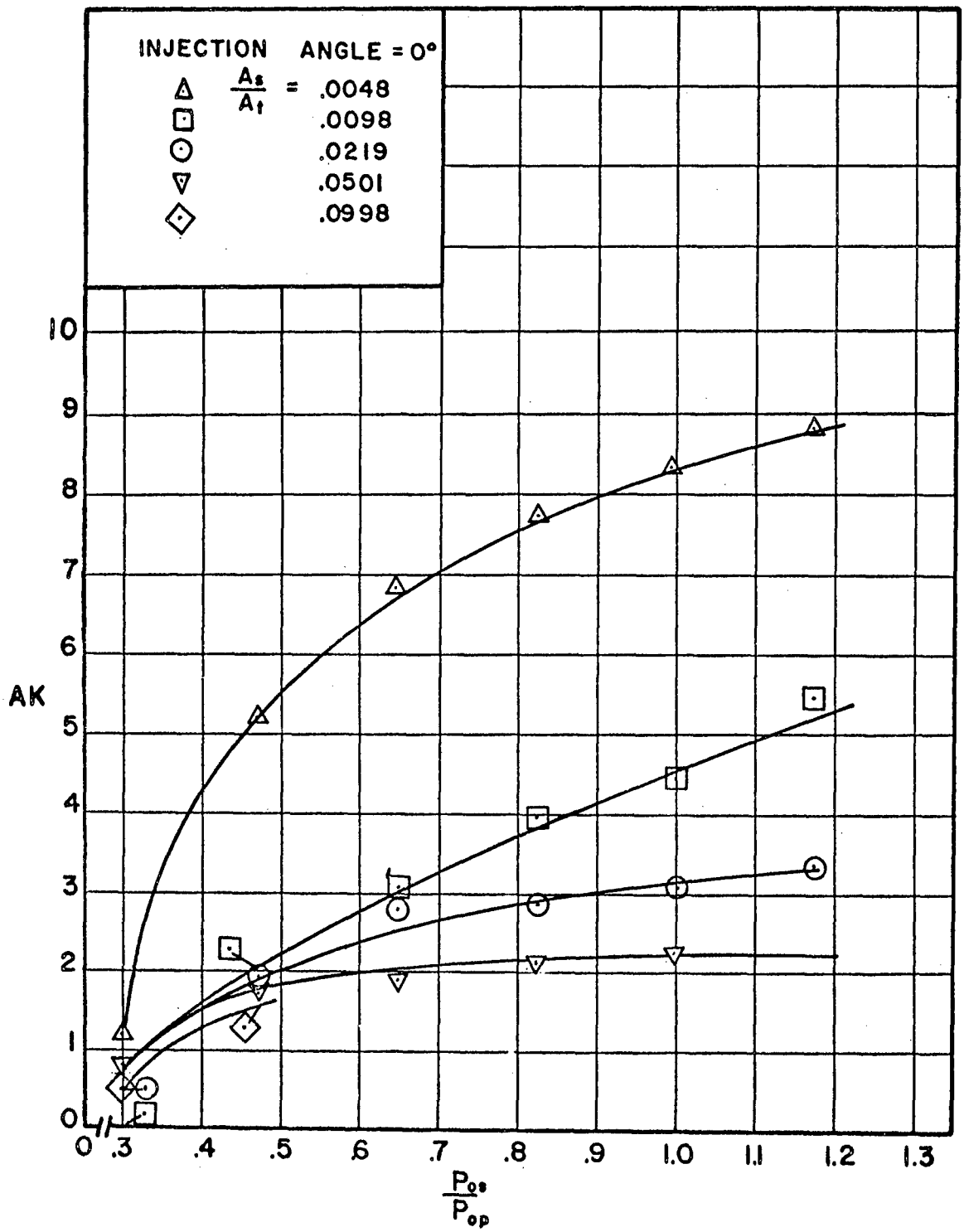

FIG. 19 EFFECT OF P_{os}/P_{op} ON AK WITH A_s/A_t AS PARAMETER ($\epsilon = 0°$) (EXPERIMENTAL)

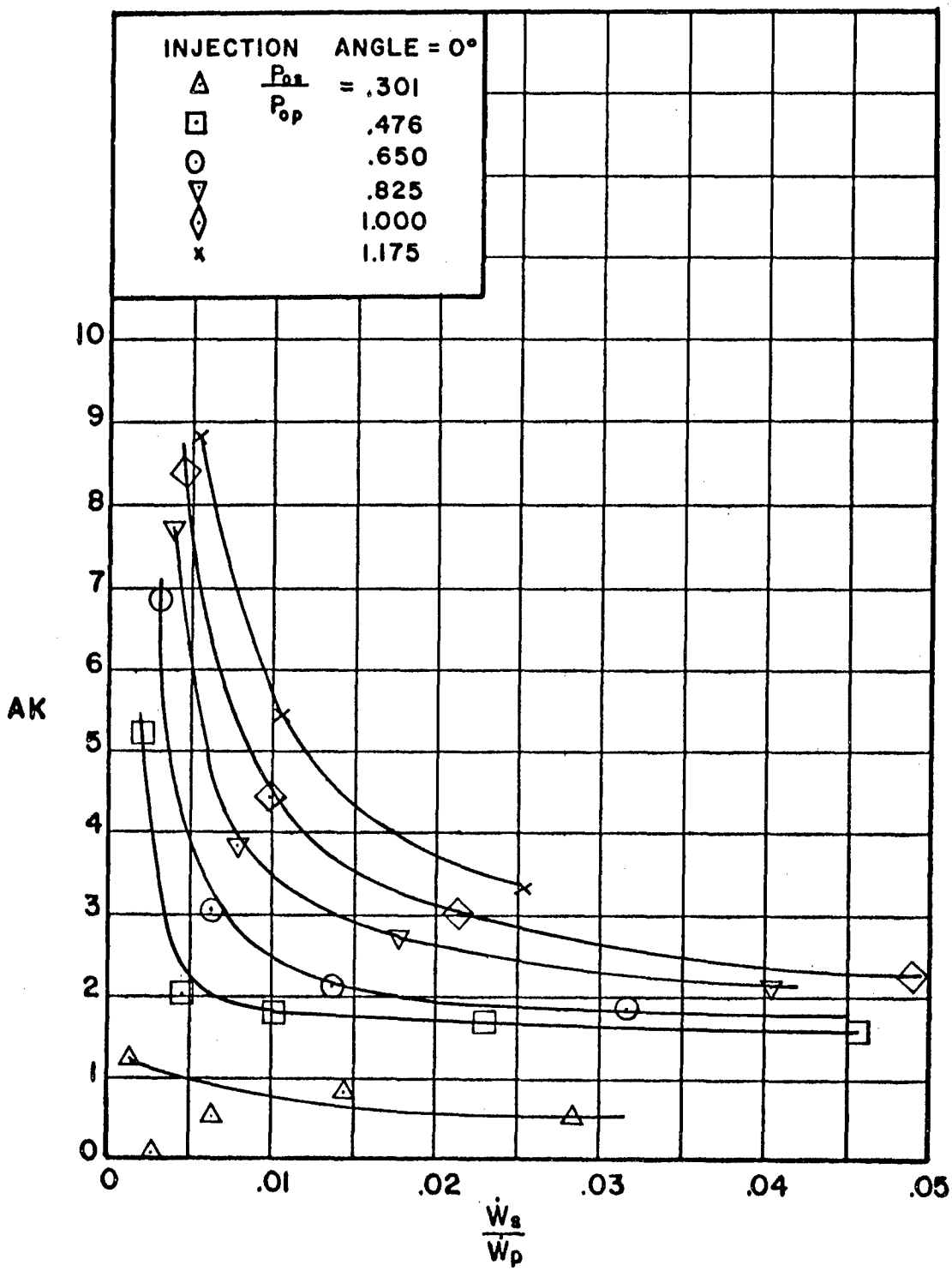

FIG. 20 EFFECT OF $\dot{W}_s/\dot{W}_p$ ON AK WITH P_{os}/P_{op} AS PARAMETER ($\epsilon = 0°$) (EXPERIMENTAL)

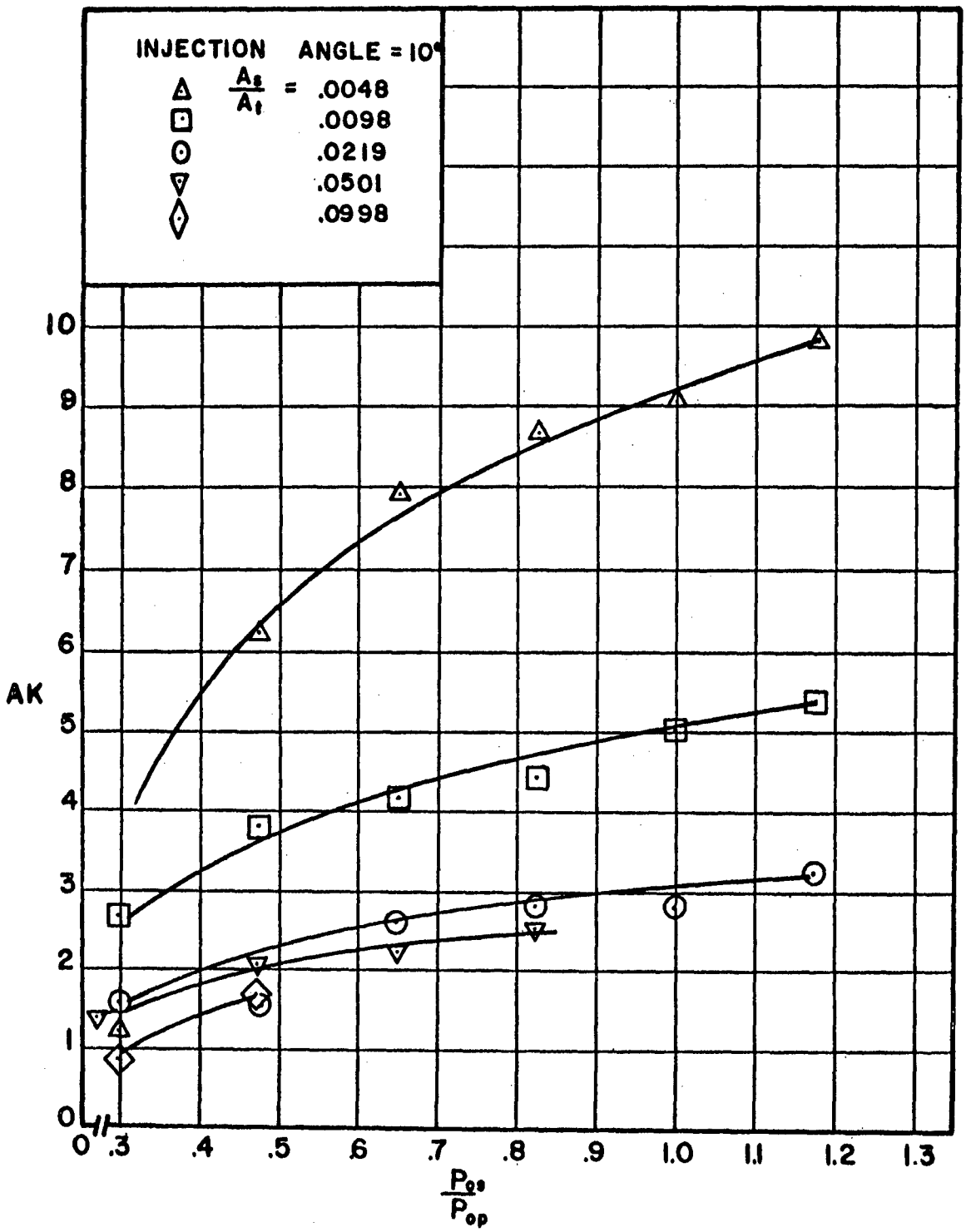

FIG. 21 EFFECT OF P_{os}/P_{op} ON AK WITH A_s/A_f AS PARAMETER ($\epsilon = 10°$) (EXPERIMENTAL)

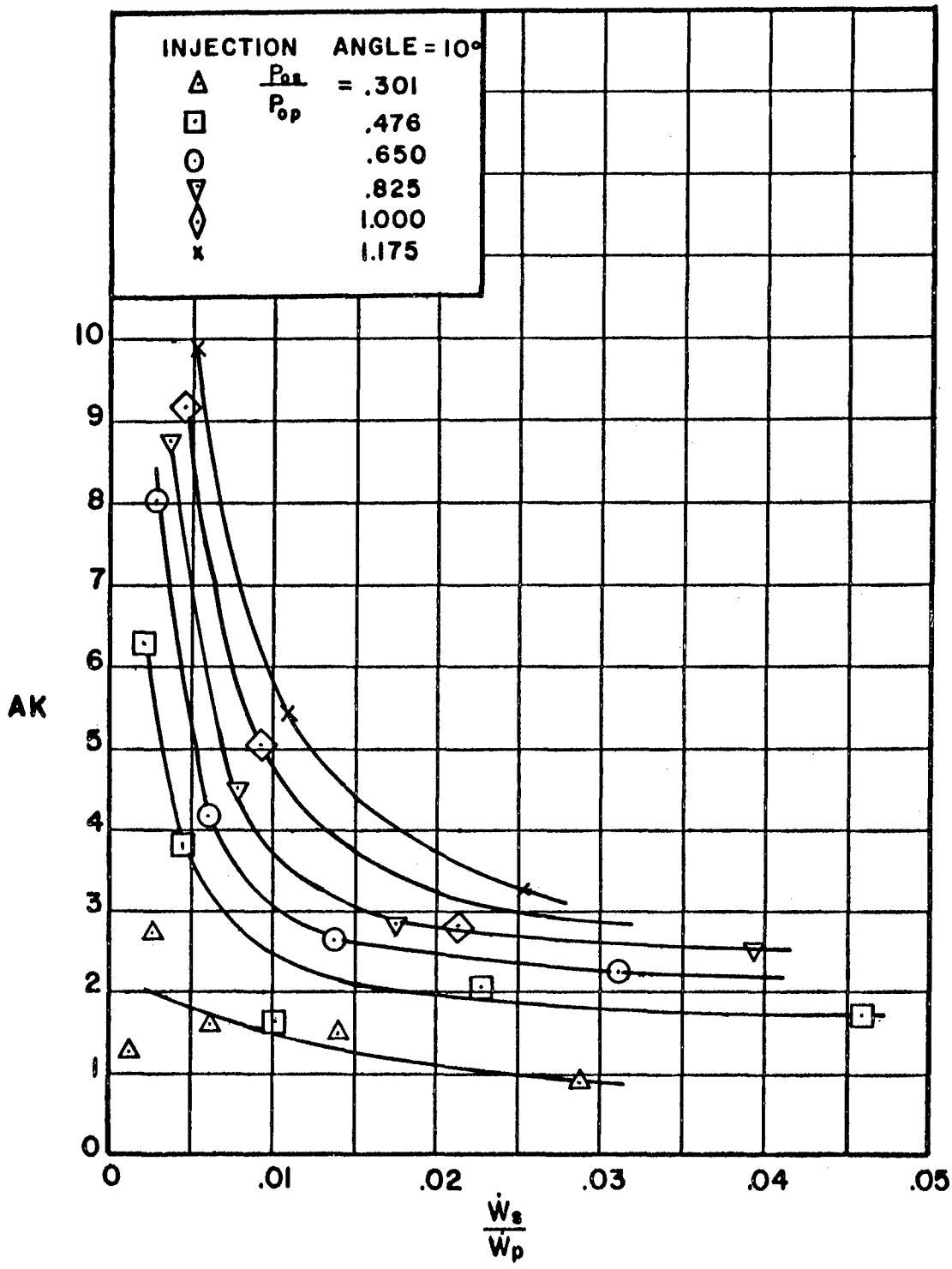

FIG. 22 EFFECT OF $\dot{W}_s/\dot{W}_p$ ON AK WITH P_{os}/P_{op} AS PARAMETER ($\epsilon = 10°$) (EXPERIMENTAL)

4. COMPARISON OF EXPERIMENTAL AND THEORETICAL RESULTS

Calculations are made utilizing two of the available theories, namely those presented in (5) and (6), in which equations have been developed for predicting the side force produced by secondary injection. The results of the application of these theories using the same conditions as reported in Chapter 3 for the experimental program are then compared with the experimental results.

4.1 Estimated Side Force Values According to Selected Theories

Two of the theories reviewed in Section 1.1, due to Wu, Chapkis, and Mager (5) and Broadwell (6), are employed, after some modification, for the determination of the side force produced due to the injection of a secondary gas. Section 4.1.1 is devoted to the theory and the calculated results (corresponding to the experimental conditions reported herein) based on the boundary layer separation theory due to Wu, et al (5). Section 4.1.2 deals with the theory and the calculated results based on the blast wave theory due to Broadwell (6).

4.1.1 Calculations Based on the Boundary Layer Model

The analysis reported in reference (5) has been appropriately modified for the purposes of the present investigation by noting that

the governing equations for mass, momentum and energy of the primary and secondary streams, as well as the boundary conditions, remain the same. The geometric relationships for obtaining the point of separation and the area acted on by the shock are, of course, altered for the present two-dimensional system. The following equations then result which may be used in calculating the side force (symbols are defined in Appendix I; Fig. 2 may also be seen).

$$\gamma_p^2 M_1^2 \left(1 + \frac{\gamma_p - 1}{2} M_1^2\right) = \left[\left(1 + \gamma_p M_1^2\right) + \frac{p_4}{p_1}\left(\frac{A_4}{A_1} - 1\right) - \frac{\bar{p}_s A_4}{p_1 A_1}\right]$$

$$\left[\frac{\gamma_p + 1}{2} \frac{p_4}{p_1}\left(1 - \frac{A_4}{A_1}\right) + \frac{\gamma_p - 1}{2}\left(1 + \gamma_p M_1^2 - \frac{\bar{p}_s A_4}{p_1 A_1}\right)\right] \qquad (4.1)$$

$$2 \gamma_s^2 M_s^2 \left(1 + \frac{\gamma_s - 1}{2} M_s^2\right) = \left[\left(\frac{A_4}{A_s}\right)^2 \left(\frac{p_1}{p_s}\right)^2 \left(\frac{\bar{p}_s}{p_1} - \frac{p_4}{p_1}\right)\right]$$

$$\left[\left(\gamma_s + 1\right) \frac{p_4}{p_1} + \left(\gamma_s - 1\right) \frac{\bar{p}_s}{p_1}\right] \qquad (4.2)$$

$$\bar{p}_s = \frac{2}{3} p_{b1} + \frac{1}{3} p_s \qquad (4.3)$$

$$\frac{p_{b1}}{p_1} = \frac{1 + G}{\left(1 + \frac{p_b}{p_1} G_1\right)} \qquad (4.4)$$

$$G_1 = \frac{- 0.328 K \sqrt{M_1^2 - 1}}{1 + \frac{\gamma_p - 1}{2} K M_1^2} \qquad (4.5)$$

$$\frac{p_b}{p_1} = 1 + \frac{\gamma_p M_1^2 (1 - K)}{2 + (\gamma_p - 1) M_1^2} \tag{4.6}$$

$$X = A_4 (\cot \delta + \tan \epsilon) \tag{4.7}$$

$$\cot \delta = \frac{1}{\left[\frac{(5 \frac{p_{b1}}{p_1} - 1)}{7 M_1^2 - 5 (\frac{p_{b1}}{p_1} - 1)}\right] \left[\frac{7 M_1^2 - (\frac{6 p_{b1}}{p_1} + 1)}{(\frac{6 p_{b1}}{p_1} + 1)}\right]}^{1/2} \tag{4.8}$$

$$F_s = (p_{b1} - p_1) X + A_s \quad p_s (1 + \gamma_s M_s^2) - p_4 \quad \cos \epsilon \tag{4.9}$$

Equations 4.1 through 4.9 are nine equations involving nine unknowns. The side force is then calculated for the same values of the parameters, namely:

1. the primary and secondary stagnation pressures,
2. the primary and secondary stagnation temperatures, and
3. the geometrical parameters

as for the experiments reported in Section 3.2. The computed results are presented graphically in Figs. 23 through 30.

Figure 23 presents the side force, F_s, plotted versus the secondary stagnation pressure, P_{o_s}, with the slot area, A_s, as parameter, for normal injection (see Fig. 15 which presents the corresponding experimental results).

Figure 24 presents F_s plotted versus the secondary weight flow rate,

$\dot{W}_s$, with P_{o_s} as parameter, for normal injection (see Fig. 16 for experimental results).

Figures 25 and 26 present the corresponding results for injection at an angle of 10^o measured upstream from a normal to the nozzle axis (see Figs. 17 and 18 for experimental results).

Figure 27 presents the amplification factor, AK, plotted versus the ratio of the secondary to primary stagnation pressures, P_{o_s}/P_{o_p}, with the ratio of the areas of the injection slot to the throat of the primary nozzle, A_s/A_t, as parameter, for normal injection (see Fig. 19 for experimental results).

Figure 28 presents AK plotted versus the ratio of the secondary to primary weight flow rates, $\dot{W}_s/\dot{W}_p$, with P_{o_s}/P_{o_p} as parameter, for normal injection (see Fig. 20 for experimental results).

Figures 29 and 30 present the corresponding results for injection at an angle of 10^o measured upstream from a normal to the nozzles axis (see Figs. 21 and 22 for experimental results).

4.1.2 Calculations Based on the Blast Wave Theory

The semi-empirical equations for the side force obtained (6) for the two-dimensional case are directly applicable to the present investigation. They are repeated here for convenience.

$$F_i = 0.50 \left(1 + \frac{2 + (\gamma_p - 1) M_1^2}{2 (\gamma_p - 1) M_1^2} \frac{m_p}{m_s} \frac{T_{o_s}}{T_{o_p}}\right) M_1 V_1 \dot{m}_s \qquad (4.10)$$

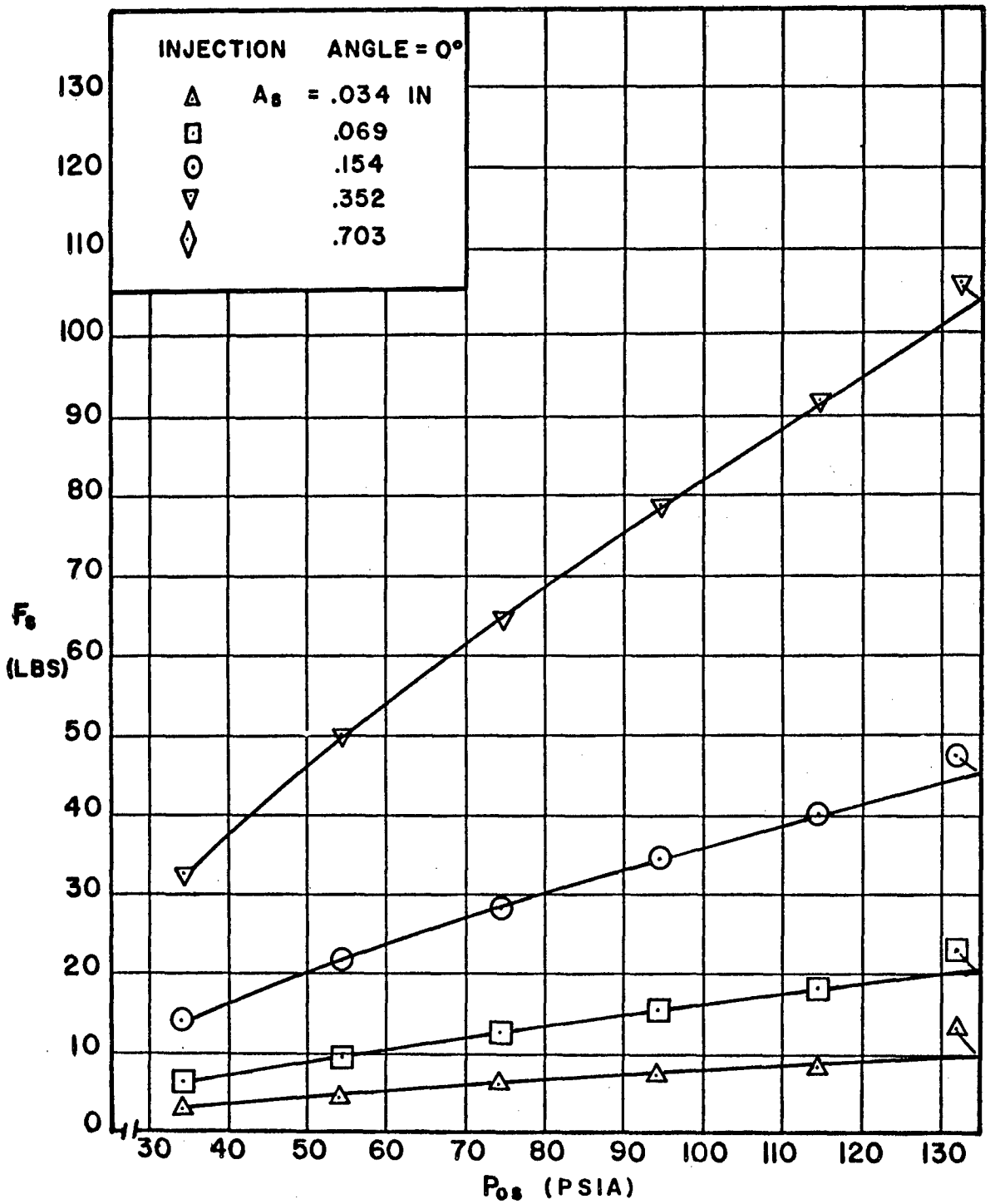

FIG. 23 EFFECT OF P_{os} ON F_s WITH A_s AS PARAMETER ($\epsilon = 0°$) (WU, ET AL)

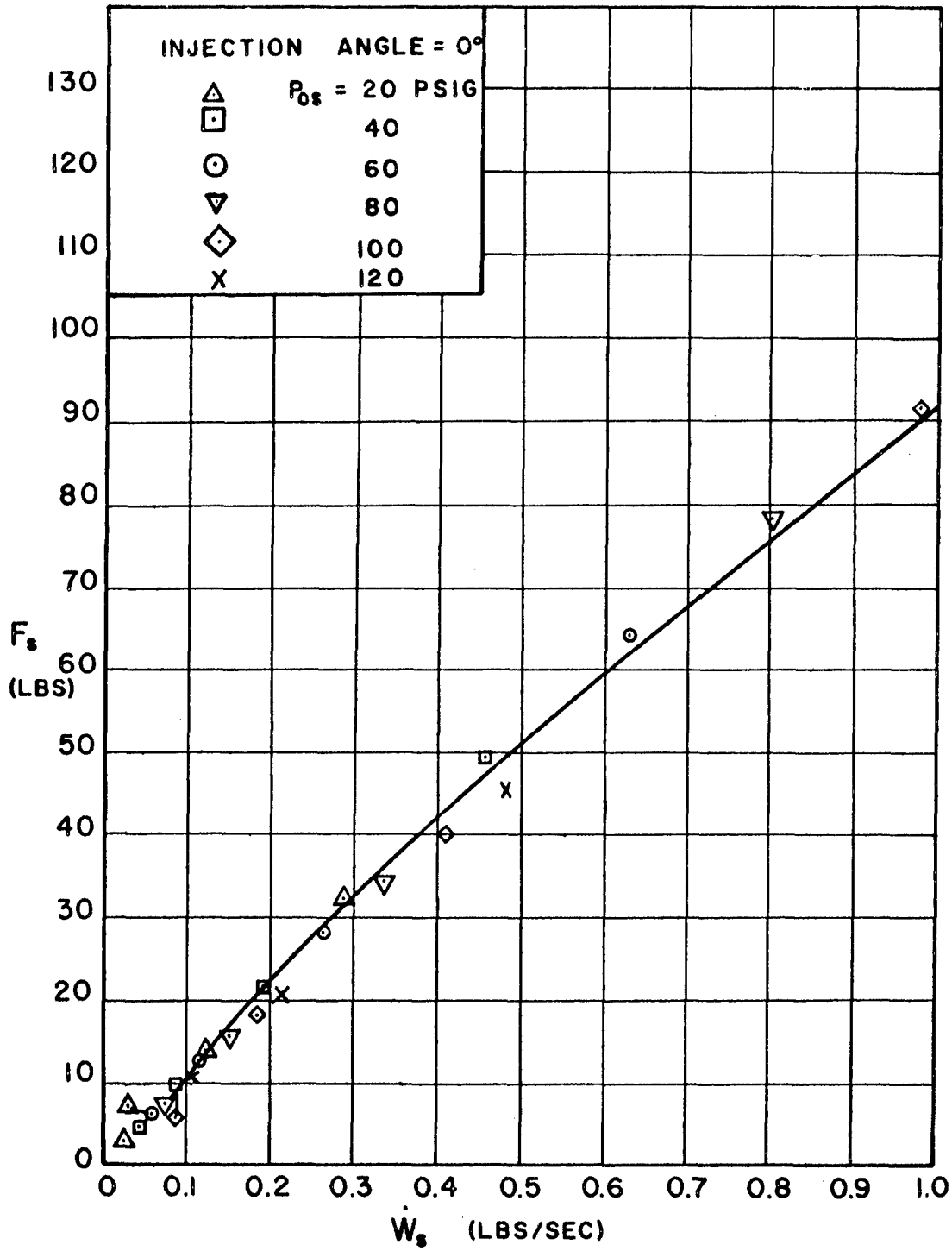

FIG. 24 EFFECT OF $\dot{W}_s$ ON F_s WITH P_{0s} AS PARAMETER ($\epsilon = 0°$) (WU, ET AL)

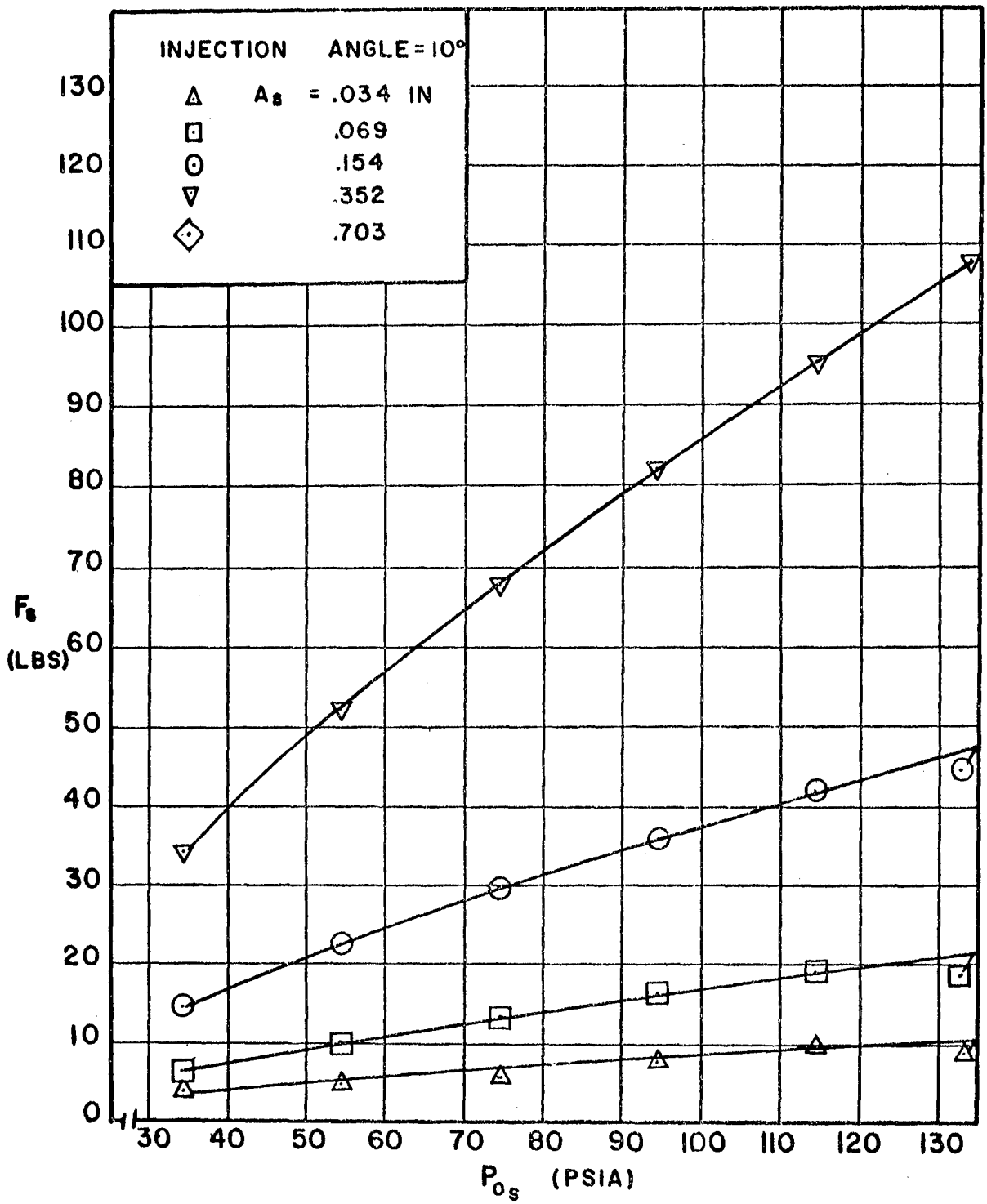

FIG. 25 EFFECT OF P_{os} ON F_s WITH A_s AS PARAMETER ($\epsilon = 10°$) (WU, ET AL)

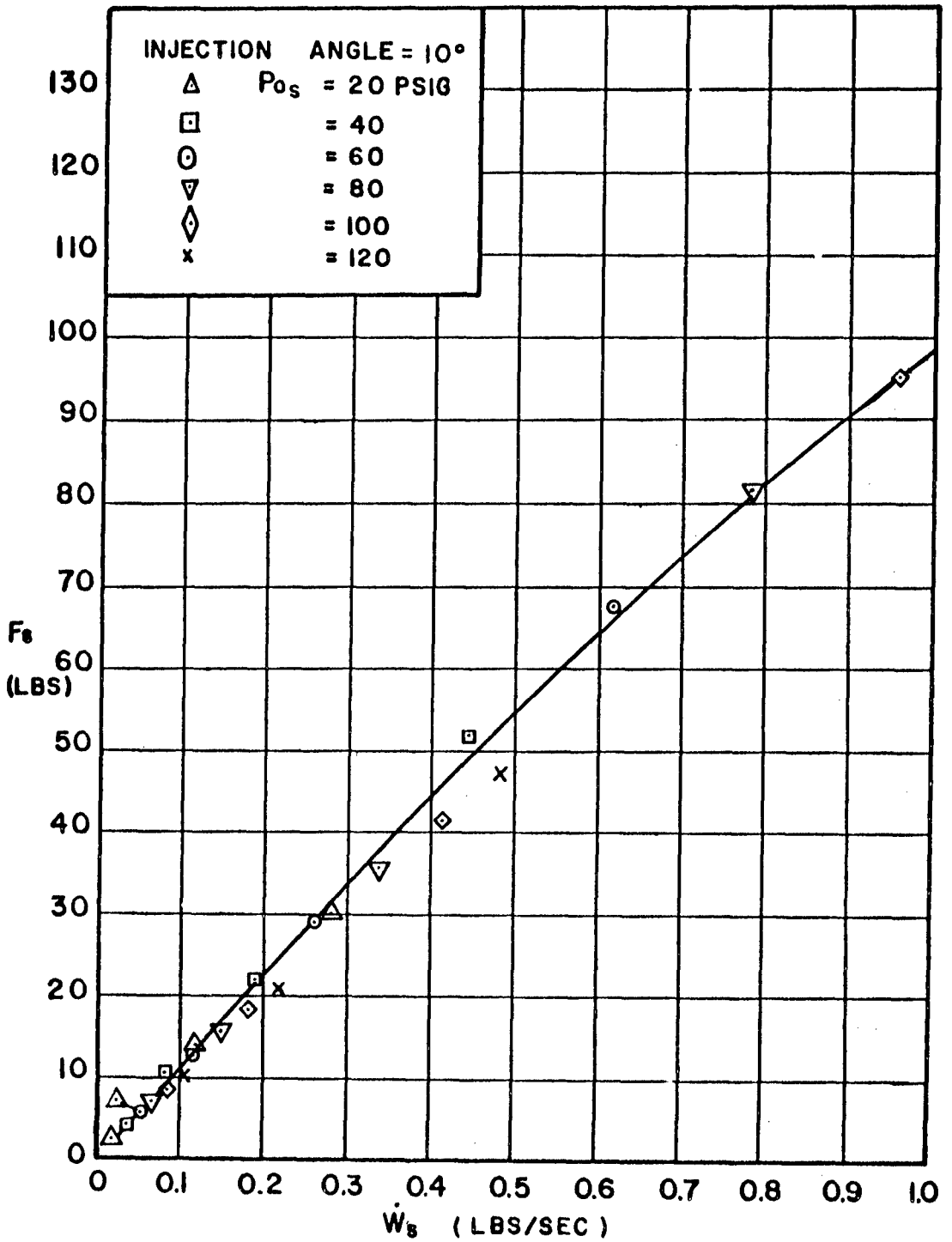

FIG. 26 EFFECT OF W_s ON F_s WITH P_{os} AS PARAMETER ($\epsilon = 10°$) (WU, ET AL)

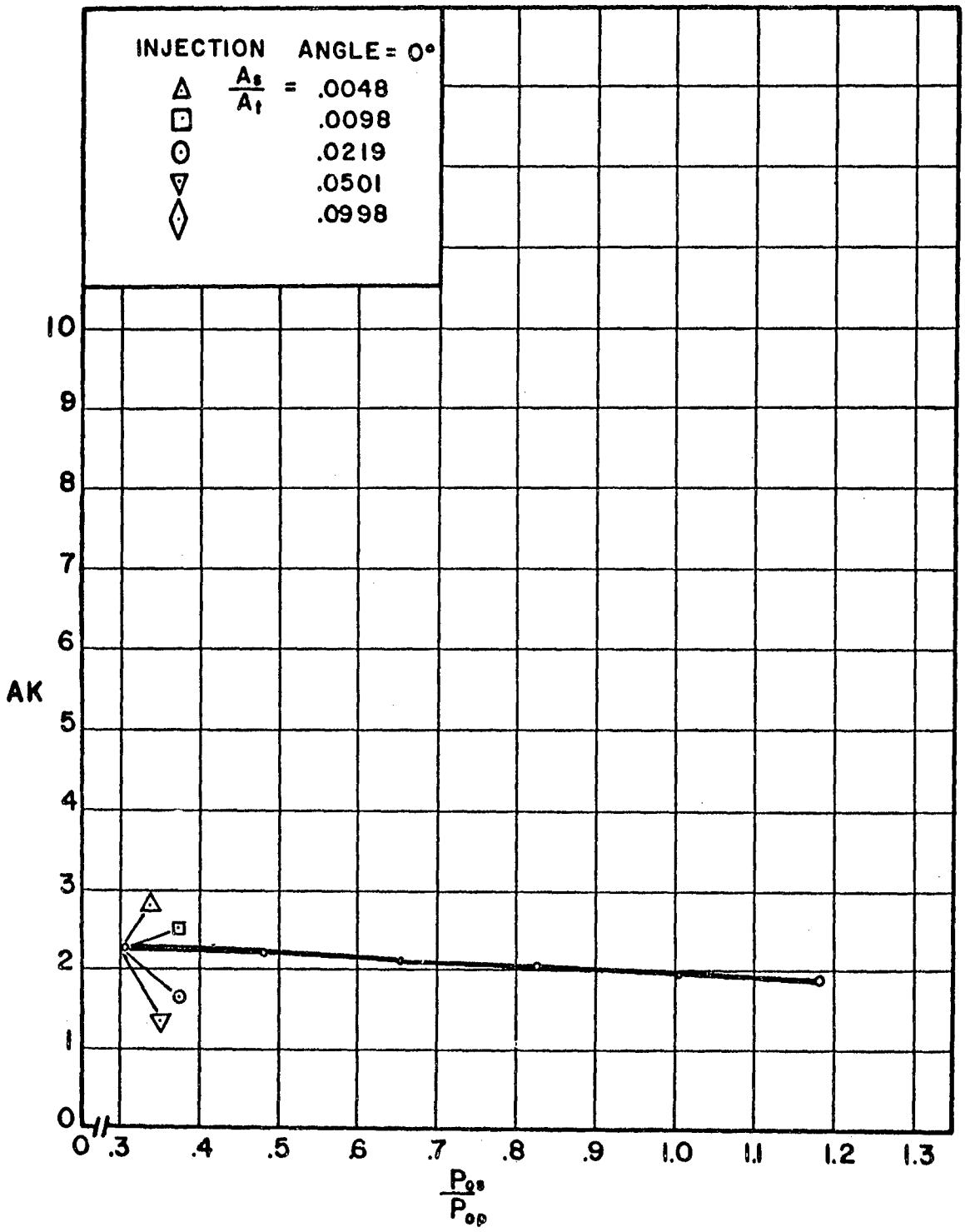

FIG. 27 EFFECT OF P_{os}/P_{op} ON AK WITH A_s/A_t AS PARAMETER ($\epsilon = 0°$)
(WU, ET AL)

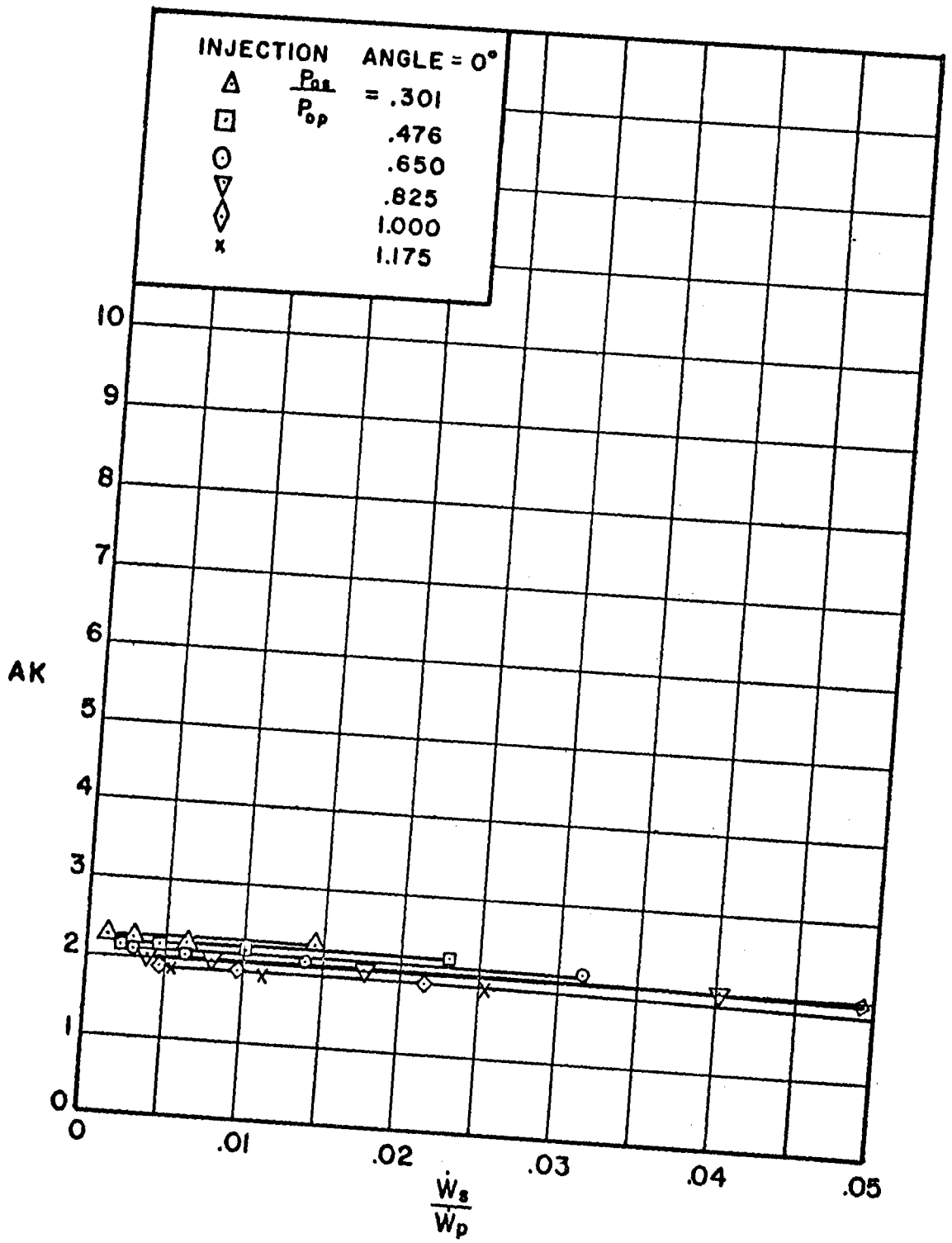

FIG. 28. EFFECT OF $\dot{W}_s/\dot{W}_p$ ON AK WITH P_{os}/P_{op} AS PARAMETER ($\epsilon = 0°$) (WU, ET AL)

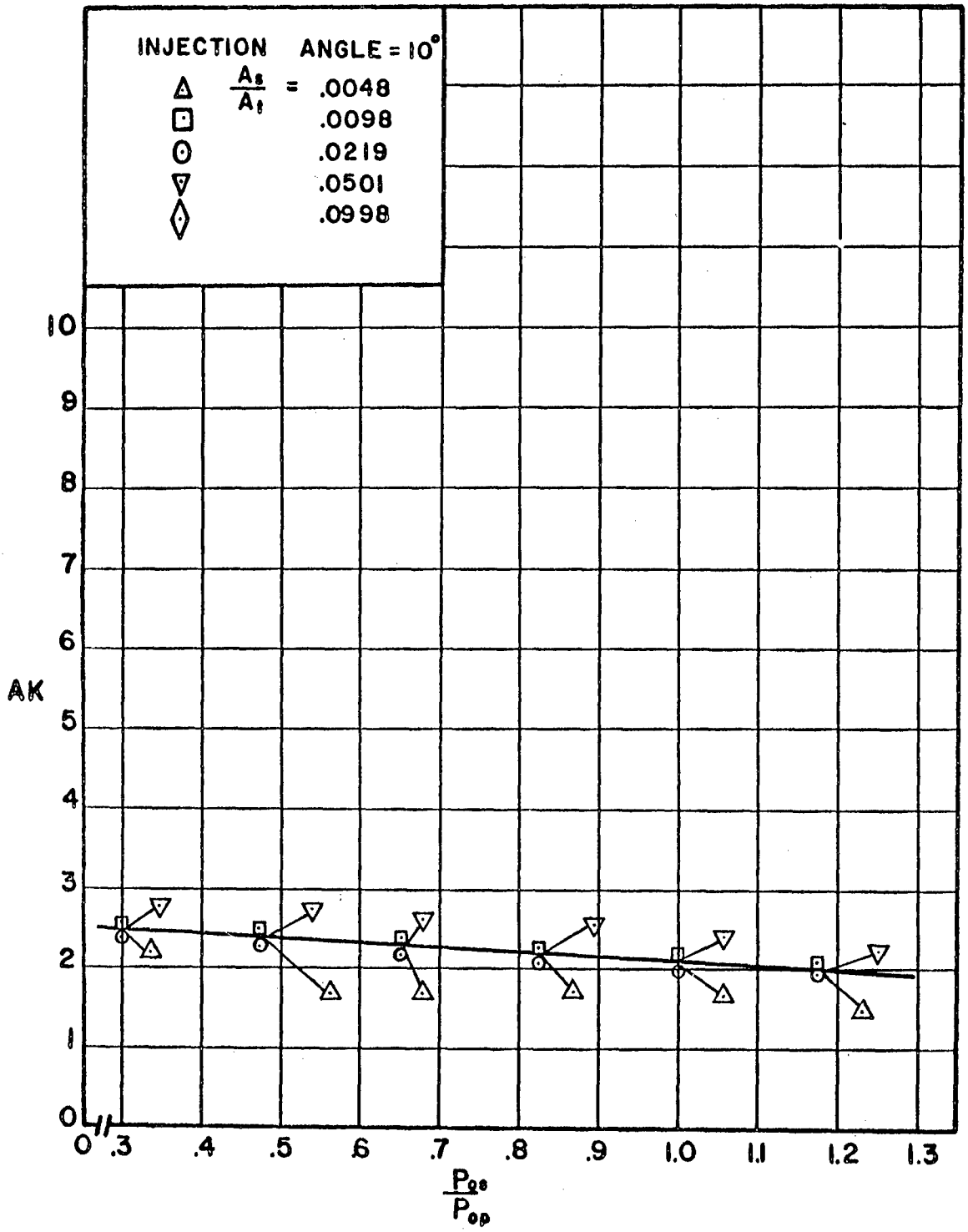

FIG. 29. EFFECT OF P_{os}/P_{op} ON AK WITH A_s/A_t AS PARAMETER ($\epsilon = 10°$)
(WU, ET AL)

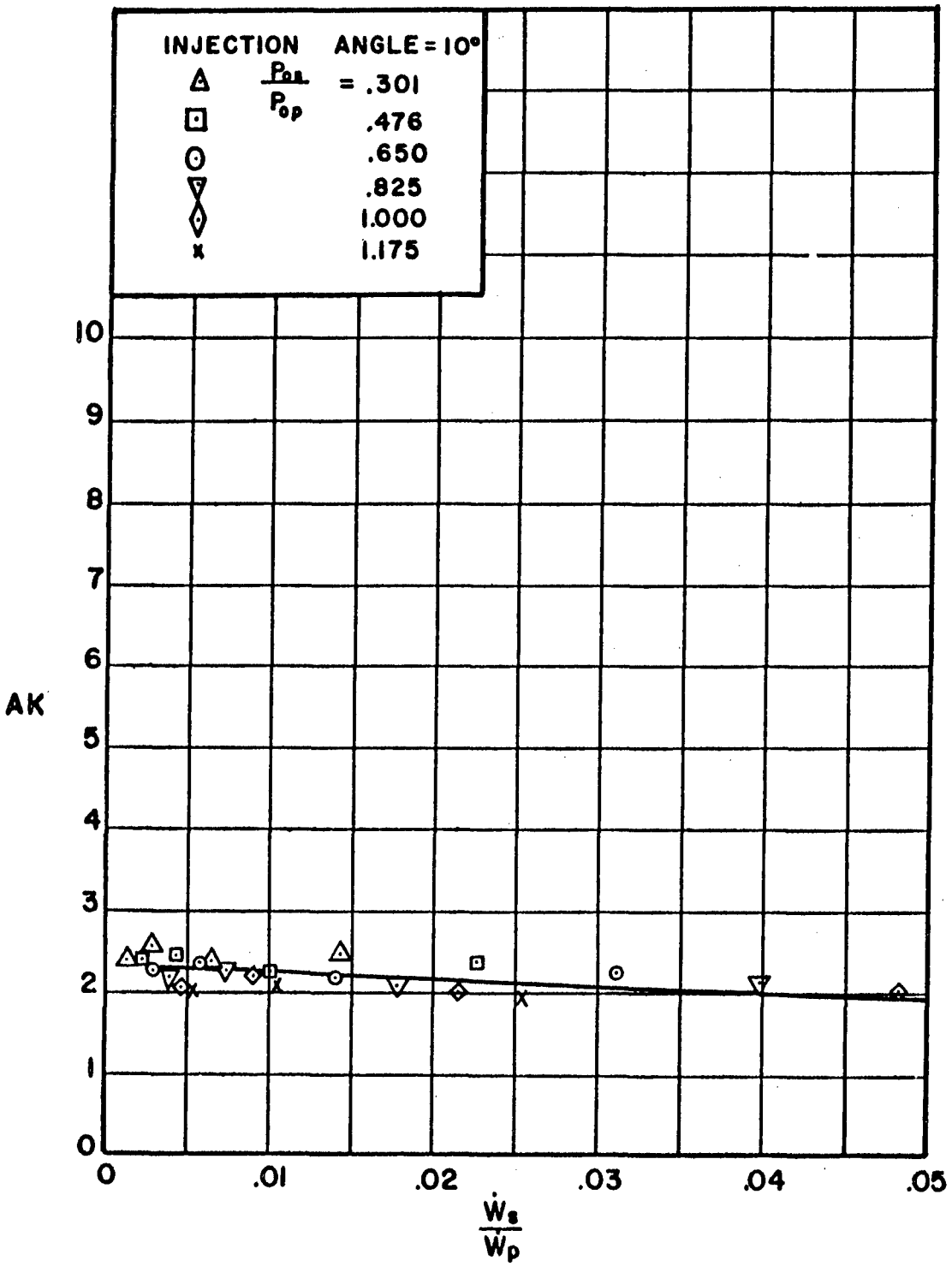

FIG. 30. EFFECT OF $\dot{W}_s/\dot{W}_p$ ON AK WITH P_{os}/P_{op} AS PARAMETER ($\epsilon = 10°$)
(WU, ET AL)

$$F_j = \left[\dot{m}_s V_s + (p_s - p_p) A_s \right] \cos \epsilon \qquad (4.11)$$

$$F_s = F_i + Fj \qquad (4.12)$$

The results of the calculations based on equations 4.10, 4.11 and 4.12 are presented graphically in Figs. 31 through 38.

Figure 31 presents the side force, F_s, plotted versus the secondary stagnation pressure, P_{o_s}, with the slot area, A_s, as parameter for normal injection (see Fig. 15 which presents the corresponding experimental results).

Figure 32 presents F_s plotted versus the secondary weight flow rate, $\dot{W}_s$, with P_{o_s}, as parameter, for normal injection (see Fig. 16 for experimental results).

Figures 33 and 34 present the corresponding results for injection at an angle of 10^o measured upstream from a normal to the nozzle axis (see Figs. 17 and 18 for experimental results).

Figure 35 presents the amplification factor, AK, plotted versus the ratio of the secondary to primary stagnation pressures, P_{o_s}/P_{o_p}, with the ratio of the areas of the injection slot to the throat of the primary nozzle, A_s/A_t, as parameter, for normal injection (see Fig. 19 for experimental results).

Figure 36 presents AK plotted versus the ratio of the secondary to primary weight flow rates, $\dot{W}_s/\dot{W}_p$, with P_{o_s}/P_{o_p} as parameter, for normal injection (see Fig. 20 for experimental results).

Figures 37 and 38 present the corresponding results for injection at an angle of 10^o measured upstream from a normal to the nozzle axis (see Figs. 21 and 22 for experimental results).

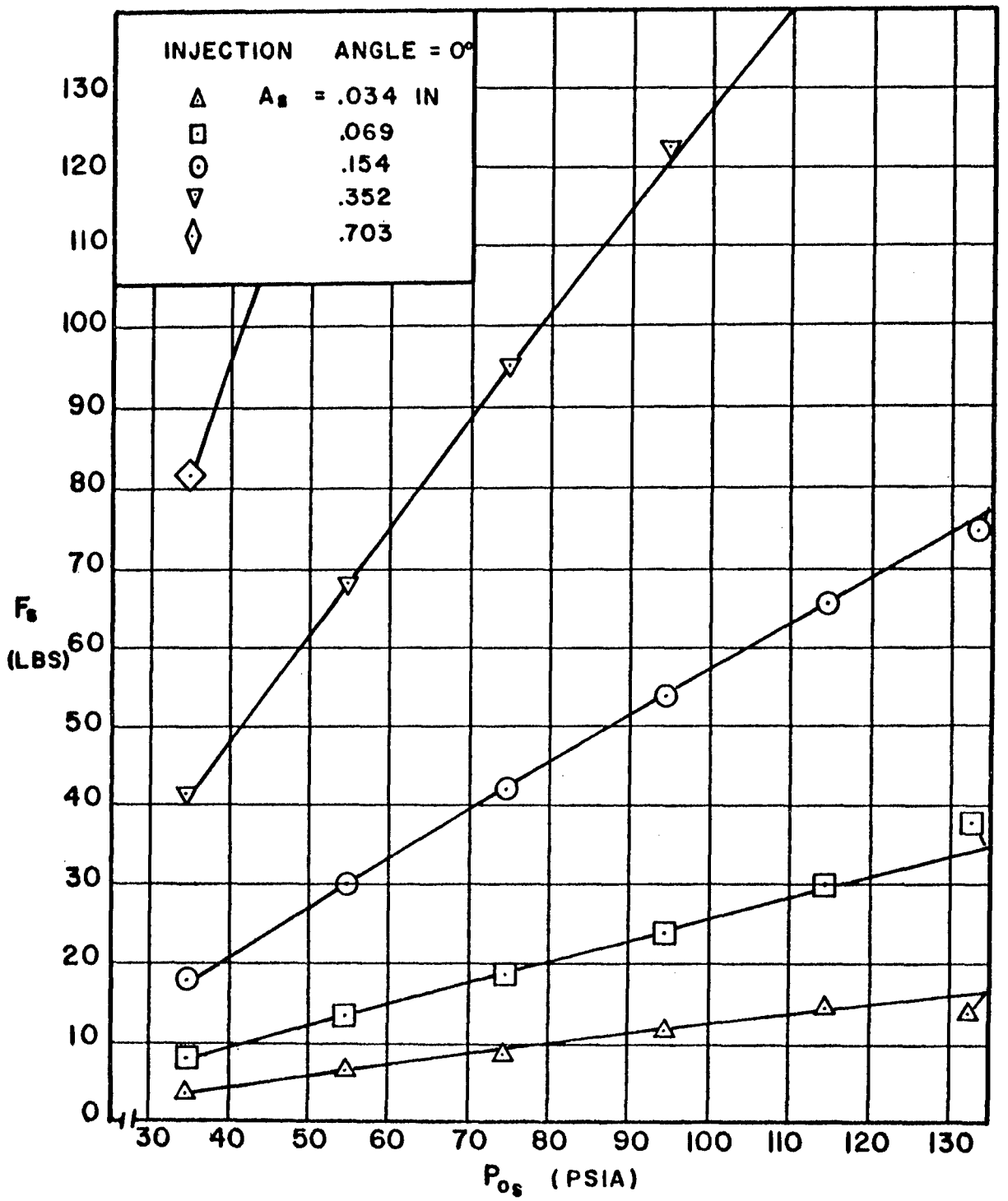

FIG. 31 EFFECT OF P_{0s} ON F_s WITH A_s AS PARAMETER ($\epsilon = 0°$) (BROADWELL)

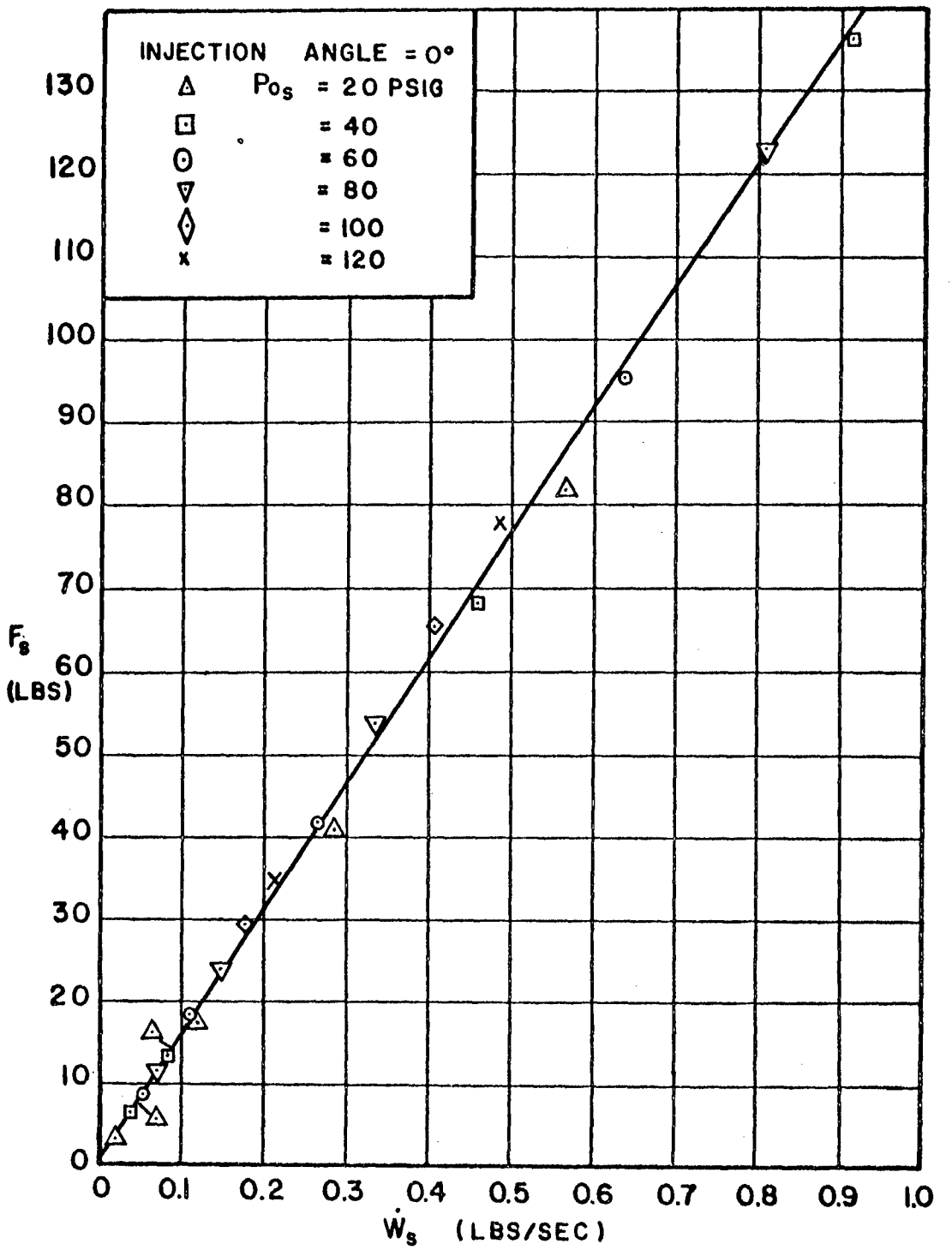

FIG. 32. EFFECT OF W_s ON F_s WITH P_{os} AS PARAMETER ($\epsilon = 0°$) (BROADWELL)

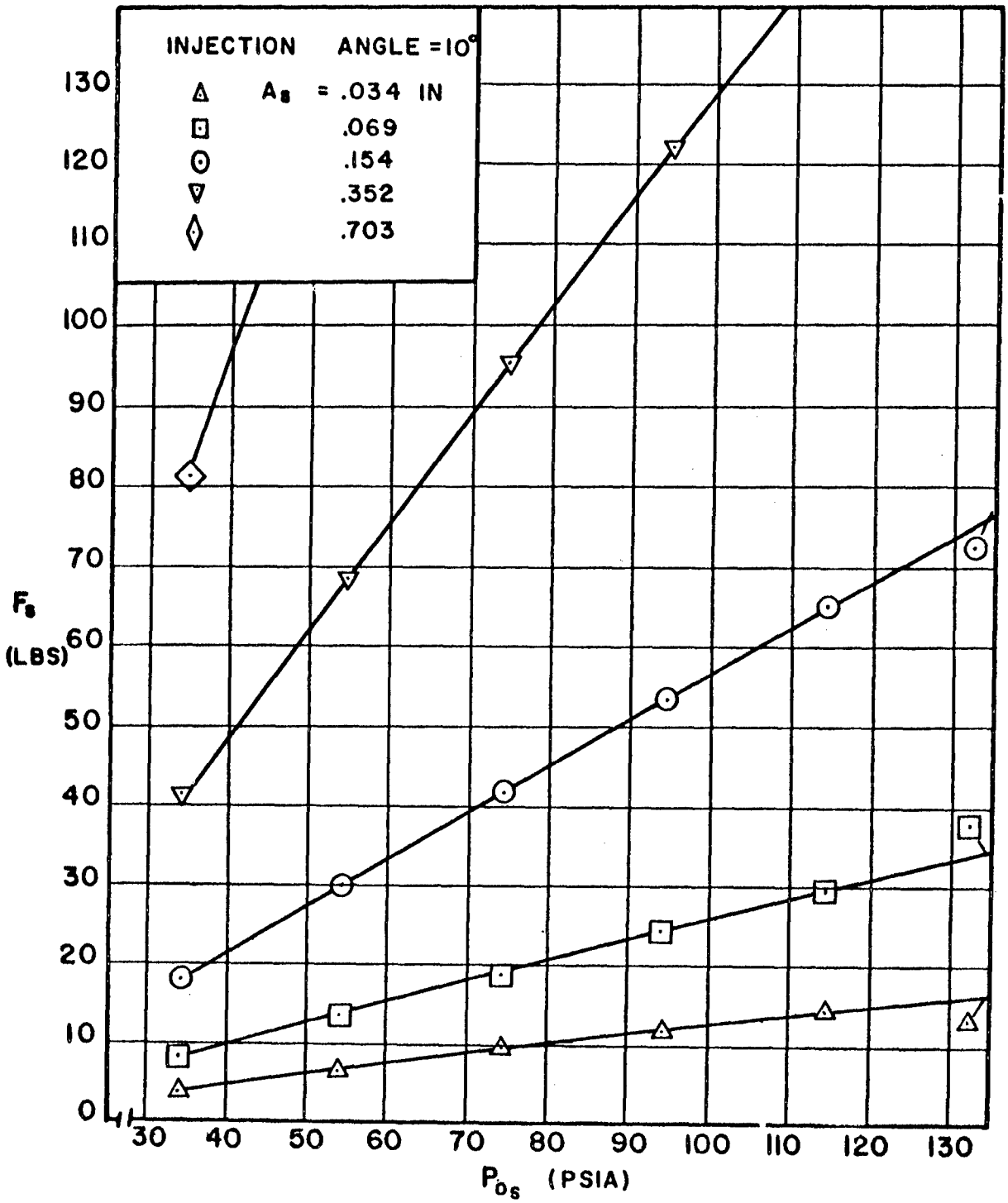

FIG. 33 EFFECT OF P_{os} ON F_s WITH A_s AS PARAMETER ($\epsilon = 10°$) (BROADWELL)

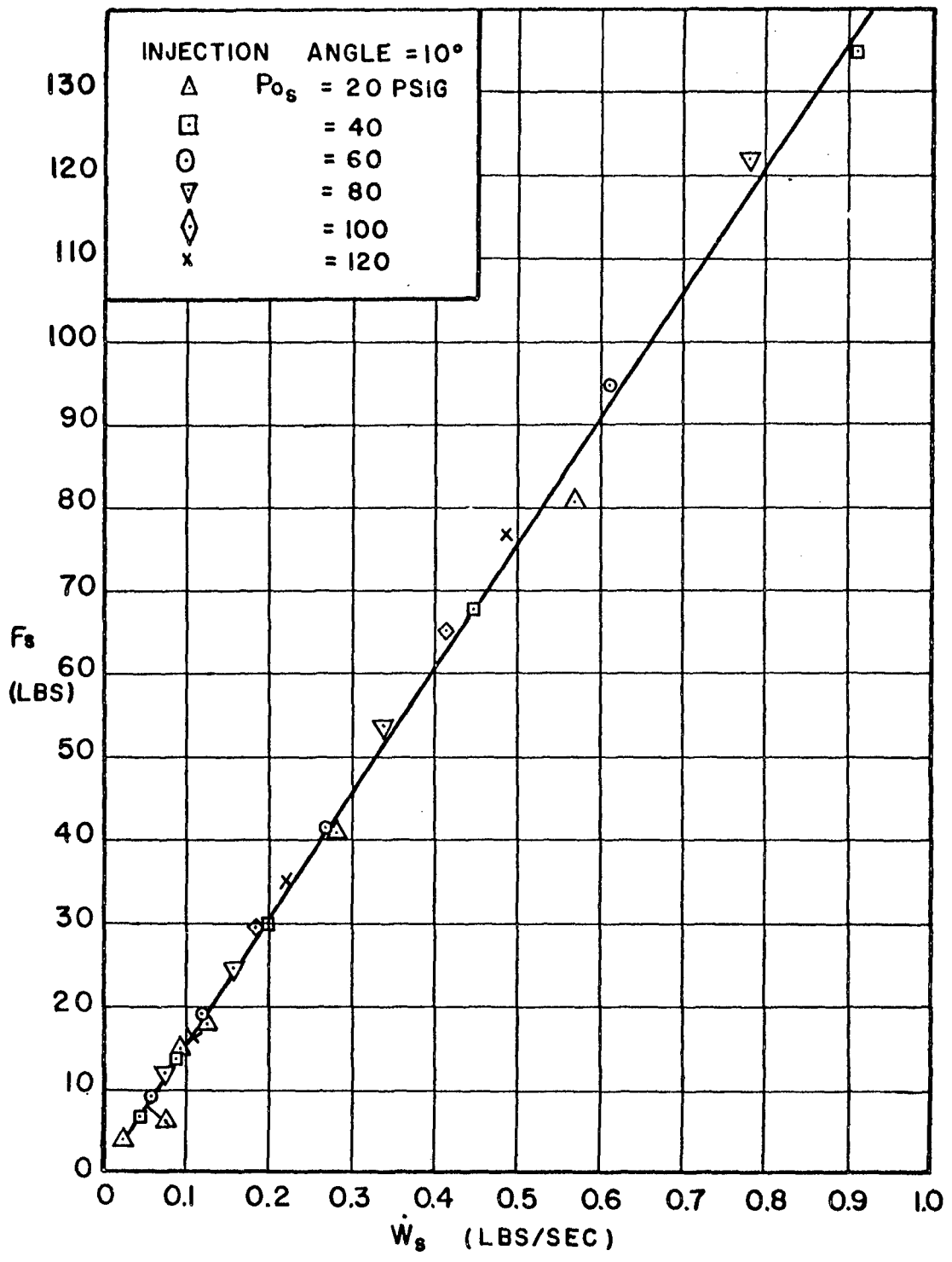

FIG. 34. EFFECT OF W_s ON F_s WITH P_{os} AS PARAMETER ($\epsilon = 10°$) (BROADWELL)

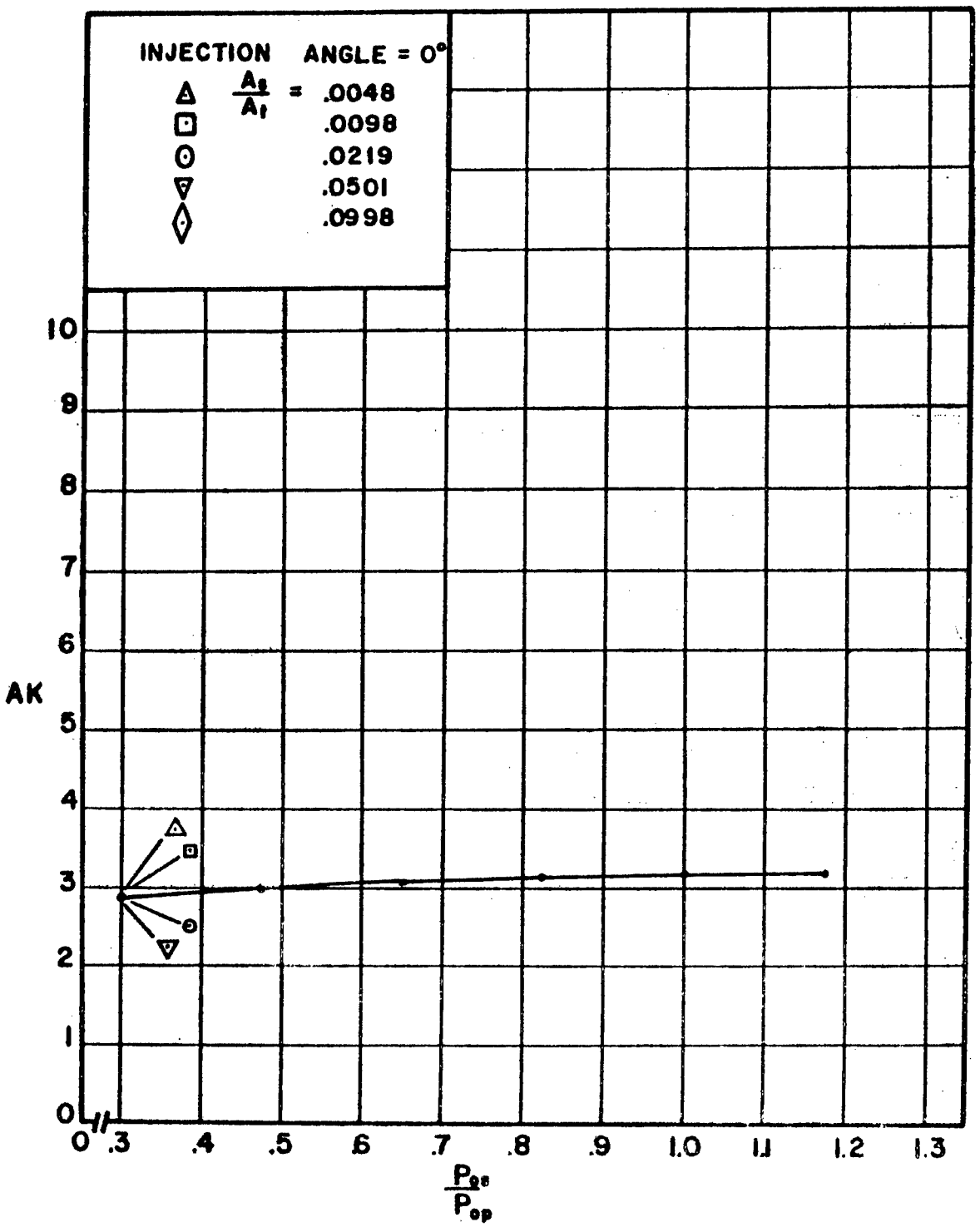

FIG. 35 EFFECT OF P_{os}/P_{op} ON AK WITH A_s/A_f AS PARAMETER ($\epsilon = 0°$) (BROADWELL)

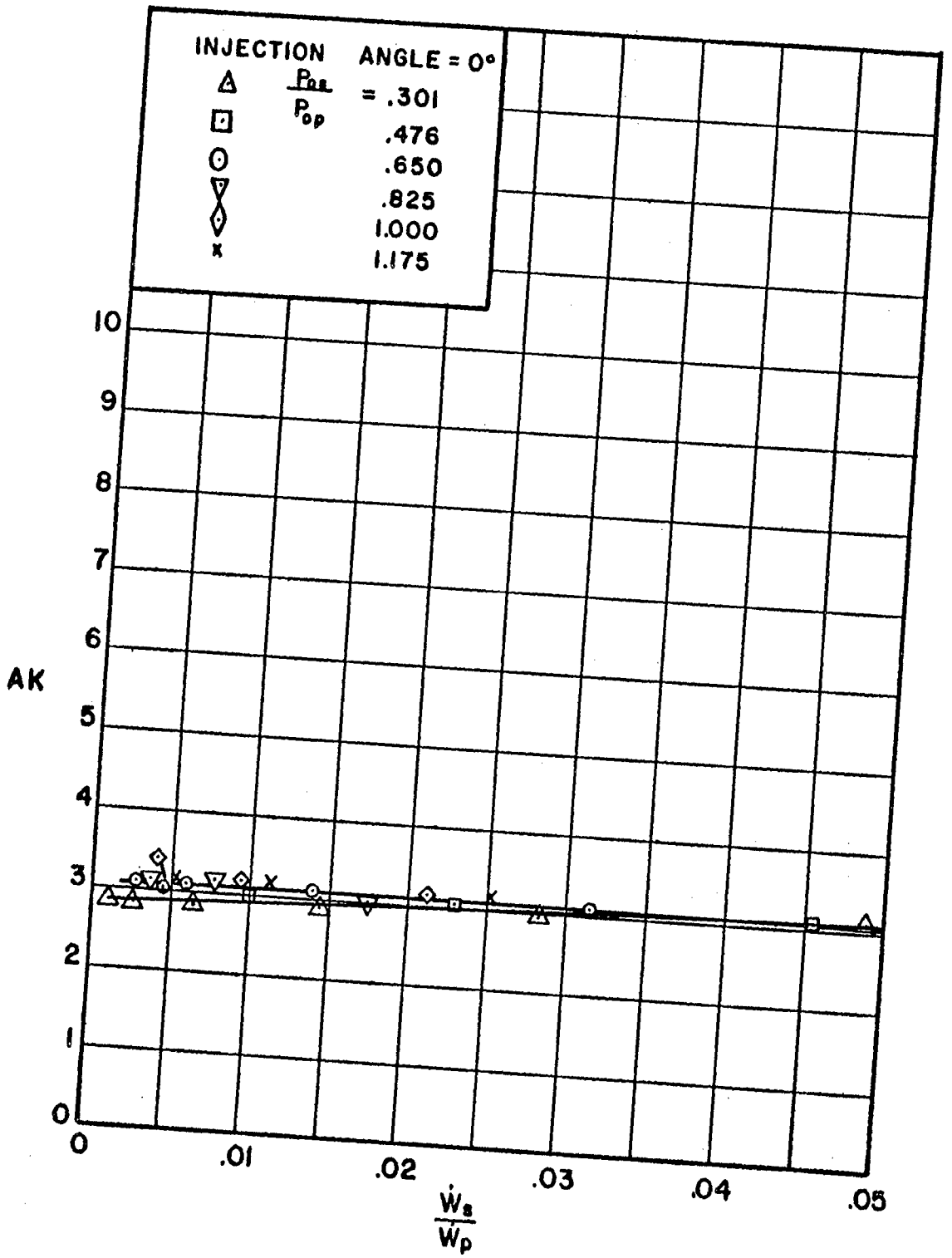

FIG. 36. EFFECT OF $\dot{W}_s/\dot{W}_p$ ON AK WITH P_{os}/P_{op} AS PARAMETER ($\epsilon = 0°$)
(BROADWELL)

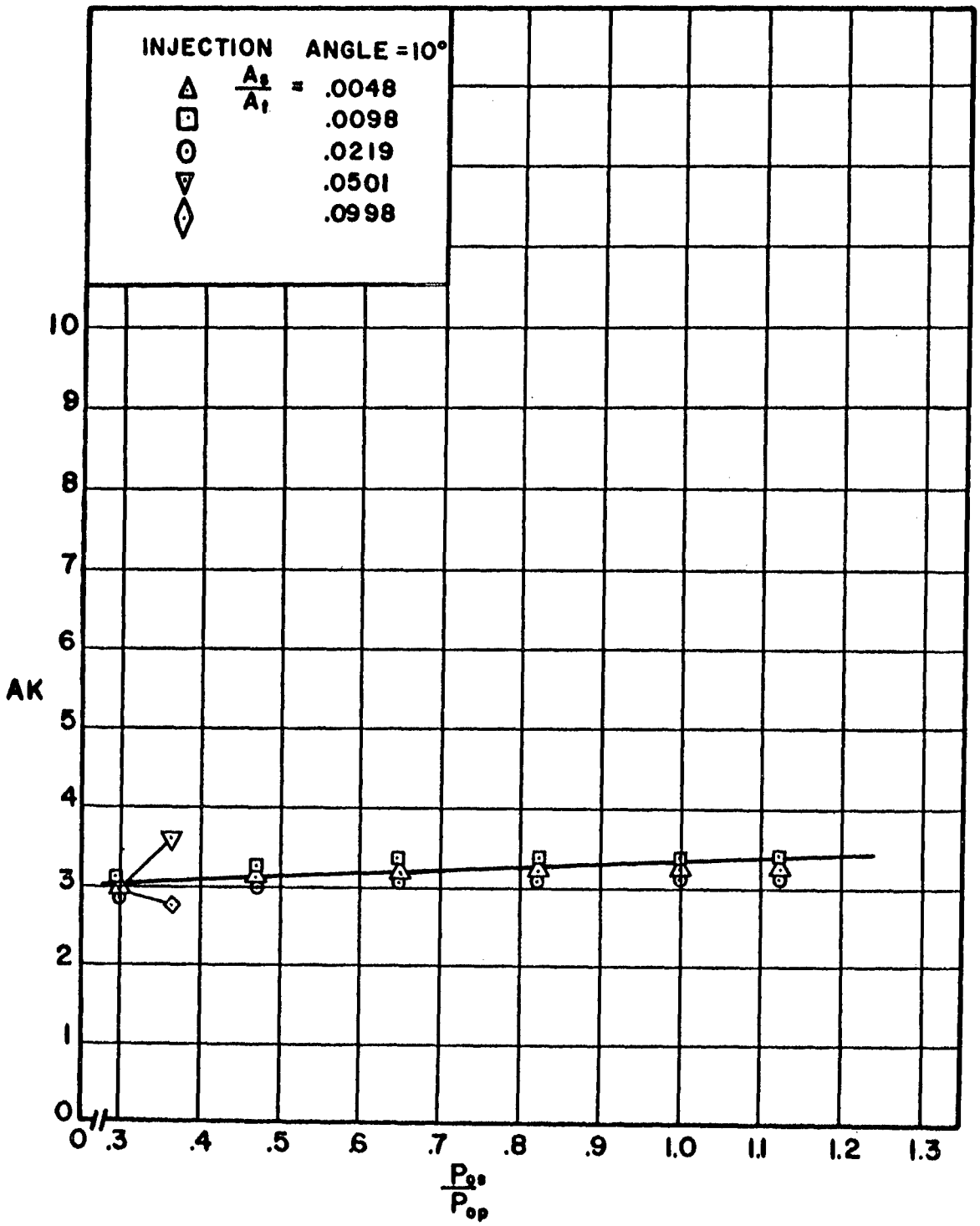

FIG. 37. EFFECT OF P_{os}/P_{op} ON AK WITH A_s/A_f AS PARAMETER ($\epsilon = 10°$)
(BROADWELL)

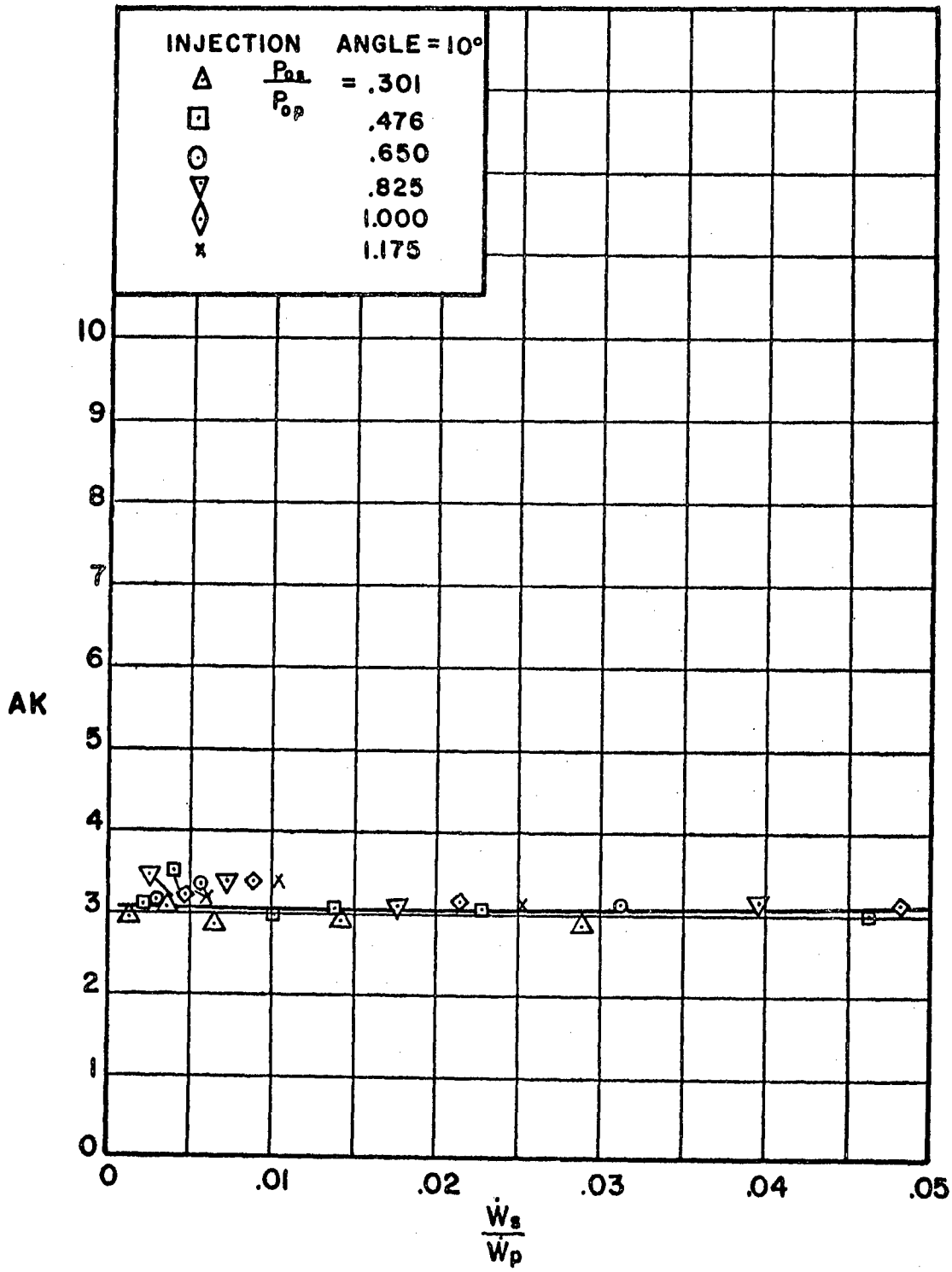

FIG. 38. EFFECT OF $\dot{W}_s/\dot{W}_p$ ON AK WITH P_{os}/P_{op} AS PARAMETER ($\epsilon = 10°$) (BROADWELL)

4.2 Comparison of Measured and Calculated Side Force Values

The results calculated on the basis of the appropriately modified theories due to Wu, et al. (5) and Broadwell (6) may be compared with the experimental results with respect to the influence of the following parameters on the estimated side force, F_s, or amplification factor, AK:

1. secondary stagnation pressure, P_{o_s},
2. injection slot area, A_s,
3. secondary stream weight flow rate, $\dot{W}_s$, and
4. the angle of injection, ϵ.

The influence of the secondary stagnation pressure as determined by theory may be compared with the experimental results by reference to Fig. 39 where the side force, F_s, is plotted versus the secondary stagnation pressure, P_{o_s}, with the injection slot area, A_s, as parameter, for normal injection.

Figure 40 presents the amplification factor, AK, plotted versus the ratio of secondary to primary stagnation pressures, P_{o_s}/P_{o_p}, with the ratio of the secondary slot area to the primary throat area, A_s/A_t, as parameter, for normal injection.

Figures 41 and 42 present the corresponding results for injection at an angle of 10^o measured upstream from a normal to the nozzle axis.

Comparison of the theoretical and experimental curves yields the following results.

1. F_s versus P_{o_s} for different A_s.

   a. For large slot areas Broadwell's theory predicts higher

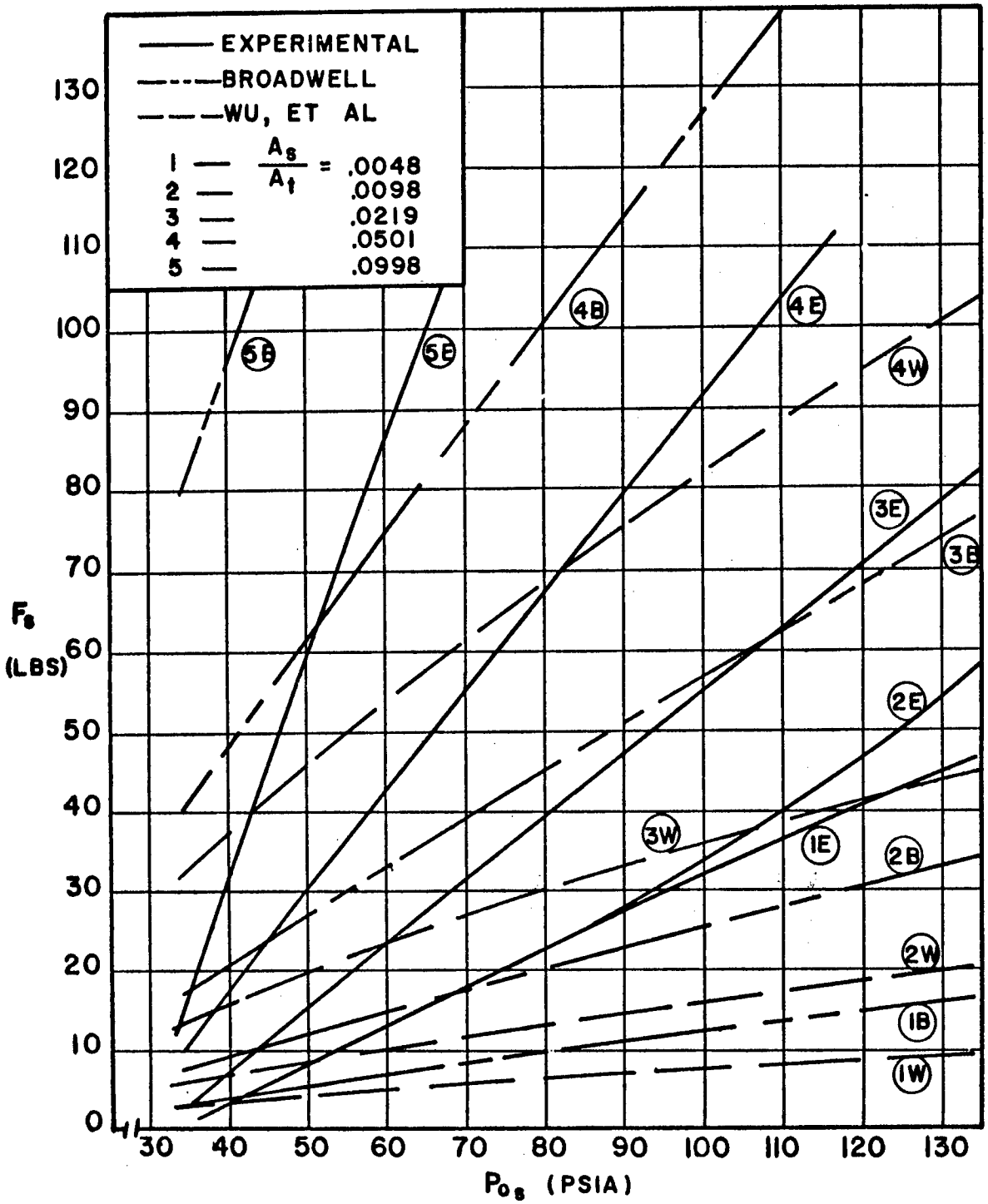

FIG. 39 EFFECT OF P_{o_s} ON F_s WITH A_s AS PARAMETER ($\epsilon = 0°$)

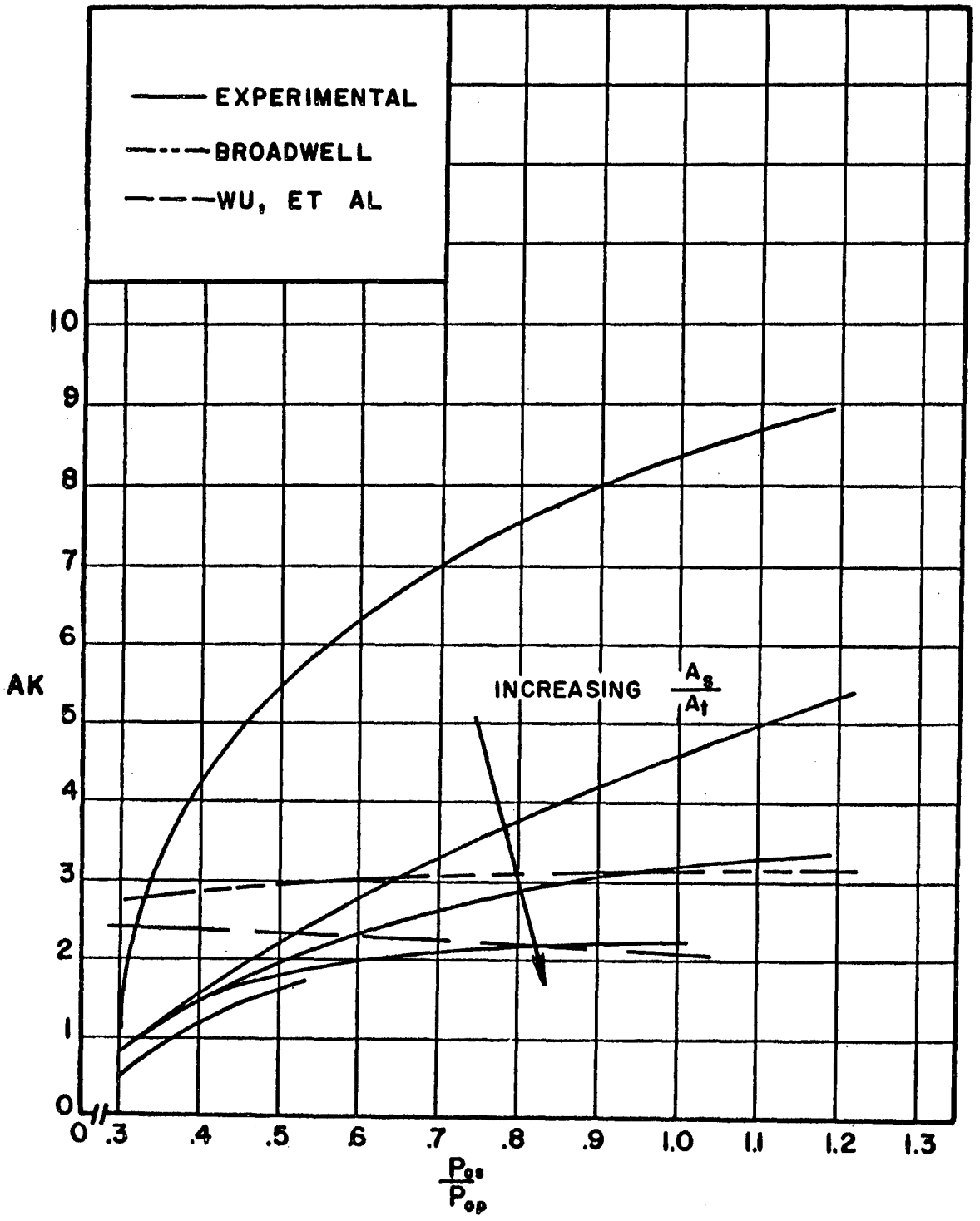

FIG. 40 EFFECT OF P_{os}/P_{op} ON AK WITH A_s/A_t AS PARAMETER ($\epsilon = 0°$) THEORY AND EXPERIMENT

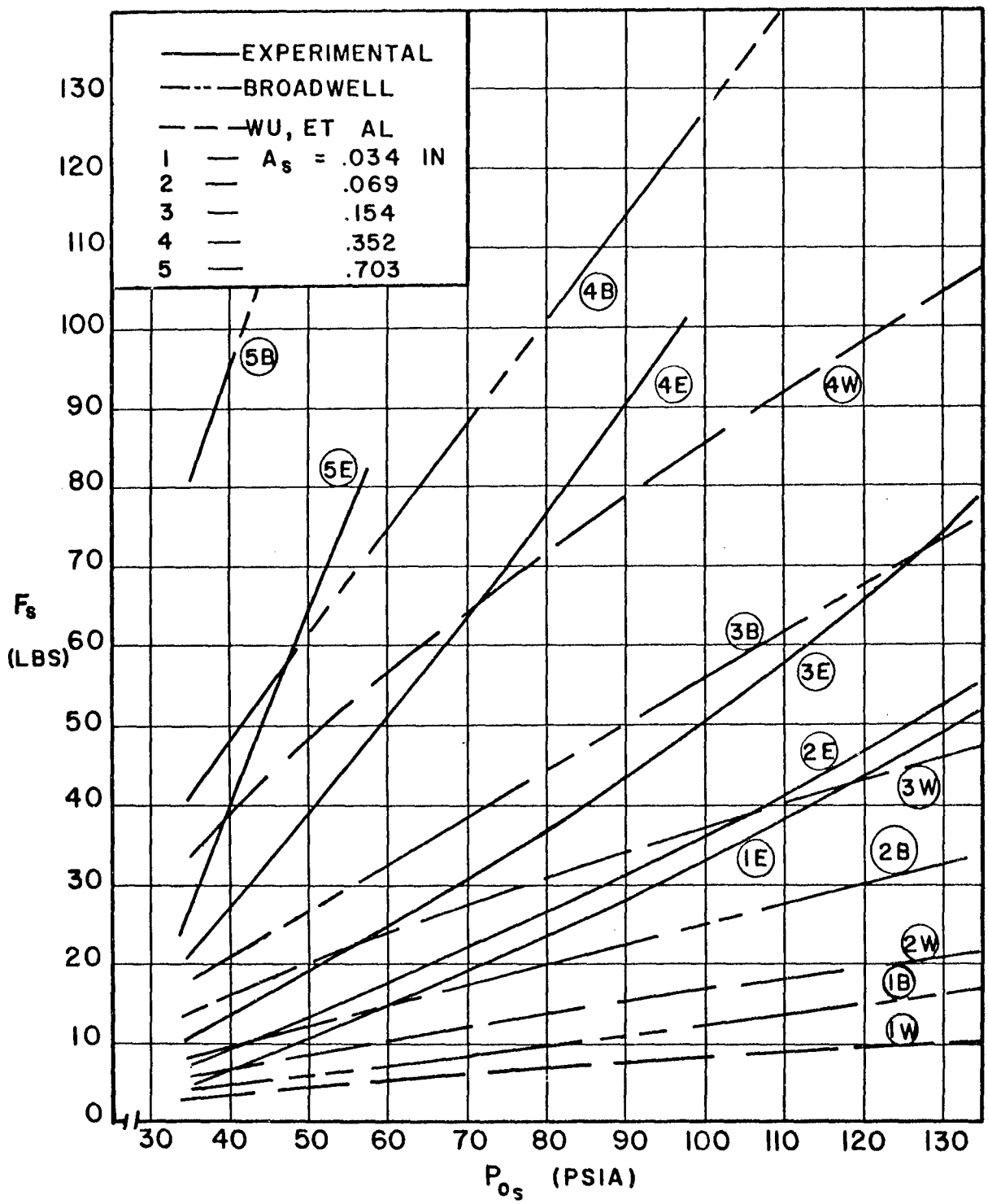

FIG. 41 EFFECT OF P_{os} ON F_s WITH A_s AS PARAMETER ($\epsilon = 10°$) THEORY AND EXPERIMENT

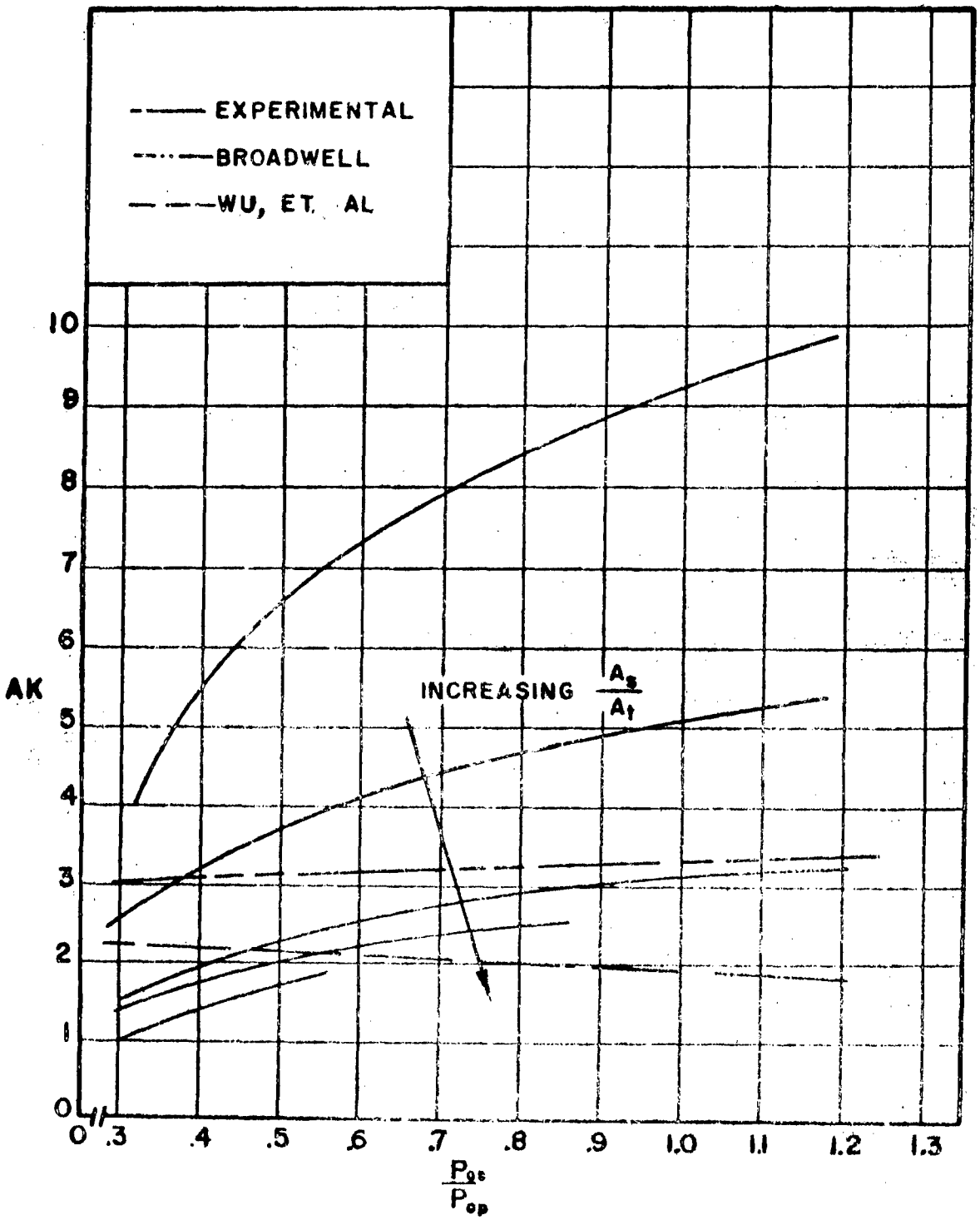

FIG. 42 EFFECT OF P_{os}/P_{op} ON AK WITH A_s/A_f AS PARAMETER ($\epsilon = 10°$) THEORY AND EXPERIMENT

values of side thrust than measured experimentally (see curves (5E), and (5B), in Fig. 39). As the slot area is decreased the experimental and theoretical side force values approach each other. As the slot area is decreased further Broadwell's theory predicts lower values of side force than are measured experimentally (see curves (1E), and (1B), in Fig. 39).

b. The theory of Wu, et al breaks down for the largest slot area examined experimentally. The largest slot area for which the analysis of Wu, et al produces results also is the slot area which compares most favorably with experimental results (see curves (4E) and (4W) in Fig. 39). For smaller values of slot area the results agree less favorably as evidenced by curves (1E) and (1W) in Fig. 39.

2. F_s versus P_{o_s} for different ϵ. The angle of injection, ϵ, has the following effect on the two theories.

a. Side force decreases as the angle of injection is increased due to the theory of Broadwell.

b. Side force increases as the angle of injection is increased according to the theory due to Wu, et al.

Since experimental results indicate that the side force increases as the angle of injection is increased it is apparent that Broadwell's theory is not in qualitative agreement with the experimental results while the analysis by Wu, et al does agree qualitatively, although not quantitatively, with the

experimental results concerning the effect of the angle of injection of the secondary gas.

3. AK versus P_{o_s}/P_{o_p} for different A_s/A_t. Neither theory shows the dependence of the slot area on the amplification factor for a given secondary to primary stagnation pressure ratio as is seen in the experimental results (see Fig. 40). It is noted that, for the range of pressures investigated, the amplification factor remains fairly constant for both theories, Wu's analysis predicting a slightly decreasing amplification factor with increasing secondary stagnation pressure and Broadwell's analysis predicting a slightly increasing amplification factor for an increasing secondary stagnation pressure. The same general conclusions can be made for injection 10° upstream.

The influence of the weight flow rate of the secondary stream as determined from theory may be compared with the results of the experiments by reference to Figs. 43 through 46. These figures also indirectly reveal the influence of the secondary slot area.

Figure 43 presents the side force, F_s, plotted versus the secondary weight flow rate, $\dot{W}_s$, with the secondary stagnation pressure, P_{o_s}, as parameter, for injection normal to the axis of the primary nozzle.

Figure 44 presents the amplification factor, AK, versus the ratio of the secondary to primary weight flow rates, $\dot{W}_s/\dot{W}_p$, with secondary to primary stagnation pressure ratio, P_{o_s}/P_{o_p}, as parameter, for normal injection.

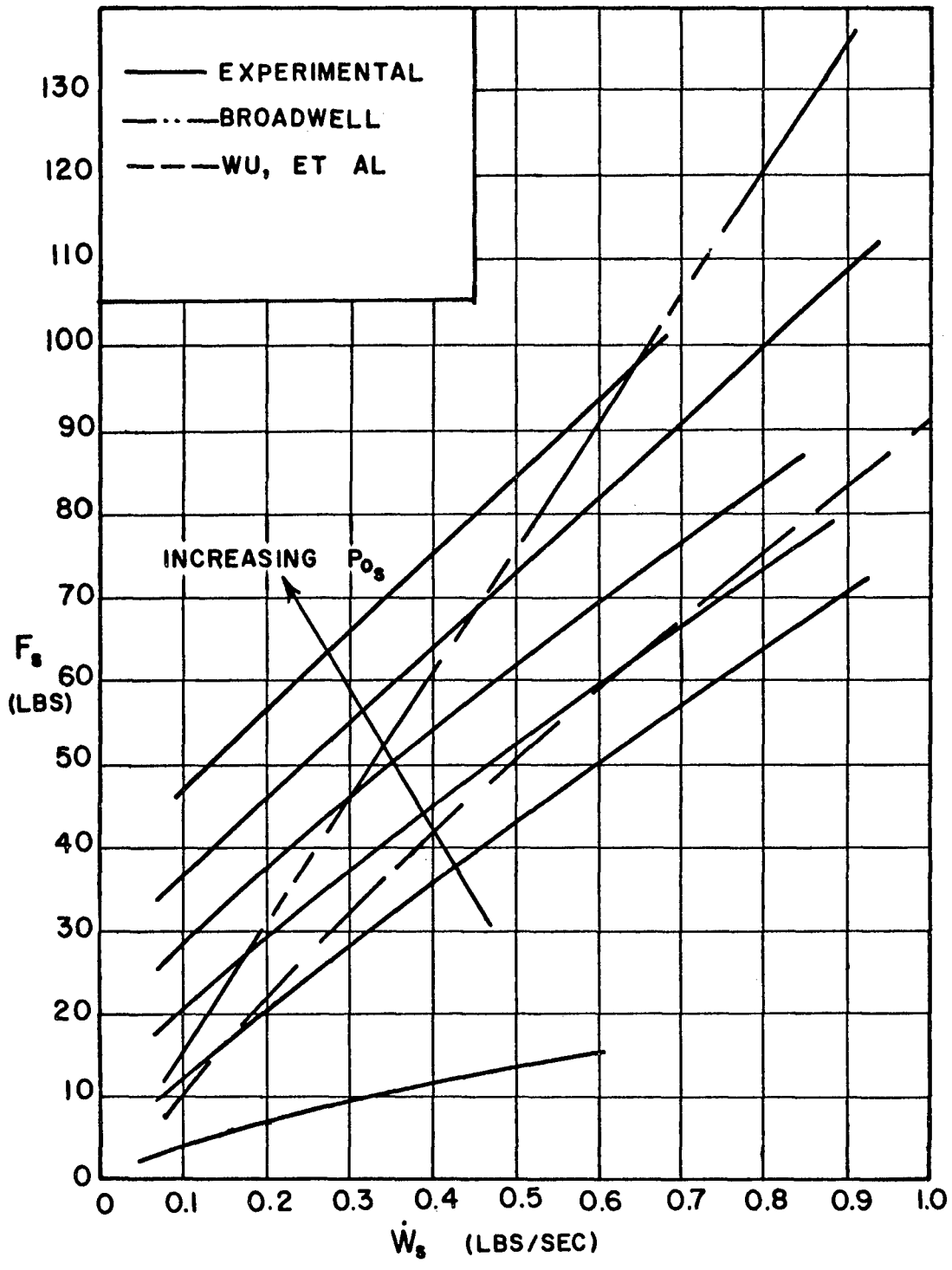

FIG. 43 EFFECT OF $\dot{W}_s$ ON F_s WITH P_{os} AS PARAMETER ($\epsilon = 0°$) THEORY AND EXPERIMENT

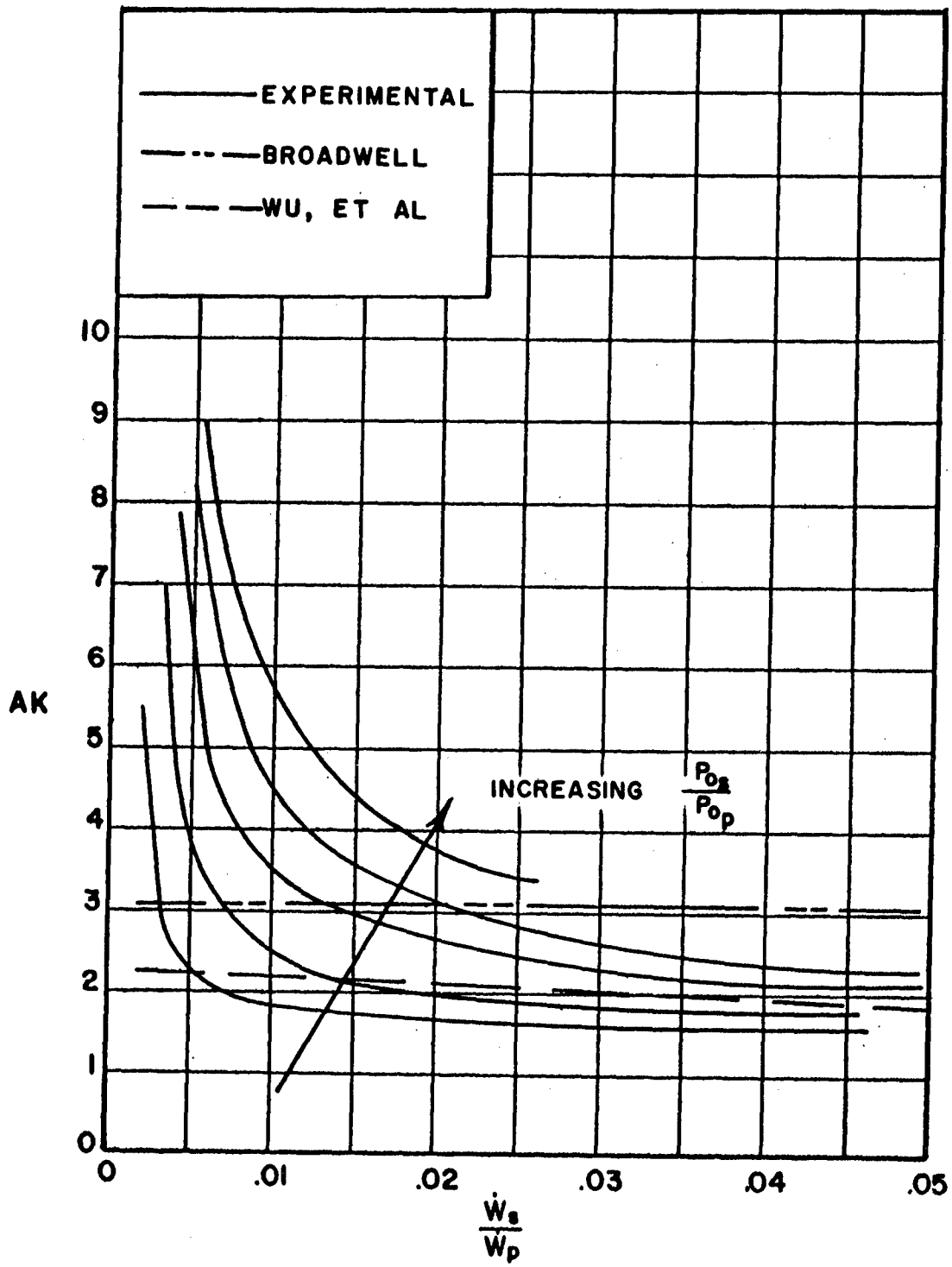

FIG. 44 EFFECT OF $\dot{W}_s/\dot{W}_p$ ON AK WITH P_{os}/P_{op} AS PARAMETER ($\epsilon = 0°$) THEORY AND EXPERIMENT

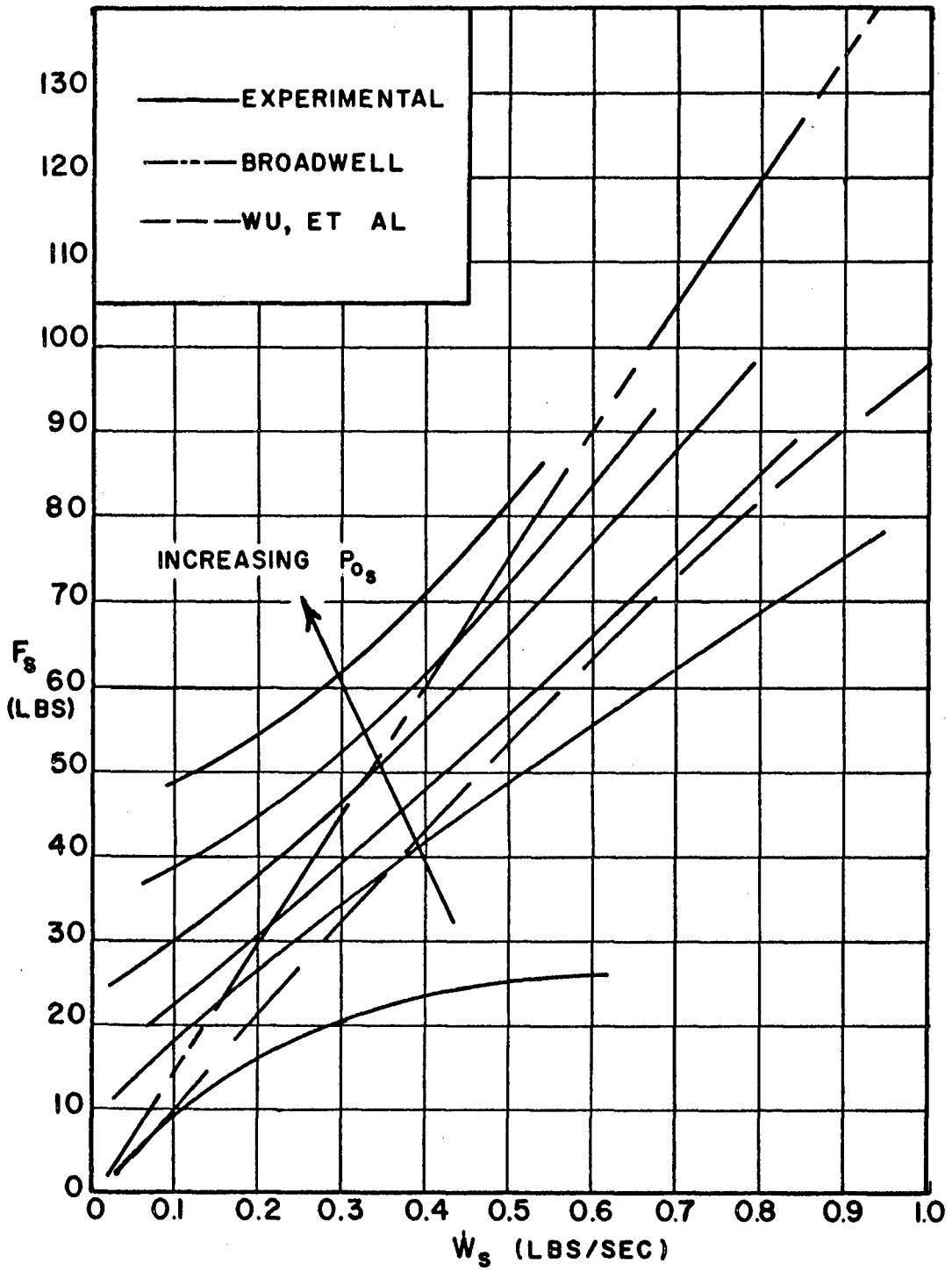

FIG. 45 EFFECT OF $\dot{W}_s$ ON F_s WITH P_{0s} AS PARAMETER ($\epsilon = 10°$) THEORY AND EXPERIMENT

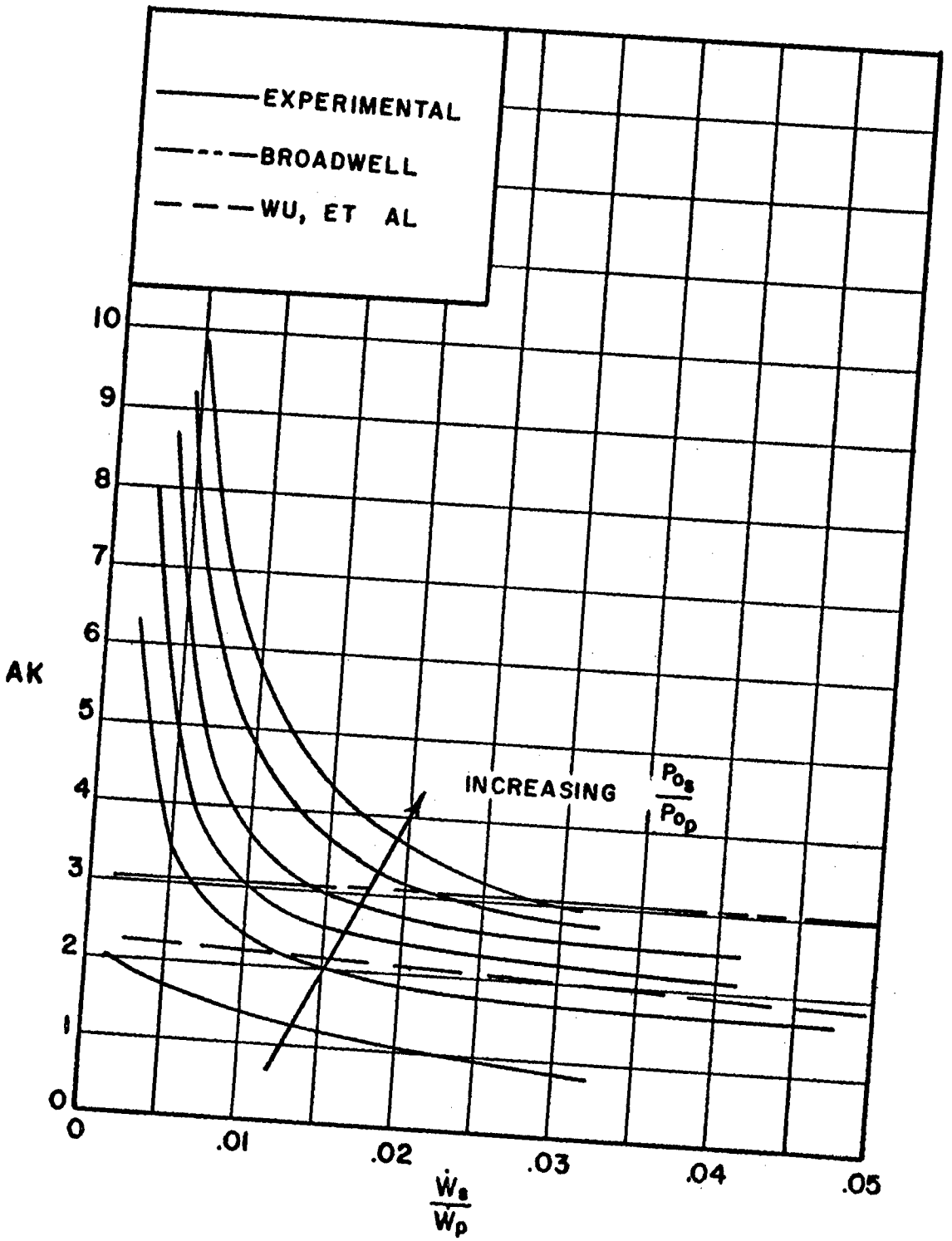

FIG. 46 EFFECT OF $\dot{W}_s/\dot{W}_p$ ON AK WITH P_{os}/P_{op} AS PARAMETER ($\epsilon = 10°$) THEORY AND EXPERIMENT

Figures 45 and 46 present the corresponding results for injection at an angle of 10° measured upstream of a normal to the nozzle axis.

Comparison of the theoretical and experimental curves yields the following results.

1. F_s versus $\dot{W}_s$ for different P_{o_s}. The two theories presented herein do not show the same dependence of the secondary stagnation pressure on the side force produced for given values of the secondary weight flow rate that is evident in the experimental results. With reference to Fig. 43 it is noted that experimentally determined values of side force are greater than those of theory for high secondary stagnation pressures and less for low secondary stagnation pressures. It appears that at a value of secondary stagnation presure of approximately 70 psia the theoretical and experimental results agree. The same general remarks pertain to injection at 10° upstream of a normal to the nozzle axis.
2. AK versus $\dot{W}_s/\dot{W}$ for different P_{o_s}/P_{o_p}. The effect of the secondary to primary stagnation pressure ratio that is apparent in the experimental results is not predicted by either of the two theories as is evident in Fig. 44. It appears that as the secondary weight flow rate is increased the theoretical and experimental values of the amplification factor agree more closely. The same general conclusions are applicable to injection at an angle of 10° upstream.

5. CONCLUSIONS

While the experimental program reported herein needs further extension, several of the parameters affecting thrust vector control by secondary gas injection have been systematically investigated with the result that useful conclusions can be made regarding their importance. In addition, the calculated results based on both of the theories presently available for computing the side force produced under given operating conditions are compared with experiment to determine under what conditions they describe with reasonable correctness the influence of various parameters.

The following two sections present the conclusions that may be drawn from the experimental and the theoretical results. Some further investigations, both experimental and theoretical are suggested in Section 5.3.

5.1 Experimental Results

From the results of the diagnostic observations and the detailed measurements of flow parameters, the following conclusions may be stated.

1. No particular flow pattern can be identified as being universally applicable in the region upstream of the point of injection. Such an absence of a typical pattern of flow is noticeable when only the weight flow rate of the secondary gas is changed, all other parameters remaining constant.
2. When the weight flow rate of the secondary gas is small, up to one percent of the primary weight flow rate, the shock appears to originate immediately upstream of the point of injection with a small associated separated region.
3. When a definite shock formation is observed, for secondary weight flow rates greater than one percent of the primary weight flow rate, the shock (for the two-dimensional case) pattern produced is made up of a strong oblique shock originating at the upstream edge of the separated region, a weaker oblique shock originating near the point of maximum penetration of the secondary jet into the primary stream and an oblique shock originating downstream of the injection slot.
4. The position of the shock system produced by the injection of a secondary gas into a supersonic stream is governed by the momentum of the secondary jet, all other parameters remaining constant.
5. The pressure in the separated region is not constant, except perhaps when the secondary gas static pressure at the entrance

to the primary nozzle is equal to the boundary layer separation pressure.

6. The amplification factor, defined as the ratio of the effective specific impulse of the secondary stream to the specific impulse of the undisturbed primary stream,
   a. decreases as the weight flow rate increases, for a constant secondary stagnation pressure,
   b. increases as the secondary stagnation pressure increases, for a constant injection slot area,
   c. increases as the angle of injection measured upstream of a normal to the axis is increased, all other parameters remaining constant, and
   d. from exploratory results of experiments conducted with helium as the injectant, increases as the ratio of the secondary gas to primary gas molecular weight decreases, which would be expected.

5.2 Theoretical Models in Relation to Diagnostic Test Results

The following conclusions may be made regarding the theoretical models proposed in Section 1.1.

1. For reasonably large flow rates of the secondary fluid, which may be employed in practical thrust vector control schemes, the method of computing the side force as given by Wu, et al (1961)(5) appears to be the most satisfactory to date.

2. In such conditions as stated under item 1, it is still necessary to modify the model in the light of
   a. the modifications to the shock pattern as observed by Charwat and Allegre (1964)(9) and
   b. the modifications that are necessary in the mixing zone downstream of the point of injection.
3. When the flow rate is considerably reduced below that considered in item 1, the model due to Zukoski and Spaid (1964)(8) appears to be satisfactory.
4. The linearized flow model due to Walker, et al (1962)(2) is applicable only for extremely small flow rates of the secondary gas.

5.3 Suggested Further Investigations

The parametric analysis established that, in addition to the parameters investigated and reported herein, the axial position of injection (or freestream Mach number at the point of injection) and the secondary gas properties are influential in determining the effectiveness of gaseous secondary injection thrust vector control. Therefore, the effect of those parameters should be investigated.

Several modifications of the experimental apparatus should be made, however, before further experiments are conducted. These modifications and/or additions are as follows.

1. The number of wall pressure taps both upstream and downstream of the injection slot should be increased to facilitate:
   a. upstream - determination of the point of boundary layer

separation and a more accurate determination of the pressure distribution in the separated region, and

b. downstream - a more accurate determination of the static pressure immediately downstream of the port and in the region of the apparent origin of the downstream shock to provide information as to the cause of this shock (it may be recalled that in Section 3.1 the shock was attributed to either boundary layer separation due to the adverse pressure gradient and/or the supersonic flow being turned by the wall).

2. Appropriate static and total pressure probes should be included at the exit plane of the nozzle to determine what effect injection of a secondary gas has on the axial thrust of the nozzle.

3. Devices for the measurement of the concentration of the secondary stream should be added. Those measurements, together with visual observations, will contribute to a better understanding of the mixing taking place and the ability or inability of the primary flow to turn the injected gas back toward the wall

It may be surmised that with such additional data, more appropriate theoretical models may be determined and identified for different flow conditions.

BIBLIOGRAPHY

1. Walker, R. E., Stone, A. R., and Shandor, M., "Secondary gas injection into a conical rocket nozzle. I. Effect of orifice diameter and molecular weight of injectant," Johns Hopkins Univ., Applied Physics Lab., Rept. CM - 1010 (February 1962).

2. Walker, R. E., Stone, A. R., and Shandor, M., "Interaction between sonic side jets and supersonic duct flow," Johns Hopkins Univ., Applied Physics Lab., Bumblebee Rept. 316 (December 1962).

3. Walker, R. E., Stone, A. R., and Shandor, M., "Secondary gas injection into a conical rocket nozzle," AIAA J. 1, 334-338 (1963).

4. Walker, R. E. and Shandor, M., "Influence of injectant properties for fluid injection thrust vector control," AIAA Solid Propellant Rocket Conference Preprint 64 - 112 (January 1964).

5. Wu, J. -M., Chapkis, R. L., and Mager, A., "An approximate analysis of thrust vector control by fluid injection," ARS J. 31, 1667-1685 (1961).

6. Broadwell, J. E., "An analysis of the fluid mechanics of secondary injection for thrust vector control (revised)," Space Technology Labs. Rept. 6120 - 7744- MU - 000 (March 1962).

7. Broadwell, J. E., "Correlation of rocket nozzle gas injection data," AIAA J. 1, 1911-1913 (1963).

8. Zukoski, E. E. and Spaid, F. W., "Secondary injection of gases into a supersonic flow," AIAA J. 2, 1689-1696 (1964).

9. Charwat, A. F. and Allegre, J., "Interaction of a supersonic stream and a transverse supersonic jet," AIAA J. 2, 1965-1972 (1964).

10. Mager, A., "On the model of the free, shock-separated, turbulent boundary layer," J. Ae. Sc. 23, 181-184 (1956).

11. Murthy, S. N. B., "The upstream effects due to injecting a jet of gas through the wall of an axi-symmetric nozzle," Purdue Univ., Jet Propulsion Center Report No. TM - 63 - 3 (January 1963).

12. Thompson, H. D., Hoffman, J. D., and Murthy, S. N. B., "Note on a parametric analysis of thrust vector control by secondary gas injection," Purdue Univ., Jet Propulsion Center Report No. TM - 63 - 5 (February 1963).

13. Sherwood, T. K. and Reed, C. E., Applied Mathematics in Chemical Engineering, New York, McGraw-Hill, 1939.

14. Thompson, H. D., "Design procedure for optimization of rocket motor nozzles," Purdue Univ., Jet Propulsion Center Report No. TM - 63 - 6 (May 1963).

15. Akpinar, A., "Supersonic turbine blades - performance estimation," M.S.M.E. Thesis, Purdue University (January 1963).

APPENDICES

APPENDIX I

NOTATION

A_s	=	injection slot area
AK	=	amplification factor
F_1	=	side force contribution from blast wave analysis
F_j	=	momentum thrust of secondary jet
F_s	=	side force
I_s/I_s^*	=	ratio of effective specific impulse of injectant to specific impulse of injectant for sonic flow into a vacuum
K	=	emperical constant = 0.55
M	=	Mach number
M_1, M_p	=	Mach number of primary stream at point of injection
P_o	=	stagnation pressure
R	=	radius of nozzle wall curvature at the throat
R/D	=	ratio of induced shock wave radius at exit plane of nozzle to duct diameter
SW	=	injection slot width
T_o	=	stagnation temperature
V	=	gas velocity
$\dot{W}$	=	weight flow rate
$(\dot{W}_j/\dot{W})^*$	=	weight flow ratio to choke supersonic steam
X	=	axial length of separated region upstream of injection port

a	=	acoustic velocity
h	=	penetration height of secondary gas into supersonic stream
ℓ	=	axial distance from injection slot to exit plane of nozzle
$\dot{m}$	=	mass flow rate
p	=	static pressure
x,y	=	coordinates of nozzle

Greek Symbols

α	=	Mach angle
δ	=	oblique shock angle
ϵ	=	angle of injection measured upstream from a normal to the nozzle axis
γ	=	specific heat ratio
m	=	molecular weight

Subscripts

a	=	ambient conditions
bl	=	boundary layer separation conditions
e	=	conditions at exit plane
l,p	=	primary stream conditions
j,s	=	secondary stream conditions
o	=	stagnation conditions
t	=	conditions at the throat

APPENDIX II

SUPERSONIC NOZZLE DESIGN

A uniform discharge, Mach 2.0, two-dimensional nozzle was employed for the secondary injection studies. The nozzle was designed to produce an exit section with a height of 6 inches and a uniform width of 2 inches.

Several methods are available for two-dimensional perfect nozzle design. The more accepted theories are included in a report by Thompson (14) along with axi-symmetric perfect nozzle design and optimization techniques for axisymmetric nozzles.

The choice of theories to be used was somewhat arbitrary. Previous nozzle designs at this laboratory (15) indicated that Foelsch's method of design was superior to Friedrich's method in the supersonic portion of the nozzle. Therefore, the nozzle was divided into three regions (see Fig. 47) for design purposes as follows:

1. subsonic to sonic contour by Friedrich's method,
2. initial expansion to obtain radial source flow at the inflection point by simple wave theory, and
3. the straightening portion to obtain parallel uniform Mach 2.0 flow at the exit section by Foelsch's method.

The three regions will be discussed separately in the following sections.

Before discussing the design it should be noted that calculations

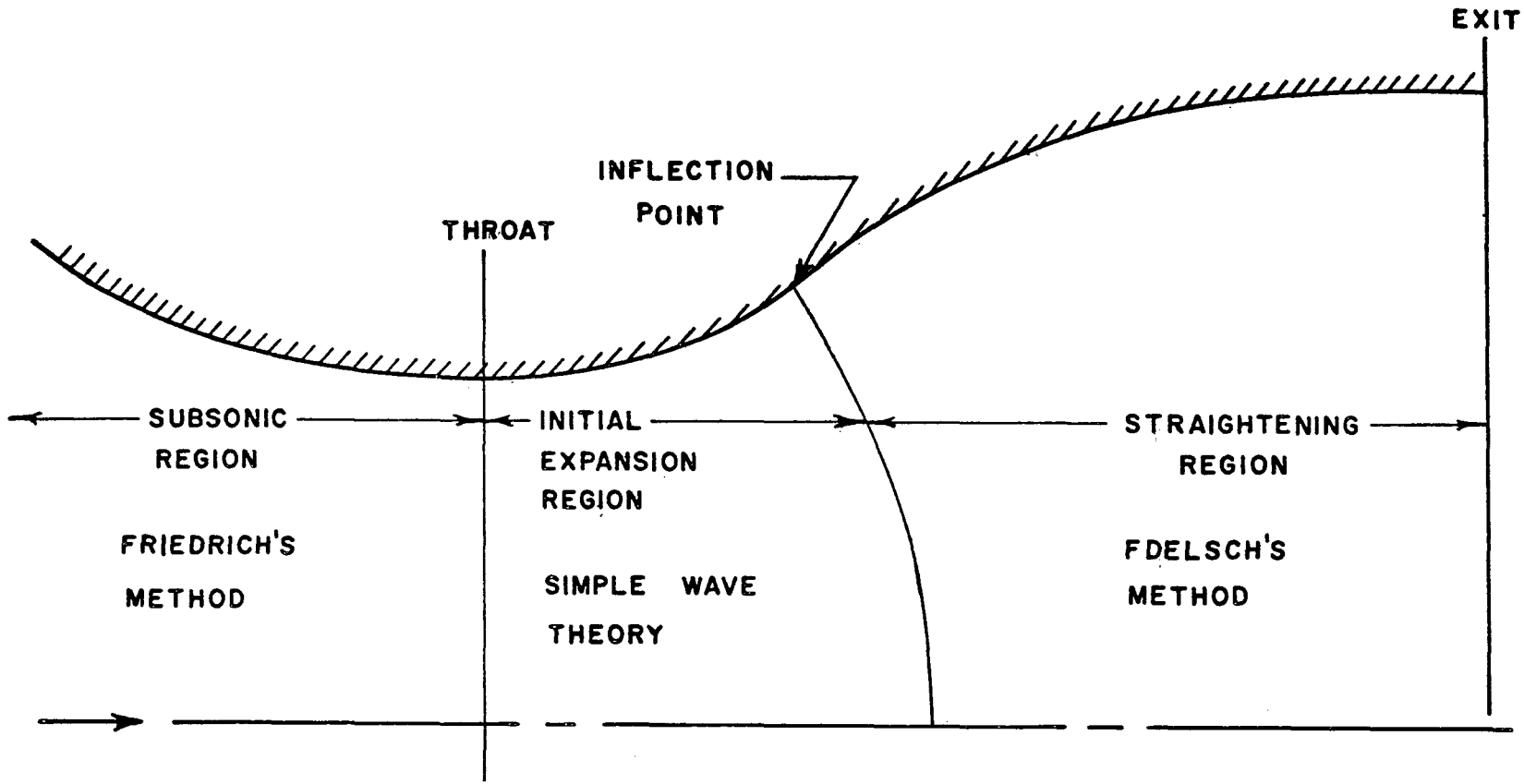

FIG. 47 DIVISION OF NOZZLE FOR ANALYSIS

were made on the IBM 7090 computer with results being obtained in the form of the x coordinate (axial) as the independent variable with the y coordinate, design Mach number and slope with respect to the x axis as dependent variables.

Determination of the Subsonic to Sonic Nozzle Contour (Friedrich's Method)

The Friedrich's method for perfect nozzle design is based on assuming a somewhat arbitrary velocity distribution along the nozzle axis and expressing the state properties of the flow field adjacent to the axis in terms of a series.

The method consists essentially of applying a necessary correction to a one-dimensional compressible flow analysis to account for the two-dimensional effect introduced by the use of a finite length. These corrected equations are in the form of a power series whose first terms are the one-dimensional approximations.

The equations obtained will not be repeated here. The reader is referred to reference (14) for a complete listing of the pertinent equations. Although algebraic, these equations are quite complicated but ideally suited for computer calculation.

Determination of the Initial Expansion Section

The use of Foelsch's method for the straightening portion of the nozzle wall contour assumes the existence of source flow on a circular arc passing through the inflection point I-I' (see Fig. 48) with the apparent center of the source flow at point O. The shape of the

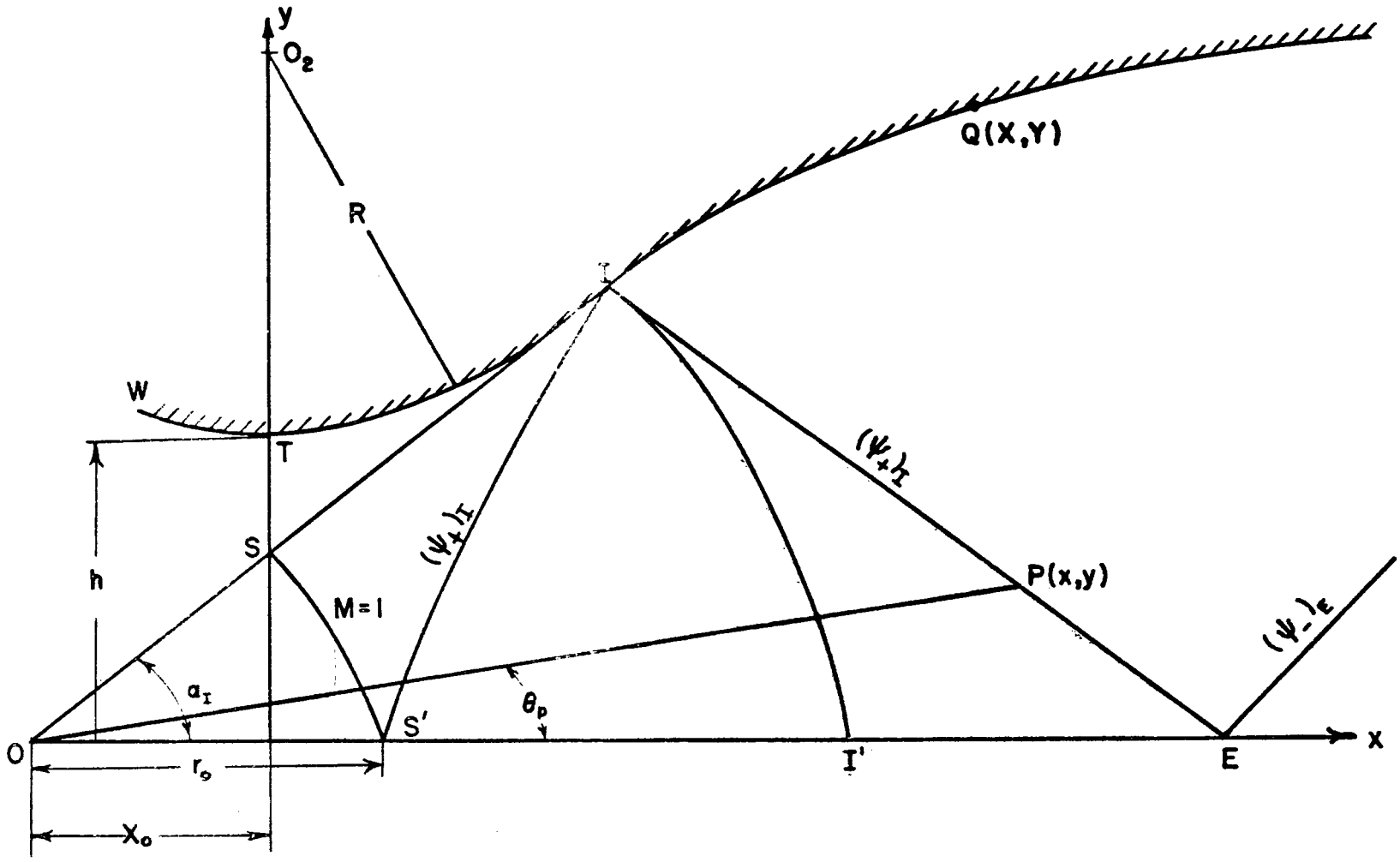

FIG. 48 INITIAL EXPANSION REGION OF THE NOZZLE

expansion contour should be such that:

1. it turns the flow a sufficient amount to give the desired conditions at the arc I-I',
2. it produces a flow which is as near to source flow as possible at the arc I-I', and
3. at point I, as well as at the throat, the nozzle coordinates, slopes, and Mach numbers match with these same parameters calculated with the aid of Foelsch's and Friedrich's method, respectively.

It may be recalled that to each point in a supersonic flow there is assigned a turning angle which is the sum of the characteristics through that point. It may be shown that (for the two-dimensional case) the shortest possible perfect nozzle may be obtained if the angle, α_1, (see Fig. 48) is one-half the turning angle assigned to the Mach number at the exit section of the nozzle. In other words the angle the contour makes with respect to the x axis at the inflection point, I, must be equal to or greater than one-half the total turning angle assigned to the exit Mach number. For the nozzle design reported herein the minimum value was employed.

Referring to Fig. 48, OSII'S' is the region of source flow with the origin at O and the sonic line the arc S-S'. It is apparent that the sonic line in a nozzle is not curved as is the arc SS'. It may be assumed that the sonic line produced by Friedrich's method is straight. The conversion of the circular flow section into a plane flow section may be accomplished by bending the portion of the nozzle wall adjacent

to the throat into any smooth convex curve WTI tangent to the rest of the wall at I and having at the throat a tangent parallel to the x axis. For continuity reasons the cross-sectional area at the throat must be equal to the area of the circular section.

It is convenient to let the curve WTI in Fig. 48 be the arc of a circle having radius R and center at O_2. R can then be chosen thereby locating point I. For the design reported herein the x coordinate of point I was chosen as 3 inches (with respect to the throat) which corresponded to a radius, R, of approximately 13 inches. Given R, the x coordinate of I and the slope of the contour at point I the coordinates of the expansion portion of the nozzle are known.

Although this region is not a simple wave region, approximate values of the Mach number corresponding to particular positions along the contour may be found by assuming simple wave flow. The equations employed for simple wave flow are reported in reference (14).

Foelsch's Method for the Straightening Portion

It is a general theorem that only a zone of simple waves may be patched to a uniform, parallel flow, i.e. the contour IQ... in Fig. 48 must be curved such that all left-running waves that strike it are cancelled. This is accomplished by curving the wall toward the nozzle axis, the curvature of the wall being the same as that of a streamline moving along the wall under the influence of waves from the opposite wall.

Since region EIQ... is a simple wave region it is a relatively simple task to determine the contour of the straightening portion of

the nozzle. The appropriate equations are presented in reference (14) and will not be repeated here.

Selected Coordinates of the Nozzle Contour

As was stated before the calculations were conducted using the IBM 7090 computer. Table 4 presents some selected coordinates of the nozzle along with the calculated Mach number and slope of the nozzle measured with respect to the nozzle axis. The values of the y coordinate are measured from the nozzle centerline so that in Table 4 the origin of the coordinate system is located at the intersection of the upstream edge and the centerline of the nozzle.

Table 4

Selected Coordinates of the Nozzle Contour

x (inches)	y (inches)	Mach Number	Wall angle with respect to axis (degrees)
0.0	2.500	0.461	
0.5	2.407	0.487	
1.0	2.319	0.513	
1.5	2.238	0.541	Not calculated
2.0	2.164	0.571	for subsonic
2.5	2.097	0.601	portion
3.0	2.036	0.634	
3.5	1.982	0.668	
4.0	1.933	0.704	
4.5	1.892	0.741	
5.0	1.857	0.780	
5.5	1.828	0.820	
6.0	1.806	0.862	
6.5	1.799	0.905	
7.0	1.781	0.949	
7.5	1.778	0.995	
7.552	1.778	1.000	0.0
8.0	1.785	1.130	1.945
8.5	1.812	1.220	4.115
9.0	1.857	1.304	6.291
9.5	1.922	1.382	8.474
10.0	2.007	1.458	10.674
10.5	2.111	1.533	12.886
11.0	2.223	1.581	12.092
11.5	2.325	1.619	10.943
12.0	2.417	1.654	9.909
12.5	2.500	1.687	8.963
13.0	2.575	1.717	8.086
13.5	2.642	1.745	7.267
14.0	2.703	1.771	6.494
14.5	2.756	1.796	5.777
15.0	2.804	1.820	5.092
15.5	2.845	1.842	4.446
16.0	2.882	1.864	3.831
16.5	2.912	1.884	3.241
17.0	2.938	1.904	2.690
17.5	2.959	1.923	2.152
18.0	2.976	1.941	1.626
18.5	2.988	1.954	1.137
19.0	2.996	1.977	0.651
19.5	3.000	1.993	0.207
19.722	3.000	2.000	0.000

APPENDIX III

CALIBRATION

Prior to gaseous injection the nozzle was checked to insure that it produced shock-free flow. Early tests indicated that a series of shocks originated immediately downstream of the nozzle inflection point. These shocks were clearly visible in shadowgraphs. It was determined that during the polishing, a series of depressions were inadvertantly made in the contour immediately downstream of the injection point. Hand filing removed the depressions and eliminated the shocks.

Once the shocks were eliminated the actual Mach number was checked with the design Mach number down the nozzle. This was accomplished by measuring the wall static pressure at different axial positions and calculating the Mach number using the isentropic relationship

$$\frac{P}{p} = \left(1 + \frac{\gamma-1}{2} M^2\right)^{\frac{\gamma}{\gamma-1}} \qquad \text{(III.1)}$$

These values were then compared with the Mach numbers calculated during the nozzle design. Figure 49 is a plot of the design and measured Mach numbers versus the axial distance from the entrance of the nozzle. The measured values are average values for 12 different tests.

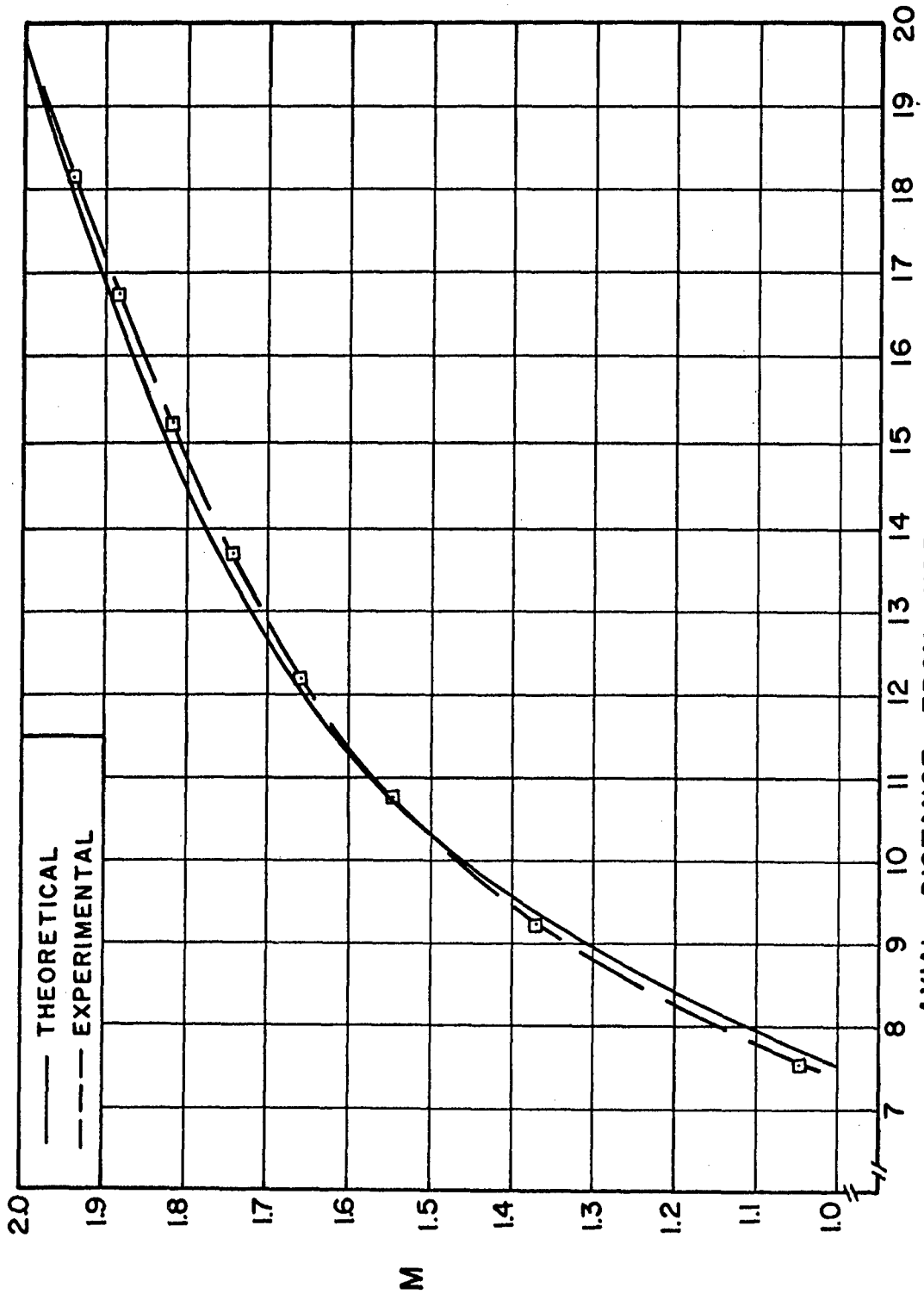

FIG. 49 COMPARISON OF CALCULATED AND MEASURED MACH NUMBERS